2013

Head Gasket Finite Element Model Correlation

Jeff Scott Eagleson
University of Windsor

Head Gasket Finite Element Model Correlation

By

Jeffrey Scott Eagleson

A Thesis
Submitted to the Faculty of Graduate Studies
through the Department of Mechanical, Automotive and Materials Engineering
in Partial Fulfillment of the Requirements for
the Degree of Master of Applied Science
at the University of Windsor

Windsor, Ontario, Canada

2013

Head Gasket Finite Model Element Model Correlation

by

Jeffrey Scott Eagleson

APPROVED BY:

_____

Dr. R. Bowers
Department of Mechanical, Automotive and Materials Engineering

_____

Dr. D. Green
Department of Mechanical, Automotive and Materials Engineering

_____

Dr. A. Sobiesiak, Advisor
Department of Mechanical, Automotive and Materials Engineering

May 10, 2013

DECLARATION OF ORIGINALITY

I hereby certify that I am the sole author of this thesis and that no part of this thesis has been published or submitted for publication.

I certify that, to the best of my knowledge, my thesis does not infringe upon anyone's copyright nor violate any proprietary rights and that any ideas, techniques, quotations, or any other material from the work of other people included in my thesis, published or otherwise, are fully acknowledged in accordance with the standard referencing practices. Furthermore, to the extent that I have included copyrighted material that surpasses the bounds of fair dealing within the meaning of the Canada Copyright Act, I certify that I have obtained a written permission from the copyright owner(s) to include such material(s) in my thesis and have included copies of such copyright clearances to my appendix.

I declare that this is a true copy of my thesis, including any final revisions, as approved by my thesis committee and the Graduate Studies office, and that this thesis has not been submitted for a higher degree to any other University or Institution.

ABSTRACT

Finite element analysis studies are increasingly being relied upon to improve the design and decrease overall production time of powertrain components. Multi-layer steel head gaskets are important, passive sealing components that exist in almost all internal combustion engines and are crucial for proper engine performance. In industry there currently exist many different approaches for studying this component using finite element analysis.

This study attempted to give insight into what finite element methods are currently being used by analysts and if their results correlate with physical test results. The category of finite elements studied for use in the gasket assembly were dependent on the type of results required and included conventional shell, continuum shell, gasket type and three-dimensional solid elements. By use of ABAQUS software and Fuji Pressure Film comparisons, it was found that each element type has strengths and limitations regarding real world correlation, computational expense and ease of procedure.

DEDICATION

Dedicated to all of my friends and family.

ACKNOWLEDGMENTS

I would like to thank the following people, whom I could not have completed the project without:

- Dr. Peter Frise and Ms. Jan Stewart from Auto 21 and the University of Windsor for the fantastic organizational job they have done with the entire Masters program.
- Dr. Sobiesiak for his hard work, patience and information provided on powertrain components.
- Mr. Mohammed Malik for his continued support throughout the entire two year program.
- Mr. Patrick Baer for his patience, guidance and genuine interest in the entire project.
- Mr. Paul Gardiner for his continued help with the project.
- Mr. Raffaele Bonavolonta and the CRF team for their hospitality, hard work and support during my time in Torino.
- Mr. Adrian Trifan for his constant support and guidance while learning the ABAQUS software
- Dr. Cristiana Delprete and the Politecnico di Torino staff for their support throughout the project
- Ms. Raffaella Fiora for her hard work and hospitality during our time in Italy.

TABLE OF CONTENTS

LIST OF TABLES

LIST OF FIGURES

LIST OF ABBREVIATIONS/SYMBOLS

1D	One Dimensional
2D	Two Dimensional
3D	Three Dimensional
AFR	Air-Fuel Ratio
BC	Boundary Condition
CAD	Computer aided design
CAE	Computer aided engineering
CC	Cold Clamping
CF	Cold Firing
CPU	Central processing unit
CTC	Chrysler Technical Center
FE	Finite Element
FEA	Finite Element Analysis
FEM	Finite Element Method
FIAT	Fabbrica Italiana Automobili Torino
GPa	Gigapascal
GVRA	General Victor Reinz Approach
HC	Hot Clamping
HCV	Higher Calorific Value
HF	Hot Firing
ISO	International Organization for Standardization
mm	Millimeter
MLS	Multi Layer Steel
MPa	Megapascal
N	Newton
NLGEOM	Non-Linear Geometry Option
OEM	Original Equipment Manufacturers
PCP	Peak Combustion Pressure
PdT	Politecnico di Torino
RAM	Random access memory
RPM	Revolutions per Minute
SDI	Severe Discontinuity Iteration
USB	Universal serial bus
VM	Von Mises

NOMENCLATURE

X	Angle of Bead
Y	Height of Bead
V	Width of Full Bead
k_s	Stiffness of Studs
k_H	Stiffness of Head
k_B	Stiffness of Block
k_L	Stiffness of Engine Liner
k_G	Stiffness of Entire Gasket
k_1	Stiffness of Gasket Layer 1
k_2	Stiffness of Gasket Layer 2
k_3	Stiffness of Gasket Layer 3
k_4	Stiffness of Gasket Layer 4
ε_x	Strain in x-Direction
u	Displacement
σ_x	Stress in x-Direction
E	Modulus of Elasticity
{F}	Global nodal Force vector
[K]	Structure global stiffness matrix
{d}	Vector of displacements
I_S^c	Maximum amount of severe discontinuity iterations
P_{MOD}	Modified Cylinder Pressure
P_{MAX}	Maximum Cylinder Pressure
R_C	Cylinder Radius
R_I	Intake Valve Radius
R_E	Exhaust Valve Radius
S	Stresses (Gasket)
E	Strains (Gasket)
S11	Pressure in the gasket element
S22	Direct membrane stress.
S33	Direct membrane stress
S12	Transverse shear stress
S13	Transverse shear stress
S23	Membrane shear stress
E11	Gasket closure
E22	Direct membrane strain
E33	Direct membrane strain
E12	Transverse shear motion
E13	Transverse shear motion
E23	Membrane shear strain
U	Membrane shear strain
RF	Reaction Forces

η_{OTTO}	Efficiency of the Otto Cycle
ρ	Density
m_{AIR} (kg)	Mass
r_v	Compression Ratio of Engine
k	Ratio of Specific heat capacities
P_n	Pressure at step n of Otto Cycle
v_n	Volume at step n of Otto Cycle
v_r	Relative specific volume of air
q_n	Heat transfer per unit mass
u_n	Specific Internal Energy
cv	Constant Volume Specific Heat
cp	Constant Pressure Specific Heat
r	Axisymmetric Radial Coordinate
z	Axisymmetric Height Coordinate
θ	Axisymmetric Angular Coordinate

Chapter 1: Introduction

The head gasket is the most important passive sealing element in the internal combustion engine. It is positioned between the cylinder head and block and its purpose is to provide a gas tight seal between the cylinder(s), the water jackets, oil passages and the ambient air, liquids and gases. The area of the gasket around the cylinder must be robust enough to withstand the same pressures that are exerted on the pistons while ensuring that there is no leakage of coolant or combustion gases among the three volumes. It must be able to accomplish this at all engine temperatures and pressures without malfunction, as a failure of the engine gasket usually results in a failure of the full engine.

The current Dodge NASCAR engine uses a multi-layer steel (MLS) construction that consists of four layers of stainless steel sheets that are pressed firmly together by the compressive forces of the cylinder head bolts. Between layers 2 and 3 exists a stainless steel fire ring. The exploded view of the gasket is shown in Figure 1. Also, previous versions of the gasket have used a thin rubber coating which helps with sealing between each of the steel components. One of the major concerns is the lack of an accurate head gasket model for use during Finite Element Analysis (FEA). Preliminary testing has shown that the current digital model does not accurately represent what is occurring in the real life situation, where failures have occurred during testing. The failures are usually cracking of the gasket at the cylinders 5 and 7 exhaust locations.

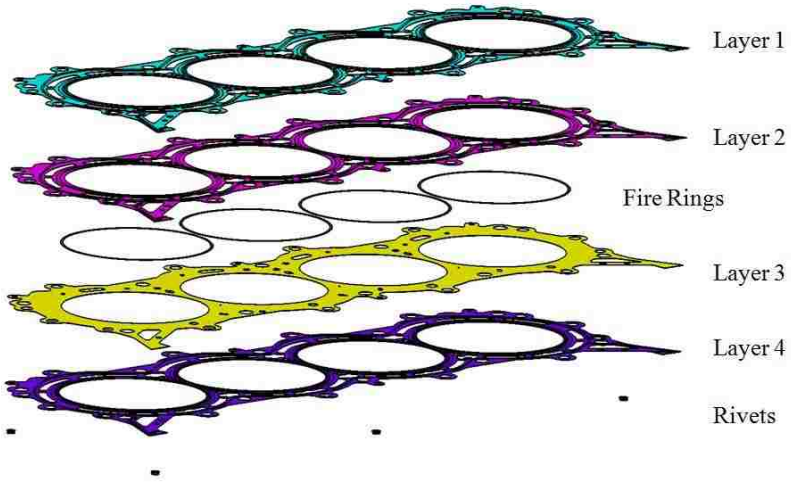

Figure 1: Exploded view of the gasket CAD

Finite Element Analysis is a powerful tool used by engineers and designers to determine how a part or assembly behaves when subjected to various boundary conditions. Some of the parameters that can be determined are stresses, strains, displacements and thermal expansions. The finite

element method is a numerical technique, ideally suited to digital computers, in which a continuous elastic structure (continuum) is divided (discretized) into small but finite well-defined substructures (elements) [Hibbit, et al, 2001]. Using matrices, the continuous elastic behaviour of each element is categorized in terms of the element's material and geometric properties, the distribution of loading (static, dynamic and thermal) within the element, and loads and displacements at the nodes of the element. The element's nodes are the fundamental governing entities of the element, as it is the node where the element connects to other elements, where elastic properties of the element are established, where boundary conditions are assigned, and where forces (contact or body) are ultimately applied [Budynas, 1999]. One of the more powerful software packages available and the one that will be used for the project is ABAQUS Standard. ABAQUS is a suite of engineering simulation programs, based on the finite element method that can solve problems ranging from relatively simple linear analysis to the most challenging nonlinear simulations. The software contains an extensive library of elements that can model any geometry. It has an equally extensive list of material models that can simulate the behaviour of most typical engineering materials including metals, rubber, polymers, composites, reinforced concrete, crushable and resilient foams, and geotechnical materials such as soils and rock [Hibbit, et al, 2001].

Head gasket designs are relatively complex and thus usually left to the gasket suppliers to design, engineer and test. When the head and block of the engine are designed by the engine development team, the contact interface is given to the gasket supplier to use for their design. The gasket supplier creates the gasket based on the information, but does not analyze their part using proper engine CAD components. Essentially, the most important seal of an engine is being designed by two separate teams with gaps of information between each other. If there is an issue with the surface contact joint of the engine, this situation is difficult to resolve due to the information gap. If a database of knowledge is built within the Chrysler, FIAT and Dodge Motorsports Team, future head gasket issues can be solved from within the company, without relying on potentially expensive outside support. The knowledge can also be used to create improved designs of engine heads and blocks.

In order to speed up the development time of engine design, it is necessary to use computational analysis as much as possible. The current finite element analysis methods used by Chrysler, FIAT and Dodge Motorsports are reliant on a provided single layer gasket model for analysis. This simplified gasket model makes many assumptions regarding stresses, strains and deflections on the real-world gasket. The primary goals of the project are to remedy the situation by thoroughly

investigating past, present and future FE techniques used in industry to analyze MLS head gasket behaviour and to determine a root cause of the current gasket failure. The results found can then be correlated to physical test data found by using Fuji Pressure Film on the real-world engine assembly. The major objective is to determine the strengths and weaknesses of FE techniques to improve company knowledge that will help analysts more accurately represent the physical head gasket during future studies. Head gaskets are fairly complex parts, so a thorough procedure for virtual simulation must be completed. Much of the physical testing is to be completed in partnership with the Penske Racing Team. Various analyses must be completed using ABAQUS FEA software to give a complete range of results. When complete, there will be a database of new knowledge regarding head gasket FEA that can be referenced by all Chrysler and FIATs designers in the future.

Although specifically dealing with NASCAR head gaskets, the completed research on head gaskets and FEA methods will decrease design time and improve engine durability for all Chrysler, Dodge and FIAT vehicles.

Chapter 2: Literature Review

The literature review was conducted using SAE papers, books and The ABAQUS user's manual. Much of the topics discussed in the thesis are based on proprietary information in industry, so only basic information was able to be found using these sources. Detailed procedures and techniques were difficult to obtain without having direct access to proprietary industrial reports.

2.1 Head Gasket Basics

The head gasket is the sealing element between the cylinder block and the head. The active sealing components of an engine are the intake/exhaust valves and the piston rings, which are constantly in cyclic motion [Stone, 1985]. Although it's role is passive, a head gasket's function is extremely important for proper engine function. The gasket must withstand the high pressures and temperatures of the combustion process and ensure that the combustion gases, coolant and oil passages remain sealed from one another. This function must occur at varying engine speeds and loads, at which the entire assembly is at varying stages of stress and temperature. Multi-layer steel head gaskets are currently the favorable choice for the internal combustion engine and are a growing technology in the heavy duty diesel industry. There are many reasons for the popularity, such as improved reliability, increased sealing with minimal stud forces, better chemical and thermal resistance, higher control of clamped gasket thickness, decreased bolt force fluctuations, improved levels of dynamic response and enhanced emission control [Chen, 2002].

2.2 Head Gasket Design

The MLS cylinder head gasket is composed of several layers of steel, which form the body of the gasket. The body material is usually composed of low stiffness steel whose function is to simply provide support to the gasket. Other materials that are commonly used are graphite and composites [Hebert, et al, 1998]. Within the layers, there of a number of distinct areas, all of which play an important role in the sealing process. Beads of a gasket are formed into the active layers of the gasket, which are the top and bottom sheets. The beads are responsible for proper sealing and convert bolt forces into sealing forces. The bead material located around the cylinder bore is known as the stopper area. This area is the first sealing line against leakage and must be the thickest and stiffest in order to provide proper sealing pressure against the combustion gases. The stopper (or fire ring) is usually a different, stiffer, material than the rest of the gasket. There are many forms of stopper areas and even gaskets that do not use a stopper. It has been found that the stopper area takes approximately 60-80% of the stress due to the bolt loading [Popielas, et al, 2003 (0484)]. Due to this, the stopper area has a major influence on the load distribution, head lift off, bore distortion, brinelling and fretting. The stopper height influences how stress is applied at

the full beads and the active layers of the gasket. It has a significant effect on the fatigue life of the gasket. The second sealing line is directly behind the stopper area and is composed of formed beads in the active layers. Beyond these layers lie the active layers of the body area, which provide sealing for the oil and coolant circuits, as well as sealing from the ambient environment. Commonly, there is coating on the gasket layers. Sometimes, there is only a coating on the top and bottom surface of the gasket at the deck interface. The coating acts as another barrier against gas and fluid leakage as well as altering the shear behaviour of the interfaces [Popielas, et al, 2000].

There are two types of beads used in a MLS gasket; the full bead and the half bead. Beyond having two different geometries, as shown in Figure 2, the beads perform different functions. The specific geometry of the beads are formed by lengths Y and V, and by angle X [Catalogue Cylinder Head Gaskets…, 2013]. During the installation of the head gasket, the full beads are compressed until they reach the height of the stopper, or until the bead resistance equals the bolt clamping force. The sealing force created by the full bead is relatively high, which is required to properly seal the combustion chambers. The main purpose of a full bead is to equalize the dynamic sealing gap oscillations between the cylinder head and cylinder block at high combustion pressures. The half bead's function is mainly to seal against coolant and oil in the areas far away from the cylinder, at bolt holes and at the outer surfaces. Since the half beads have a lower sealing force than the full beads, the full bead is able to maintain proper sealing force at the area of most importance, the combustion chamber. The main factors that affect the bead stiffness are geometry, steel quality, sheet thickness and production process [Chen, et al, 2002].

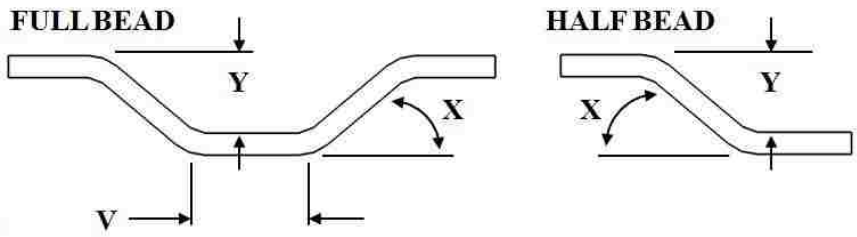

Figure 2: Full Bead (left) and Half Bead (right) of gasket layers

Engine head gasket design is a complicated process as the gasket must perform many duties while having an appropriate useful life. Therefore, it is important to balance the sealing potential versus the overall durability of the gasket. The gasket design is driven mainly by engine geometry, but other factors are of importance as well. These include: bolt clamping force, deck surface characteristics, peak cylinder pressures, engine temperatures, fluid and gas chemistries, and

compressed gasket thickness, etc [Chen, et al, 2002]. The sealing features of the gasket discussed earlier are constructed of geometric beads or embossments. The designer uses an in-plane view at the combustion chamber and each fluid passageway to properly design the sealing beads. The beads of each layer are created by stamping the thin metallic layer between two halves of the tool, which produces residual stresses in the layers. The individual layers are then stacked to attain the desired spring stiffness characteristics and required compressed thickness between the engine block and head. As shown in Figure 3, the gasket layer beads are basically small, single springs with suitable stiffness, that when assembled, create a single larger spring. Spring characteristics are determined by the layer material, thickness, hardness and geometry [Mockenhaupt, 2003]. The layout of the beads in the adjacent layers can be classified in two ways; series or parallel [Chen, et al, 2002]. The distinction is shown in Figure 4 and their use is dependent on the dynamics of the bolted joint, cyclic loading caused by the combustion process and thermal distortion of the engine assembly. In the gasket industry, there are many arrangements of the beads, therefore it is a challenge for the designer to meet the static and dynamics requirements of engine assembly. The entire gasket must provide adequate sealing at maximum, minimum and alternating loads while resisting fatigue effects over the entire gasket life. Any degradation of sealing ability will result in decreased engine performance and even failure. The preceding reasons demonstrate the need for analytical methods in the design phase of a MLS gasket. The goal of the gasket designer is to optimize the gasket contact stresses and minimize the dynamic motion of the head [Chen, et al, 2002].

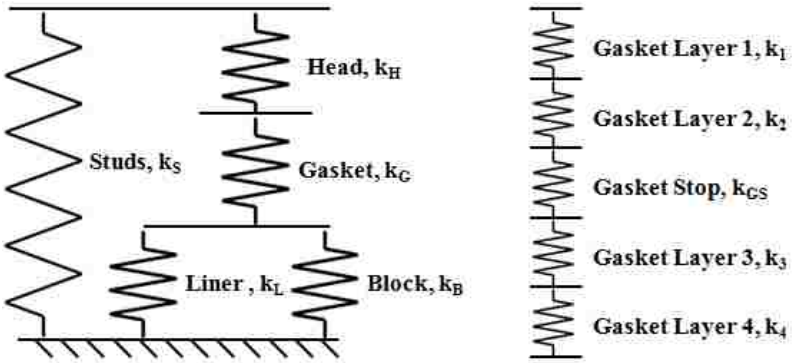

Figure 3: 1D spring stiffness diagrams of engine assembly (left) and gasket assembly (right)

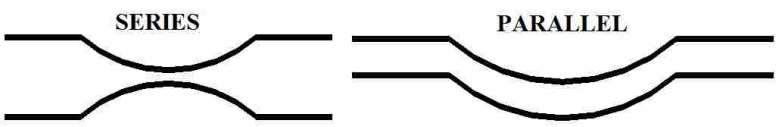

Figure 4: Types of bead profiles in gasket layers; Series (left) and Parallel (right)

2.3 Gasket Failure Modes

Metallic composition and feature geometry of the head gasket are important parameters to consider during design. As with any metallic element that is subjected to cyclic loads, head gaskets have fatigue limits that must be taken into account during the design process. The dimensions and forming parameters of the full bead of the gasket resulted in changes in gasket durability. Study results show that the selection of embossing parameters producing less deformation of the bead plate is beneficial for the improvement of durability while the flattening has marginal influence. The fatigue durability is improved with the increase of in the width of the full-bead and the radial length of the bore-side flat region [Cho, et al, 2005].

Gasket layers are usually composed of hardened stainless steel. In an annealed state, stainless steel mostly consists of austenitic material. In order to get the proper spring properties from the material it must be hardened, which can be achieved by cold rolling. This cold rolling process introduces a martensite phase into the material. The result is a smaller grain size, altered grain structure, decreased elongation, and increased mechanical properties. When the beads are stamped into the metal sheets, additional cold working is performed and the hardness and mechanical properties at these areas is increased due to the plastic deformation. This occurs on only one side of the metal sheet. On the other side there exists decreased elongation which increases the probability that the bead will fatigue crack with the addition of tensile stress. Under engine assembly, tensile stress is induced as the bead is compressed [Kestly, et al, 2000].

As the martensite is formed from cold working, defects are created in the structure. Under the repeated cyclic loading of an ICE, the stress levels change and the defects begin to increase. When a sufficient amount of defects are created, the part will crack, most likely at its weakest area. The weakest area is where there exists tensile stresses, high stress levels, and highest fluctuating stress levels.

Brinelling is defined as a contact stress that permanently deforms the surface to which it is applied. The material can flow due to the deformation under pressure. It can result in damage of the cylinder block or head deck faces and also the gasket itself. It is most likely to occur in engine components made from aluminum alloys. Fretting occurs locally on a surface and is defined as pockets, drag marks and stripes in the material. When friction is high enough between two surfaces, aluminum particles can be cold welded to the metallic gasket surface. Fretting can only occur if there is gasket movement tangent to the deck surface in addition to the usual vertical motion. In general, fretting can occur without brinelling, but under most conditions, brinelling

will not occur without fretting. One theory suggests that the scratches due to fretting are a starting point for fatigue cracking due to the stress concentrations at these areas. Also there is a theory that the scratches generate the higher friction forces and added deformation in the material which results in changes in the structure [Kestly, et al, 2000].

The two most common failure modes of a MLS gasket are excessive leakage and fatigue cracking. [Chen, 2002] Large head lift during the dynamic motion of the cylinder head is the main contributor to fatigue failure due to increased amplitudes of cyclic stresses. The two major factors that cause head lift are thermal loading and firing pressure. Small cracks that exist in the gasket layers grow slightly every cycle and eventually open to a size that causes bead failure.

The forming process of the beads in each layer is achieved by stamping the thin metallic sheets between two dies [Popielas, et al, 2000]. The process shapes the bead by deforming the material beyond its yield stress. Due to the compressive and tensile forces present, there will always exist residual stresses in the gasket layer. These stresses should not be ignored when doing a full analysis on the gasket assembly.

A major consideration of gasket sealing are the stresses created in the engine head due to its bending over the stiff gasket beads, which can lead to fatigue failure under high cylinder firing cyclic loads. The stiffness of the gasket also influences the distorted shape of the cylinder bore under cold and hot assembly conditions, which can lead to piston ring conformability problems, excessive oil consumption, and unacceptable emissions levels [Hebert, et al, 1998].

The efficiency of the head gasket sealing depends on the pre-stressing force of the hold-down bolts, without taking into consideration any thermal stresses resulting from the temperature distribution within the cylinder head. It was also found that the location of maximum contact pressure on the gasket is increased when the thermal loading is included in the analysis [Popielas, et al, 2003 (0483)]. It was found that the capacity of the gasket sealing mainly depends upon the pre-stressing of the bolts, which are also the source of maximum external loading on the inner structure of the cylinder head. When thermal loading is incorporated into the analysis, the location of the weakest contact pressure on the raised portion of the gasket is changed due to the effect of thermal stress/strain. The analytical results show that the thermal stresses provide a positive support for the efficiency of gasket sealing. Under operating conditions with gas pressure, however, there exists an opposite force to the direction of the pre-tensioned bolts, which increases the possibility of gas leakage. The solution is to increase the magnitude of the assembly force without exceeding the material strength of each component in the engine structure. By knowing

this early in the gasket design process, the gasket structure can be improved in the areas of worst sealing.

2.4 Non-linearity in Gaskets

Since cylinder head gaskets are made of multiple layers spaced apart from one another, the structure possesses material properties which are directionally dependent (anisotropic) and non-linear [Hebert, et al, 1998]. When compressed, the multiple layers are bent beyond their yield stress and undergo plastic deformation. The multiple gasket layers come into contact with each other, which results in an increasing slope of the stress-strain curve. Due hysteresis in the gasket assembly, as the load is decreased, it does not follow the same loading curve that it originally followed. For example, the curve on the left in Figure 5 shows that the loading curve will follow AB as the gasket is compressed. If the gasket is unloaded, it will follow the unloading curve BCA. ABAQUS software deals with the nonlinearities by two different methods; nonlinear elastic model with damage and nonlinear elastic-plastic models. The two different types of gasket curves are shown in Figure 5 below [Hibbit, et al, 2010].

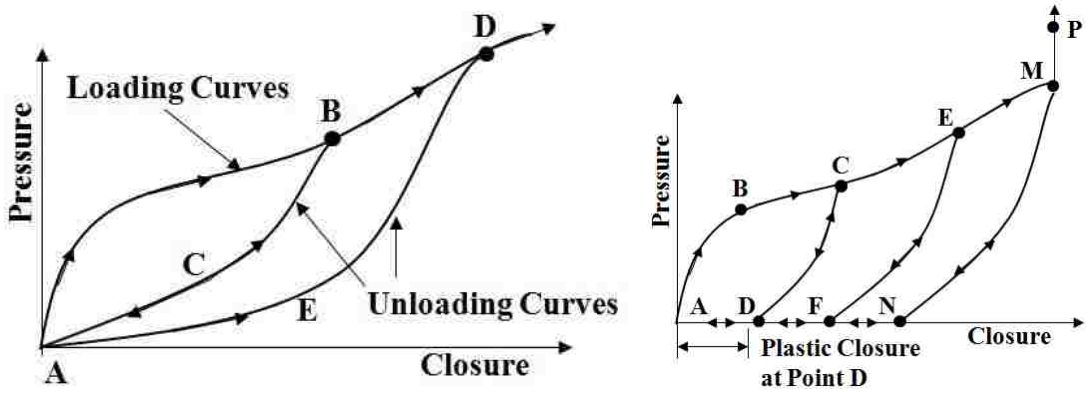

Figure 5: Pressure vs Closure curves used by ABAQUS; nonlinear elastic model with damage (left) and nonlinear elastic-plastic model (right)

2.5 Gasket Analysis Using Finite Element Methods

In order to reduce the time and costs of the engine development cycle, Computer Aided Engineering (CAE) is an important tool for gasket design. For the commercial automobile market, turnaround for engine model generation has been greatly reduced from the past [Kestly, et al, 2000]. As a result, the short development time means that it is very difficult to get real information through testing and experimentation. This means that CAE must be used to make the first design proposal and first optimizations without using any hardware. It is imperative that the

MLS gasket design meets the fit, form and function requirements of the application; thus the solid models of the engine block, head and studs must be included in the FE analysis, along with the environmental parameters and installation information. The costs and time associated with implementing MLS head gaskets are encouraging increased levels of technical knowledge early in the design process. The design process generally relies heavily on advanced experimental, analytical and numerical methods. It is very important to use the Finite Element method of the full engine assembly, including the gasket, in order to aid in the understanding of motion levels and deflections of the MLS gasket sealing features, well before production [Popielas et al, 2003 (0481)]. The pre-production analyses help the designer to understand the capability of the design to meet sealing and durability requirements of the gasket while allowing it to be brought into production faster. The numerical simulation modeling allows the engineer to review multiple loading and operating conditions, which increase the probability of an initial design being successful.

2.5.1 Axisymmetric Methods

In the past, traditional approaches to gasket analysis lacked information of the head and block due to customer confidentiality, and therefore used only 2D axisymmetric models and oversimplified assumptions (permanently rigid mating surfaces, room temperature working temperatures, etc). Interactions at the deck faces were usually ignored. MLS gaskets are subjected to high compressive stresses during loading and the compressive responses are non-linear. Complexities in the geometry and material behaviour make detailed modeling of gaskets using continuum elements extremely time consuming for internal stress analysis. Therefore, two-dimensional axisymmetric analysis was the only approach to the complicated problem. This type of analysis not only provides a solution to the longer running time for the three-dimensional models, but also provides a large amount of information on the behaviour and interaction between the engine hardware, and also within the different layers of the gaskets. Typically, a 2D axisymmetric multi-layer model consists of the different layers of the gasket geometry, the rubber coating on the metal, and the residual stresses due to the forming process. The steps involved are as follows [Popielas, et al. 2003 (0483)]:

1. The results file from a specialty software is outputted. The single layer forming process calculation is then converted into an input file for multi-layer analysis using specialized sub-routines.
2. The engine head, block and liner are modeled as rigid surfaces.

3. The Input file for Multi-layer 2D axis-symmetric model is created for different load cases depending on engine operating parameters. Which are:

Step 1: Apply the specified bolt load. Bolt load to be used for the simulation is calculated as below:

Load = [Number of bolts/Cylinder * Bolt load per bolt] * 50 % for gasoline engines

Load = [Number of bolts/Cylinder * Bolt load per bolt] * 75 % for heavy-duty engines

Step 2: Apply specified head lift off (experimental data used or the calculated lift off of a 3D calculation)

Step 3: Apply reduced bolt load

Step 4: Apply specified head lift off (Using experimental data)

The next evolution was to model the deformed surface with topography over the entire sealing surface by using "Super Elements" [Popielas et al, 2000]. Although an improvement over the previous methods, the deformed surface was fixed at a certain working condition and therefore could not accurately represent transition conditions. The analyses were very limited and not accurate enough to satisfy customer requirements. As computer hardware and FEA software improved, MLS gaskets were able to be studied in more depth. FEA was now able to simulate the forming process of the gasket layers and reveal the residual stress distribution within the material. The FEA analyst could model the male and female die shapes by using rigid elements and place deformable material between them. Due to contact problems, these are usually left to 2D axisymmetric models. After conversion from 2D to 3D, some commercial FEA codes will allow the analyst to export the results with residual stress into a simplified 3D engine assembly for further analysis. However, the prior simulation has many deficiencies such as unknown coefficients of friction between the die and gasket layers, difficulties in modeling the rubber gasket coating and proper simulation of the speed of the die itself [Popielas, et al, 2000].

2.5.2 Proteus® Software

In recent years, programs have been created in order to further investigate the phenomenon of gasket residual stresses. One of the major programs is entitled Proteus®. For the 2D Analysis, the Proteus® software is first used to determine the deformed shape of the bead layer as well as residual stresses due to the manufacturing process. The program is also able to determine the fatigue life of the elements under operating conditions, the weakest element area and the number

of cycles until cracking. Important parameters that are used by the program include: material parameters, friction coefficient between the gasket coating and tooling, bead width and height, tooling radius, coating thickness, etc. After these parameters are found, the information from the Proteus® software is exported into a commercial software, such as ABAQUS or Marc. [Popielas, et al, 2000]

2.5.3 The Victor Reinz Approach

Currently, OEMs want to determine the effects of the interaction between the gasket, engine block and head, so the historical, less detailed methods are not appropriate. A typical procedure involves the construction of the 3D engine block, cylinder head and conventional gasket between them. The MLS gasket is then modeled and replaces the conventional gasket so that the differences can be compared. This simulation would typically involve the preload of the bolts, peak firing pressure, bolt load from stretch tests, thermal map and other variables.

One of the largest manufacturers of MLS head gasket is Victor Reinz. They have developed a specific method for gasket analysis, known as The Victor Reinz CAE Approach and is displayed in Figure 6 below. The first step for any analysis is to define the goal of the calculation. In gasket analysis, there are many parameters and it does not makes sense to consider them all at the same time. The types of parameters that need to be studied include, but are not limited to [Popielas, et al, 2000].

- Residual stress/strain distribution in the beads due to the manufacturing forming process.
- Durability of the beads in the various layers
- Load/deflection curves of the beads and the entire gasket assembly
- Influence on corresponding components (head, block and studs)
- Load distribution of the gasket at the deck faces of the assembly
- Specific loads on the gasket sealing areas
- Distortion of head, block, liner, studs, valve guides, valves, etc
- Head lift off under peak temperature and pressure
- Dynamic sealing gap oscillation during the combustion process

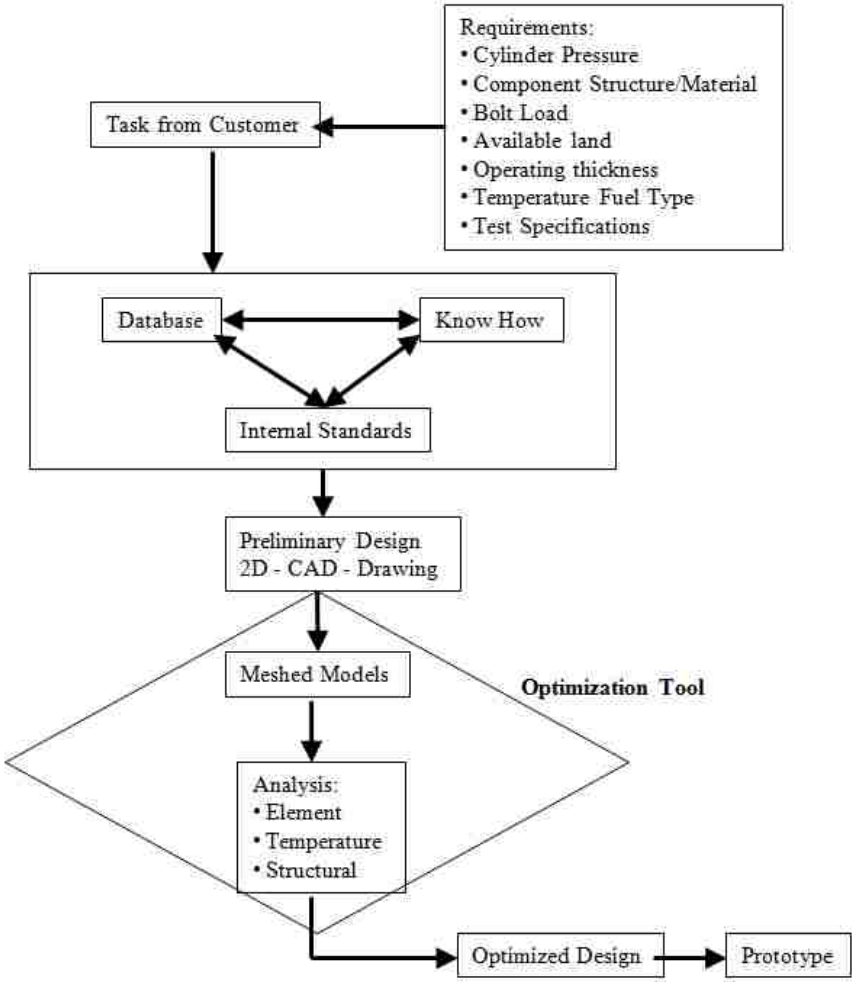

Figure 6: Victor Reinz CAE Approach [Popielas et al., 2003 (0483)]

The behaviour of the gasket must be studied under working conditions with consideration of the history of the layer, especially the bead. The special Proteus® Software was developed in order to determine stress levels, stress distribution, load/deflection curve and durability of the beads themselves. The information obtained allows for a first design optimization. After a suitable design is obtained, there are two possibilities: put the full gasket explicitly into the system or use the gaskets or special elements with the use the calculated load/deflection curve data [Popielas, et al, 2000]. There are two critical aspect of using the full gasket. The explicit use of the gasket would increase the number of elements, and at the same time the number of degrees of freedom, dramatically. To handle the processing time a "super computer" system and a considerable amount of running time would be required. Also, accurate representation of gasket coatings is difficult to accomplish. [Popielas, et al, 2000]

There are two different types of structural engine analyses: static and dynamic. For the static case, the pressure is considered static, and therefore the results do not correspond to real engine operation. The approximation allows individual parts to be analyzed due to the asymmetric nature of the engine firing sequence. Smaller models can also be analyzed. For a dynamic analysis, pressure loading as a function of time is reproduced for various operating conditions. The entire engine must be analyzed. This type of analysis allows for the assessment of the vibration behaviour of the engine components. Also, it allows for the analysis of the gasket behaviour as a function of engine speed and combustion pressure. Non-linear analysis is only feasible due to the plastic/elastic deformation characteristics of the MLS gasket and possibly due to the elongation of the bolt. The individual elements of a MLS gasket will exhibit different amounts of plastic deformation, depending on their location and applied load. This will result in varying unload characteristics as well. For both cases, the CFD temperature map is needed. The loading sequence for the analysis must follow the real world case, which is [Popielas, et al, 2000];

For the Static analysis case, the load cycle is:

1. Bolt tightening at room temperature

2. Cold setting of the threads, by an amount determined experimentally or taken from empirical data

3. Heating up to operating temperature

4. Static pressure loading with max. combustion pressure for the dynamic case, the load cycle is:

    A. Bolt tightening

    B. Setting of the threads by an amount determined experimentally or taken from empirical data

    C. Dynamic pressure loading with simultaneous heating to the operating temperature

The computational results can be compared with experimental findings. After the cold condition bolt tightening, the pressure distribution can be compared with Fuji film. The calculated gap between the head and block deck faces can be compared to the measured static-sealing gap (operating thickness). Bolt clamping forces can be compared for the cooled down engine. Dynamic gap measurements of the real engine and computational case can be compared. Various results are compared from their computational analysis and experimental analysis.

The CAE approach is separated into Part A and Part B. For Part A, model preparation includes the 1-cylinder model, the whole engine model and the thermal analysis model. Gasket analysis starts

with the element study, which includes the forming operation in creating the sealing elements (beads), along with the material limit and functionality study. Optimization early in this design stage increases the opportunity for an improved final design. The proceeding step assembles the previously calculated elements into a multi-layer system to mimic the real gasket. This procedure simulates loading and unloading conditions by using simplified structures such as rigid elements and basic deformable bodies. This gives an initial look into the contact pressure on the engine component surfaces. The flow diagram is shown in Figure 7. CAE Approach Part B involves the system simulation of the 3D 1-cylinder model and the whole bank engine. The single cylinder analysis serves as a parameter study for gasket and engine parameters and also as an optimization loop. The whole bank analysis is always the last analysis. The influence of the neighboring cylinders can be observed in FEA as the stiffness of the engine varies over the entire sealing deck. Possible weak areas can only be found using a 3D study. The 3D simulation ends the FEA part of the analysis. The flow diagram is shown in Figure 8 [Popielas, et al, 2003 (0483)].

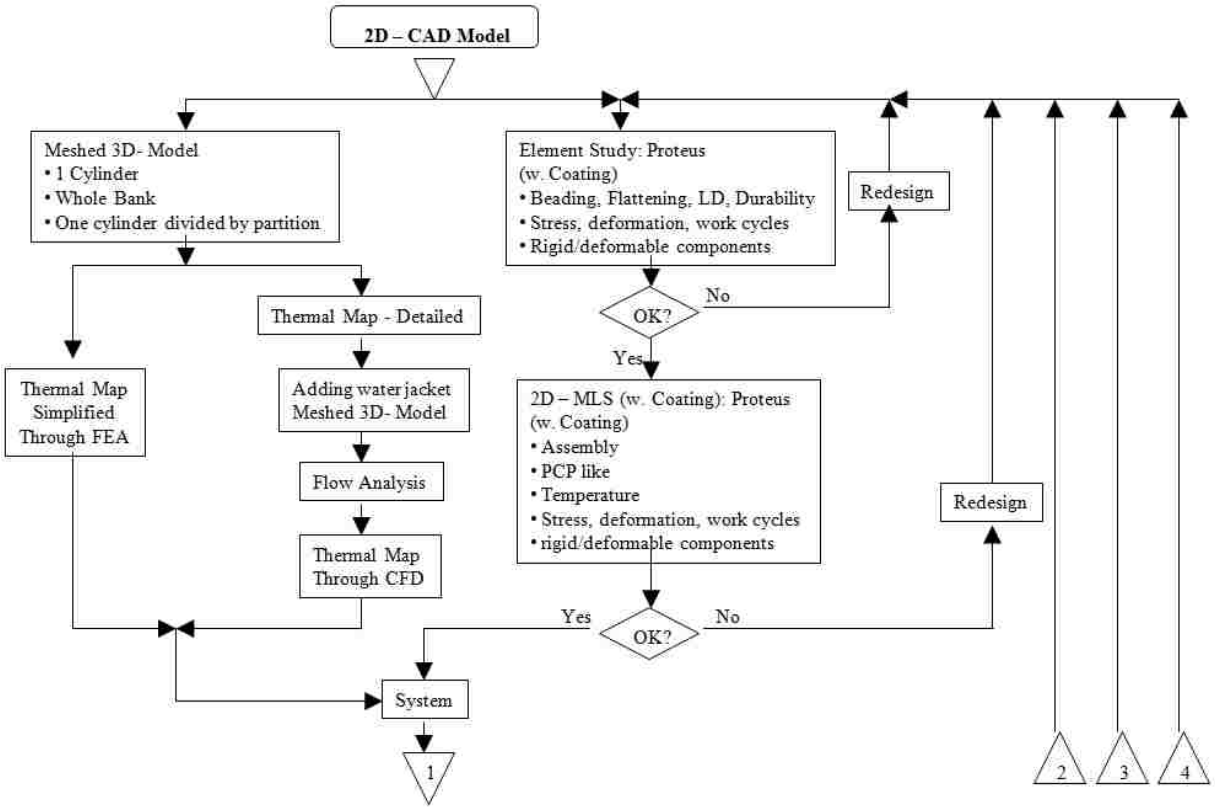

Figure 7: Victor Reinz CAE Approach - Part A [Popielas et al., 2003 (0483)]

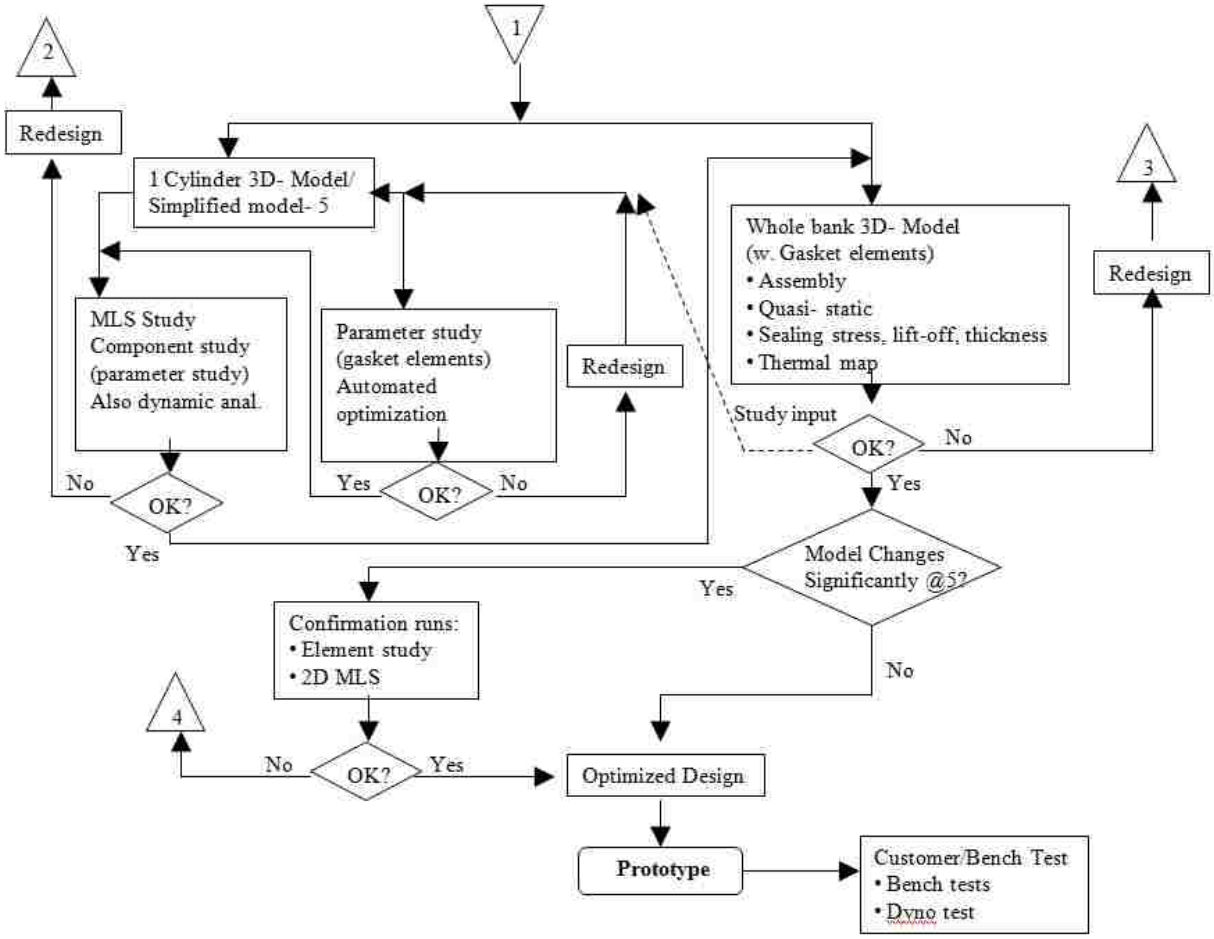

Figure 8: Victor Reinz CAE Approach - Part B [Popielas et al., 2003 (0483)]

If an engine liner is present, it is necessary to use a deformable geometry of the head, block and liner to simulate the influence of the liner on the internal stress of the gasket layers. The head cross section is usually modeled with the deck thickness along with the entire cross section of the liner and the cross section of the block to the nearest coolant or oil hole. The results from this type of simulation are as follows [Popielas, et al, 2003 (0483)]:

- Stress and strain distribution
- Load-deflection curve of the gasket
- Interaction between the different layers
- Interaction between the gasket and hardware
- Contact pressure at the sealing interface and between the layers
- Stress and strain amplitudes in order to estimate the durability
- Uniformity of bead compression in each layer

- Spring travel of the beads during firing
- Influence of temperature on sealing pressure
- Influence of coating on the sealing pressure at the sealing areas.

For verification of the 2D results, load deflection curves can be plotted to give information regarding balance load studies. These results should be compared against experimental results.

It is important to understand the coolant behaviour in an engine to design a critical engine component such as a head gasket. The coolant flow inside the engine determines the temperature distribution of the engine. Due to the complexities faced by the gasket in a real engine due to thermal expansions and loads, the 3D analysis must include a temperature map of the engine. This can be found using CFD software and then applied to the FEA analysis. Victor Reinz uses three methods for incorporating temperature into 3D analysis; using data measured by thermocouples, using customer data, and using data from CFD thermal analysis. It is important to use the temperature data in the FEA to determine thermal warpage.

For new gasket designs, it is important to understand the full sealing system (cylinder head, block, gasket and bolts). A proven method is by use of a single cylinder FEA engine model. Usually the middle cylinder with proposed uniform bead height gasket design is selected for investigation of the stiffness of the structure using a simulation. The geometry files of the head and block are meshed using continuum elements, usually hexahedral with fine mesh of linear (C3D6, C3D4, etc), reduced integration or incompatible mode elements (C3D8I, C3D6I, etc) are ideal. The head and block are usually complex, therefore wedge or tetrahedral elements may be necessary. The linear forms of these elements are relatively poorer compared to hexahedral, therefore very fine meshes must be used. Usually, a model constructed with fine tetrahedral elements will increase the degrees of freedom of the assembly, and therefore takes longer to run than a simulation with brick elements. Ideally, for an entire engine bank model, a model with 500,000 elements and 1-1.5 million degrees of freedom is suitable for determining gasket performance. Due to discretization, it is feasible to model the MLS gasket as a real 3D part with multiple layers. For parameter studies of the assembly, gasket elements can be used.

The entire bank engine model analysis begins after the Proteus®, 2D axisymmetric and 3D one cylinder FEA simulations are complete. The gasket is modeled using Abaqus gasket elements. The steps for the full bank analysis are as follows [Popielas, et al, 2003 (0483)]:

1. Model assembly with 100% bolt load at room temperature. The sealing pressure contour plot can be compared to the Fuji film impression for preliminary verification and correlation purposes. Bore distortion data can be determined as well. No bolt load loss is included.

2. Peak Combustion Pressures (PCP) are added to the cylinders to determine head lift off. The operating thickness of the gasket can be checked against the lead pellet test data at room temperature. In reality, the engine temperature rises rapidly once pressure is applied, therefore, it is necessary to apply the thermal map at PCP.

3. Apply appropriate temperature map to the engine.

4. Apply nominal PCP to the engine model. The sealing pressure contour plots can be compared against the minimum sealing requirements. The objective is to evaluate if there are any weak spots at any particular location of the structure. The sealing pressure must be checked at the spacer/stopper bead area, active bead area, fluid sealing beads, and all other beads. The operating thickness may be calculated again to check thickness under working conditions. The head lift off data will help determine if the number of active layers is sufficient. Under most circumstances, the bolt load will decrease over time due to material relaxation and thermal expansion of the head. 80% or 70% of the bolt load may be used as the assembly load. Different thermal maps can be applied to the simulation for different operating conditions. With the decreased clamping load, varying thermal maps and the over rated PCP, the worst case condition of the engine can be evaluated.

5. For heavy duty applications extra load cases can be added. Examples include, but are not limited to, assembly with bolt load and PCP for cold starting or uphill/downhill load conditions.

A separate approach is to study the interaction between the different layers of the gasket by using a multi-layer 3D model. This method allows for evaluation of the gasket and it's sealing capabilities in detail. Information is given at the bolts where the highest load can over press the gasket and in areas away from the bolts where the lowest load could cause leakage. The 3D analysis shows supporting effects from one area to the neighbour areas. This type of analysis allows for the observation of detailed data as in the 2D axisymmetric analysis, however the structural stiffness is closer to reality [Popielas, et al, 2003 (0483)].

2.6 Finite Element Theory

Finite element theory was based on the methods provided in [Logan, 2002] and [Budynas, 1999]. The main approach to the finite element method involves modeling any structure with small,

interconnected elements called finite elements. At every finite element there is an associated displacement function. All of the finite elements are directly or indirectly linked to every other element through shared interfaces. It is possible to determine the behaviour at any node in the structure in regards to the properties of all other elements of the structure by applying the stress/strain properties of the material defining the structure. All of the equations used to describe the behaviour of each node results in a sequence of algebraic equations. These equations are put into matrix notation for ease of computation.

For a structural mechanics problem, there are traditionally two general direct approaches that are used with the finite element method. The first approach is called the force method and uses internal forces for the unknowns of the analysis. The equilibrium equations are used to initially determine the governing equations. To obtain any additional necessary equations, compatibility equations are introduced. This results in a set of algebraic equations for determining the unknown forces. The second approach is called the displacement or stiffness method, and uses the nodal displacements as the unknowns of the analysis. Governing equations are expressed regarding the nodal displacements using the equations of equilibrium and an appropriate relation between forces and displacements. The displacement method is better for computational purposes because it formulation is simpler for most structural analysis problems.

Another method used for developing the governing equations is the variational method. One of the principles uses the theorem of minimum potential energy that is applicable to materials that behave in a linear-elastic way. A second principle used to develop the governing equations for the variational method is the principle of virtual work. This principle can be used for materials that behave in a linear-elastic way and for materials that behave nonlinearly.

The first step is to divide the structure into an equivalent structure of finite elements and nodes. This is usually referred to a discretizing the structure. The most appropriate element type must be chosen and is related to the type of analysis that will be performed. Also, the size of each element is important to the overall performance of the analysis. Elements must be small enough to give accurate results, but large enough to decrease computational cost. It is a matter of engineering experience and judgment to determine which element sizes should be used. Generally, where there is expected rapid change in results, smaller or higher order elements should be used. Where results are expected to be constant, large elements can be used. The assembly of elements is called a mesh and is usually automatically created using a pre-processor. Manual meshes can be created when necessary as well. Elements must be chosen based on the physical structure of the actual

body being loaded and how accurately the loading conditions would like to be represented. There are many types of elements that can be used for a finite element analysis. The main elements are;

- One dimensional line element. Types include 2-node elements (linear) or 3-nodes (quadratic).
- Two dimensional plane elements. Types include 3-node triangular elements (linear), 4-node quadrilateral elements (linear), 6-node triangular elements (quadratic) and 8-node quadrilateral elements(quadratic).
- Three dimensional elements. Types include 4-node tetrahedral (linear), 8-node hexahedral (linear), 10-node tetrahedral (quadratic) and 20-node hexahedral (quadratic).

The second step entails choosing a displacement function within every element by using the nodal values of the element. Due to their simplicity in finite element formulation, linear, quadratic and cubic polynomials functions are frequently used. Trigonometric series' can be used for the functions as well. The displacement functions are functions of the coordinates of the node. For example, a two-dimensional element will have its function expressed in relation to the nodal unknowns in its x and y component. Identical general displacement functions are used for all of the elements. The finite element method takes a continuous quantity and approximates it by use of a discrete model composed of sets of piece-wise continuous functions defined for each finite element.

The third step involves using the strain/displacement and stress/strain relationship to derive the equations for each finite element. For a one dimensional case in the x direction, for small displacements

$$\varepsilon_x = \frac{du}{dx} \qquad \text{(Equation 1)}$$

where ε_x is strain and u is the displacement. Stress are related to strains through stress/strain laws, or constitutive laws. The simplest of these laws is Hooke's law, which is

$$\sigma_x = E\varepsilon_x \qquad \text{(Equation 2)}$$

where σ_x is the stress in the x direction and E is the modulus of elasticity.

The fourth step involves the derivation of the element stiffness matrix and equations. There are three commonly used methods for achieving this; the direct equilibrium method, the work or

energy methods, and the methods of weighted residuals. Each method develops the individual element nodal equilibrium equations.

The fifth step involves the assembly of the element equations to obtain the global or total equations, and to also introduce boundary conditions. The individual element nodal equilibrium equations are assembled into global nodal equilibrium equation, which can be written as

$$\{F\} = [K]\{d\} \qquad \text{(Equation 3)}$$

where {F} is the vector of global nodal forces, [K] is the structure global stiffness matrix (usually square and symmetric) and {d} is the vector of known and unknown nodal degrees of freedom or generalized displacements. Known loads are included in the nodal force vector. The global stiffness matrix [K] at this stage is a singular matrix. In order to remove the singularity, boundary conditions (BCs) must be added at appropriate areas of the structure. The boundary conditions act as supports or constraints as to remove any rigid body motion. Addition of the BCs results in the modification of the of the global equation, usually the elimination of degrees of freedom.

The purpose of the 6th step is to solve the global equation for d_1, d_2 ... d_n using an elimination method such as Gauss's method, or an iterative method such as the Gauss-Seidel method. The ds are called primary unknowns since they are the first values to be determined using the stiffness finite element method.

The 7th step solves for the element strains and stresses. Important secondary values of strain and stress (or moment and shear force) are obtained easily by using Hooke's Law, as they are directly expressed in relation to the displacements found in Step 6.

The final, 8th step involves the interpretation and analysis of the results. Location of large deformations and large stresses are important in the design phase of the structure and can be determined using a post-processor program.

2.6.1 Gasket Elements

A common approach is to model the MLS gasket is using a single layer of 3D specialized gasket elements and non-linear description of the gasket model behaviour. This approach represents the gasket's material behaviour by using non-linear spring elements based on physical test data. The gasket element geometry is physically linear, however, its built-in behaviour is nonlinear. The two ways to determine the gasket material behaviour are from experimental data or from a 2D gasket FE analysis. The existing residual stresses within the gasket from the forming of the embossments

ensure that a forming analysis should be performed to obtain an accurate emboss geometry and accurate load deflection curves. A second approach is to accurately re-produce every detail of the gasket's physical geometry and assign proper material properties to each region. This approach is characterized by geometric and material non-linearity. These types of analyses are much more complicated and computationally expensive compared to the first approach. [Hibbit, et al, 2010]

Improvements have been made using the gasket elements. It was found that a way to improve gasket modeling to get accurate normal and transverse motion was to model each gasket layer as one-layer gasket elements [Baig, et al, 2007]. These elements were stacked together according to the number of layers in the physical gasket. Since each layer was included, the interlayer shear effects were present during the analysis. This type of stacked gasket element model was found to more accurately predict head gasket normal and shear displacement fields. Also, the results tended to compare well with a secondary model that used continuum elements for the gasket, but required much less CPU time.

MLS gaskets are complicated geometric constructions that are subjected to large compressive strains, in which their response to compression is highly non-linear [Hibbit, et al, 2010]. These complexities make it very difficult and impractical to model the gasket using continuum elements for full engine analysis. ABAQUS code and software uses gasket elements created especially for simulating the complicated gasket behaviours by eliminating the contact issues between layers. The gasket is modeled as a single layer with uniform thickness. All of the important data such as bead locations, material properties and loading curves are built into the gasket model. However, the major deficiency of the single layer model is that it does not consider dynamic behaviour of the system [Popielas, et al, 2000].

The behaviour of the gasket through the thickness of the gasket is difficult to model using traditional continuum elements, therefore, ABAQUS has developed Gasket Elements specifically for studying the behaviour of gaskets. These gasket models assume that the thickness-direction, transverse shear and membrane behaviours are uncoupled. If these assumptions are followed, the gasket behaviour can be defined using a gasket behaviour model. The current Fel-Pro supplied gasket uses this method. For the case in which the behaviours of the gasket are coupled, or tensile stresses are present, a built in or user-defined material model must be used. Gasket behaviour is usually determined by performing a compression test on the physical gasket assembly. The resulting behaviour found with the experiment can be used to model a discretized, single layer of gasket elements.

This type of method makes two assumptions. The first is that the gasket does not possess the same physical properties in all three directions, thus the gasket is modeled using linear elastic material properties in the two in-plane directions and all three shear directions. The second assumption is that Poisson's effect within the gasket is negligible, since the normal strain generates almost no in-plane stress. This is because the user is only interested in the normal stresses in the gasket, which will be the same for any value of Poisson's ratio. The in-plane strain depends on the normal stress, Young's Modulus and Poisson's ratio, but since results are not concerned with in-plane stress results, the value of Poisson's ratio is of little importance. Also, since the gasket is treated as a structure and not a material, under normal loading conditions the layers of the gasket are compressed and brought closer together. The majority of the strain energy is used to bring the layers into contact with one another, therefore very little in-plane stress is sustained [Hebert, et al, 1998].

The geometry of a typical ABAQUS gasket element is shown in Figure 9 below. A gasket element is composed of two faces, a top face and a bottom face, separated by a thickness. Relative motions between the top and bottom faces is the thickness direction behaviour, and is measured along the thickness direction, which is the local 1-direction. This direction is obtained by defining the thickness direction at the integration points. Changes in the relative positions of the top and bottom faces measured in a plane orthogonal to the thickness direction quantify the transverse shear behaviour of the gasket. The planes to define the transverse shear behaviour are the local 1-2 and 1-3 planes. Finally, the shearing and stretching of the midsurface of the element quantifies the membrane behaviour of the element, which is defined in the 2-3 plane. To define the local 2-direction of the 3D gasket element, the tangent to the midsurface is projected onto a plane orthogonal to the local 1-direction. The local 3-direction is obtained by the cross product of the local 1-direction and 2-direction.

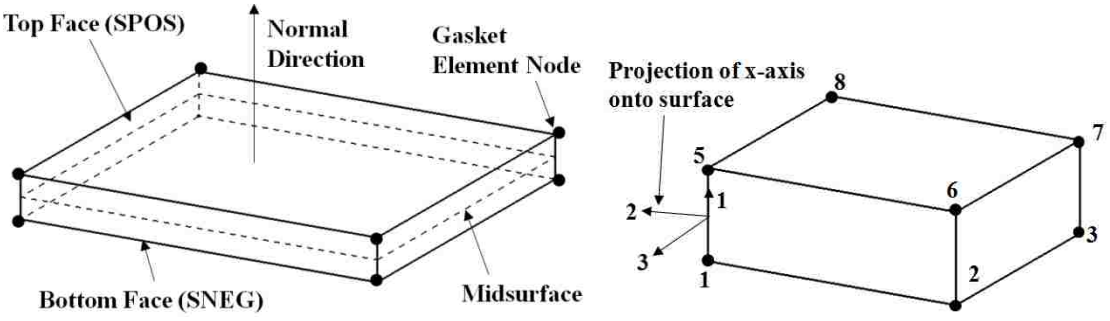

Figure 9: ABAQUS representation of Specialized Gasket Elements

The elements do not have mass, and therefore, no density as well. Within ABAQUS, there are different types of gasket elements. These include; two-dimensional elements, three-dimensional elements, axisymmetric elements, thickness-direction behaviour only elements, and thickness direction, membrane and transverse shear behaviour elements. Gasket elements can be applied to static, static perturbation, quasi-static, dynamic and frequency analyses.

For the general gasket element, there are two classes of gasket elements. The first class allows for the gasket nodes to have all degrees of freedom active. This type is necessary when the membrane and/or transverse shear behaviour is of importance, as well as the thickness direction behaviour. The three behaviours are defined as uncoupled behaviours only. It is also possible to model the gasket with only thickness-direction and transverse shear behaviours, if needed. The second class of gasket element is able to measure deformation in the thickness direction only. The two other deformation modes are not included. The nodes of this gasket element have only one degree of freedom in the thickness direction of the gasket. In these elements, frictional forces cannot be transmitted, and thermal expansion or stretching is not accounted for. The three modes of gasket behaviour are shown in Figure 10.

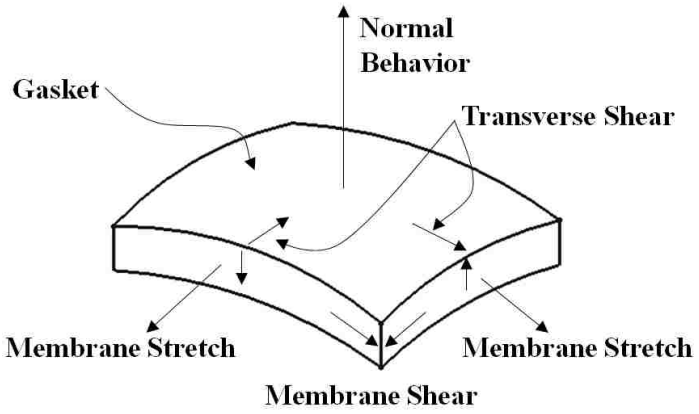

Figure 10: Gasket Element showing three uncoupled behaviours

When assembling a gasket model into an engine assembly, the easiest method is to have the gasket nodes share the nodes with the other elements adjacent to them. However, generally the meshes are not connected using the same nodes, so contact pairs must be used for these cases. The gasket material behaviour is usually much softer than the adjacent engine material, and the discretization of the gasket is usually much finer. Because of these facts, the slave surfaces should be on the gasket and the master surfaces should be on the head or block deck face. In this case,

mismatched meshes can result in inaccurate pressure distribution at the gasket and deck faces. For this reason, it is important to have similar sized elements at the adjacent faces.

2.6.2 Shell Element Theory

Shell elements are generally used to model structures in which one dimension is significantly smaller than the other two dimensions. This is the case for a layer of a gasket, which is an extremely thin sheet of metal. ABAQUS uses two different types of Shell elements; Conventional and Continuum [Hibbit, et al, 2010].

For a Conventional shell element, the geometry is represented by a reference surface whose thickness is defined by a section property. The elements are discretized over the surface. These elements have displacement and rotational degrees of freedom. The elements use linear or quadratic interpolation and allow mechanical and/or thermal (uncoupled) loading. They can be used in static or dynamic procedures. Depending on the type of Conventional element, the effect of transverse shear deformation and thickness change may or may not be included. Also, some elements allow for large rotations and finite membrane strain, while others allow for large rotations but small strains. For a gasket assembly in compression, there will be large displacements, rotations and finite membrane strains, therefore it is necessary to choose an element with these compatibilities. An important factor in choosing the appropriate element regards the transverse shear deformation. General-purpose conventional shell elements use thick shell theory as the thickness increases, but become thin shell elements as the thickness decreases. For conventional shells, stress in the thickness direction is zero and strain results only from the Poisson's effect. [Hibbit, et al, 2010]

In contrast, Continuum Shell elements are based off of an entire three-dimensional body. The thickness is determined by the geometry of the part and only contain displacement degrees of freedom. Continuum elements therefore look like a three-dimensional continuum solid, however behave similar to a conventional shell element. They use linear interpolation and allow mechanical and/or thermal (uncoupled) loading for static and dynamic procedures. Continuum shell elements are used for general purpose analyses that allow for finite deformation and large rotations. These elements are therefore suitable for nonlinear geometric analyses. Continuum shell elements allow for stress in the thickness direction which may cause additional strain than that due to Poisson's strain.

2.6.3 Axisymmetric Shell Element Theory

Axisymmetric elements are used to model structures which have a geometry which is rotated about an axis and is under axially symmetric loading conditions. This type of analysis is best described using cylindrical coordinates r, z and θ. This type of analysis can be used to gain insight into a single cylinder engine model. Although normally, a gasket is not a true axisymmetric structure, the analysis can be used to gain insight into what occurs between gasket layers during cold clamping. Since only cross sections of the gasket are taken at pre-determined locations, the analyses are very computational friendly and can usually be completed without the use of a powerful server. The ABAQUS axisymmetric element layout is shown in Figure 11 [Hibbit, et al, 2010].

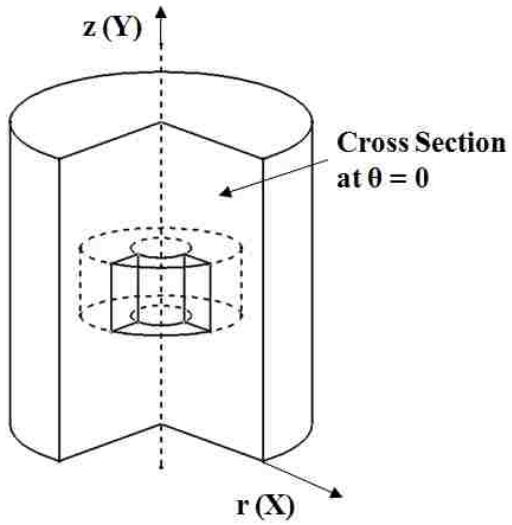

Figure 11: Representation of Axisymmetric Element

2.7 Fuji Pressure Sensing Film

Fuji Film is composed of mylar material that contains a tiny layer of microcapsules. When a force is applied to the film, the microcapsules rupture, which produces an instantaneous and permanent high resolution topographical image of pressure variation across the contact area. The greater the pressure, the more intense the color of the area. The film is from 4 to 8 mils thick (0.004-0.008mm) which allows it to conform to curved surfaces. Pressure ranges of the film are from extremely low (7.2-28 PSI) to Super High (18,500 psi to 43,200 psi). Spatial resolution of the film is 5 to 15 microns and has a ±10% visual accuracy and a ±2% accuracy when used with an optical measurement system. [www.spareonweb.com, 2013]

Chapter 3: Scope of Research

The most important passive seal of the engine is the head gasket, which sits pressed between the head and block of most engine assemblies. As discussed earlier, the engine head gasket must perform multiple duties, such as providing a mechanical seal between the engine head and block that can withstand the fluctuating internal pressure within the cylinder, and providing a seal for which engine coolant and oil can freely flow between the structures. In order for these duties to be realized, there must always exist a certain level of pressures at the interface. Due to the complexity of the engine head and block, the pressure distribution is not easily determined by calculations and fluctuates as the internal pressures and temperature of the assembly changes. The Finite Element Method is a powerful tool that can be used by the engine designer to gain insight into engine performance at the design level. No matter what the purpose of the piece, all engine parts are designed using FEA throughout their life cycle.

The purpose of this study was to look at the various techniques used in industry in order to develop a method (or methods) that can be used by the engine design team in order to quickly obtain accurate results at the head gasket interface. A 5 month work term was completed at FIAT, in Torino Italy, and simulations were run at ARDC in Windsor, Ontario, which consisted of research and development of various computer models and FEA Head Gaskets. The goal was to research the many different techniques for gasket analysis and to correlate FEA model results with physical test results obtained using Fuji Paper in order to improve the accuracy of the CAD knowledgebase. With the knowledge and experience gained, future failure modes will be decreased due to increased accuracy of studies. The implementation of the design should help to reduce project costs due to the reduction in testing times for new engine designs.

Completing an entire Finite Element Analysis on a full engine is a time consuming process that must undergo many iterations and increments in order to complete. Basic ideal gas law calculations were completed in order to gain an understanding of engine operations. Due to the complexity of the problem and lack of experience of the student, the analyses were completed in stages of increasing scale and complexity. The 2D axisymmetric analyses were a starting point for the simulations. A single cylinder simulation was the next logical step, as it would allow for easy changes of the model setup and minimal computational time. The single cylinder consisted of an assembly made up of a quarter gasket, head and block a such that only one cylinder was analyzed. Once these simulations were completed, the Full Bank simulation was created and used to observe the results on all cylinders of one side of the engine. The full bank consisted of the full

gasket, head and studs and a half model of the engine block with a thermal map applied. Both engine banks were eventually modeled. A summary of each analysis is as follows:

- Series 1: Axisymmetric assembly using 2D Axisymmetric Elements under cold clamping conditions
- Series 2: Single cylinder 3D model using Gasket Elements, Conventional Shell Elements, Continuum Shell Elements and 3D Solid Elements under cold clamp conditions
- Series 3: Full bank 3D model using Gasket Elements under cold clamping, cold firing, hot clamping and hot firing conditions.

Overviews are given at the beginning of each Series which describe in detail the differences between the simulations. Any analysis that uses gasket elements are based on the gasket element model supplied by the gasket manufacturer.

Chapter 4: Methodology

4.1 Ideal Gas Law Calculations

A simple, yet useful step during engine analysis to complete calculations involving ideal gas laws of the Otto cycle. The calculated pressures can be used to compare to the experimental values provided by Penske Racing. The engine data was taken from a dyno run of the engine and corresponds to maximum RPM of 9000. The raw data provided is shown in Appendix B.

If air standard assumptions are made, the ideal Otto cycle laws can be utilized. This cycle consists of four internally reversible processes:

1-2 Isentropic compression

2-3 Constant-volume heat addition

3-4 Isentropic expansion

4-1 Constant-volume heat rejection

The ideal gas law calculations were taken from [Stone, 1985] and [Cengel, 2002]. They focused on finding the pressures in the cylinders based on the engine geometry. The architecture of the engine is shown in Table 1 below. The parameters are based off of CAD data and NASCAR rulings.

Engine	Dodge NASCAR Engine
Layout	V8: 90° Bank Angle
Displacement (cm^3)	5867
Compressions Ratio	12:1
Bore (mm)	106.3
Stroke (mm)	82.63
Displacement, 1 cyl (cm3)	733.375
Comb Chamber Vol. (cm^3)	66.66
Maxium RPM	9000

Table 1: Engine Data

The efficiency of the Otto cycle, η_{OTTO}, is based on compression ratio of the engine, r_v, and the ratio of specific heat capacities, k. From [Stone], Equation 4 was used to determine the efficiency. k is assumed to be 1.4.

$$\eta_{OTTO} = 1 - \frac{1}{r_v^{k-1}} \qquad \text{(Equation 4)}$$

No work is involved during the two heat transfer processes since both take place at constant volume. Thus, heat transfer to and from the working fluid is expressed by:

$$\boldsymbol{q_{in} = u_3 - u_2} \qquad \text{(Equation 5)}$$

$$\boldsymbol{q_{out} = u_4 - u_1} \qquad \text{(Equation 6)}$$

where q is the heat transfer per unit mass and u is the specific internal energy. Processes 1-2 and 3-4 are isentropic, with $v_2=v_3$ and $v_4=v_1$. Thus,

$$\frac{T1}{T2} = \left(\frac{v2}{v1}\right)^{k-1} = \left(\frac{v3}{v4}\right)^{k-1} = \frac{T4}{T3} \qquad \text{(Equation 7)}$$

and,

$$\frac{P_2 v_2}{T_2} = \frac{P_1 v_1}{T_1} \qquad \text{(Equation 8)}$$

A cyclic analysis was completed using the engine parameters and equations. Table A-17 from [Cengel, 2002] was used to determine the air properties. The heat capacity at constant volume between stages 2 and 3 was found using by taking the mean between the two values. The results are shown in Table 2 below.

η_{OTTO}	62.99%		v_{r2}	56.34
AFR (assumed)	14		T_2 (K)	755.00
ρ_{AIR} (kg/m^3)	1.18		u_2 (kJ/kg)	548.00
m_{AIR} (kg)	8.65E-04		P_2 (kPa)	3124.14
m_{FUEL} (kg)	6.18E-05		q_{23} (kJ/kg)	3378.57
HCV_{FUEL} (kJ/kg)	47300.00		Q_{IN} (kJ)	2.92
cp (kJ/kg K)	1.01		T_3 (K)	3570.48
$cv_{mean\ 2,3}$ (kJ/kg K)	1.12		P_3 (kPa)	14774.38
P_1 (kPa)	100		T_4 (K)	1368.18
T_1 (k)	290		P_4 (kPa)	5661.42
u_1 (kJ/kg)	206.91		u_4 (kJ/kg)	1080.00
v_{r1}	676.1		q_{14} (kJ/kg)	873.09

Table 2: Ideal Gas Law Results

The purpose of the preceding study was to determine the theoretical maximum pressure in the cylinders. From the experimental data completed by Penske, the maximum cylinder pressure was 9.59MPa. The calculations give a maximum pressure of 14.8MPa. This is expected as ideal gas law calculation tend to give higher results than real-world results.

4.2 Gasket Layout

When analyzing a gasket assembly, it is important to establish a logical visual representation. Since various parameters are to be studied around the circumference of the cylinder, it makes sense to look at the gasket from the top view. For the entire study of the right bank of the engine, results and discussion will follow the layout of Figure 12 below. The pressures discussed refer to the pressure on the gasket beads and not on the in-cylinder pressures.

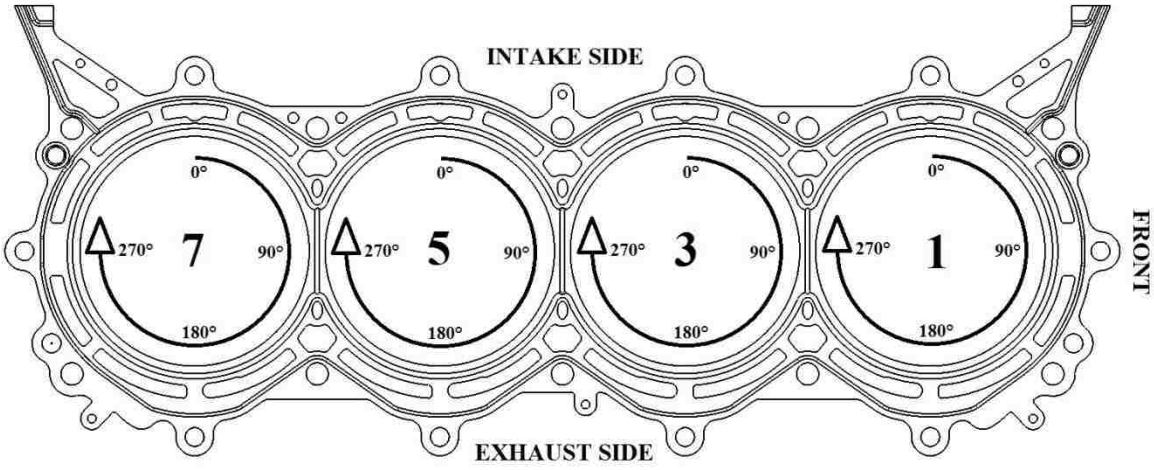

Figure 12: Top view and layout of the gasket to be used throughout report

4.3 Series 1: Axisymmetric Gasket Analysis

The Axisymmetric Method focused on single areas of the multilayered gasket during the cold clamping case. The main purpose of this procedure is to determine the gasket deflection and stresses at certain cross sections of the gasket assembly, without having to complete a full 3D analysis. Any axisymmetric FEA analysis assumes that the assembly is completely symmetric about its axis. Although there are single cylinder engines that might be axis symmetric, it is unlikely that a 3 or 4 cylinder engine bank would be completely symmetric in the geometric sense. However, cross sections about the cylinder axis can be taken at different degrees and simple analyses can be completed to give a detailed insight into the gasket behaviour during compression. The axis symmetric tests are relatively efficient compared to a full cylinder or bank analysis and can be completed on a personal computer, without the need for a large server. The proceeding method discusses the procedure to complete an Axis symmetric analysis using Catia V5 and ABAQUS 6.10. Other CAD and FEA programs should be suitable as well, and the methods should be similar. Since the head and block are modeled as rigid elements, there is no information regarding block or deck deformation.

4.3.1 Axisymmetric Procedure

The first step is to decide which cross sections of the gasket are to be analyzed. These can be based on known areas of high gasket stresses, previous gasket problems or near the head bolts. It is up to the analyst to decide how many tests will be completed. The entire method must be repeated for each cross section. Knowing that there are failures of the current gasket on the Cylinder 5 locations, it was decided to solely focus on this location for the analysis. It was decided to complete the simulation at the 0°, 90° and 180° locations. The cross section are shown in Figure 13.

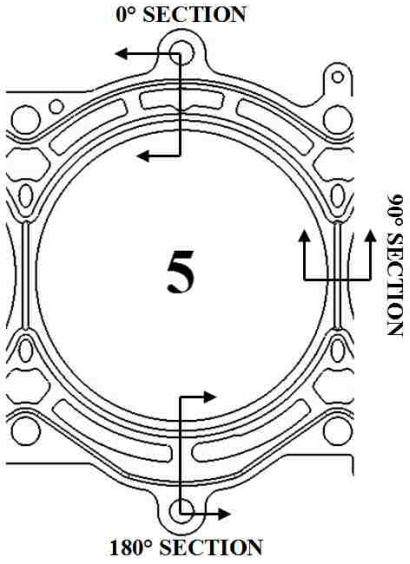

Figure 13: Sections used for the Axisymmetric analysis

ABAQUS requires that for all Axisymmetric Analyses, the cross section of the assembly must be located in the XY Plane, and only have geometry in the positive X position. This requires that the geometry of the section to be analyzed must be translated and rotated in the CAD program, so that it matches the ABAQUS requirement.

Using Catia V5, cross sections were cut at the desired gasket locations. The full gasket was supplied as a .stp or.iges CAD file, both of which are not native to Catia. Upon importing the files into Catia, the gasket was composed of thousands of individual surfaces that compose the entire gasket. It was possible to separate the gasket layers into corresponding geometrical sets, so this was done to keep the layers organized. Geometric sets were created for each cross sectional areas to be analyzed. For example, Section 90° was analyzed, so a geometric set entitled "Geometric Set- 90deg" was created.

An axis system was then inserted at the centre of each cylinder. The planes of the axis system and ones created at angles of the axis system were used to cut the cross sections of the gasket at the appropriate angles. The sections of the gasket were cut using the appropriate planes. Detached areas due to bolt holes can be ignored, as these areas are generally not compressed between the head and the block. The same procedure was completed for all of the gasket layers and the fire ring. As was mentioned before, ABAQUS only allows Axisymmetric analyses to be done when the surfaces of the assembly are contained in the XY Plane and in the positive X coordinate. Therefore, it was necessary to translate and rotate the newly created surfaces to the proper orientation, which is dependent on the original global axis. The gasket cross section assembly was first rotated about the appropriate axis in order to make it parallel with the appropriate axis. A second rotation was required in order to ensure that the cross section is in the positive X quadrant. Finally, a translation might was needed in order to ensure that the cross section was on the XY plane. The sections were "filled" in order to create the shell of the gasket assembly. The result was five 2D surfaces representing each layer of the gasket and the fire ring. The file was saved as a native Catia file. Only the needed surfaces must be shown, so all other surfaces should be hidden. The surfaces in Catia are shown in Figure 14.

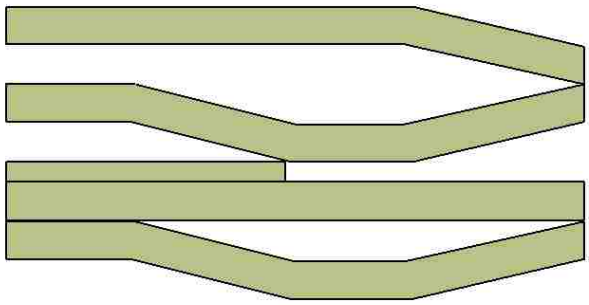

Figure 14: Surfaces of cross sections in Catia

In ABAQUS, the surfaces were now able to be imported. The Catia file was imported as a shell in Axisymmetric modeling space. Initially, ABAQUS was unable to properly import the files as an axisymmetric case, as the layers were not in the proper orientation. Once completed, the layers were imported into the ABAQUS assembly model.

A secondary head was created as a rigid shell. This enabled a concentrated force to be applied to the head, that would be distributed equally about the deformable head. References are required for rigid bodies. This was placed at the midpoint of the head. The assembly in the ABAQUS is shown

in Figure 15. The process was repeated for the locations at 0° and 180° and are shown below in Figure 16.

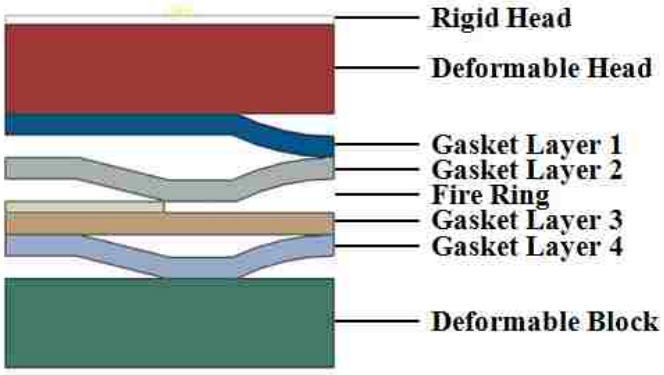

Figure 15: Axisymmetric Assembly of 90° Section in ABAQUS

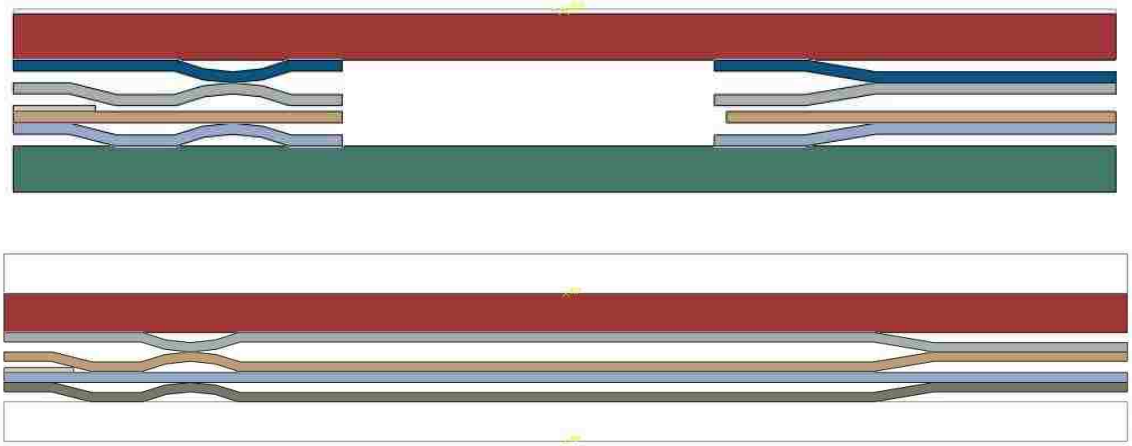

Figure 16: Axisymmetric Assembly of 0° Section (top) and 180° Section in ABAQUS

4.3.2 Axisymmetric Interactions and Constraints

The simulation has many different layers coming into contact at various times throughout the analysis. It was important to properly define interactions and constraints between each of the layers to ensure convergence. The interactions and constraint used between the gasket layers, fire ring, head and block are shown in Table 2. Since the fire ring is laser welded to the gasket layer, it was assumed that it was completely constrained to its corresponding layer. Friction numbers were based on values provided by the gasket manufacturer.

Type	Master	Slave	Type	Friction Coeff
Interaction	Deformable Head	Gasket Layer 1	Finite Sliding, Surf to Surf	0.15
Interaction	Gasket Layer 1	Gasket Layer 2	Finite Sliding, Surf to Surf	0.15
Interaction	Gasket Layer 2	Gasket Layer 3	Finite Sliding, Surf to Surf	0.15
Interaction	Gasket Layer 3	Gasket Layer 4	Finite Sliding, Surf to Surf	0.15
Interaction	Deformable Block	Gasket Layer 4	Finite Sliding, Surf to Surf	0.15
Interaction	Gasket Layer 2	Fire Ring	Finite Sliding, Surf to Surf	0.15
Tie Constraint	Rigid Head	Deformable Head		
Tie Constraint	Layer 3	Fire Ring		

Table 3: Interactions and Constraints used in the Axisymmetric analysis

4.3.3 Axisymmetric Mesh and Materials

The mesh of the layers must be detailed enough to accurately predict the behaviour of the real world gasket, but large enough as to be computationally efficient. Since gasket layers are relatively thin, the seed size should be small enough to represent this feature. A seed size of 0.05mm was used for each layer. The element type used was a CAX4R, which is a 4-node bilinear axisymmetric quadrilateral, reduced integration, hourglass control. Linear elements must be used when contact is an issue, as is the case for a MLS gasket [Hibbit, et al, 2010].

From the gasket supplier, it was determined that the gasket layers are comprised of 301 stainless steel and the fire rings are composed of 304 stainless steel. The elastic and plastic properties of the stainless steel gasket layers were defined within the material properties box. The true stress-true strain data was determined from [Olsson, 2001] and shown below. The stress strain properties are shown in Figure 17.

Part	Material	Modulus of Elasticity (Mpa)	Poisson's Ratio	Elasticity
Rigid Head	None	N/A	N/A	N/A
Deformable Head	Aluminum	71000	0.3	No
Deformable Block	Cast Iron	130000	0.26	No
Gasket Layer 1	Stainless Steel 301	193000	0.28	Graph
Gasket Layer 2	Stainless Steel 301	193000	0.28	Graph
Gasket Layer 3	Stainless Steel 301	193000	0.28	Graph
Gasket Layer 4	Stainless Steel 301	193000	0.28	Graph
Fire Ring	Stainless Steel 304	193000	0.28	No

Table 4: Material information used for the axisymmetric analysis

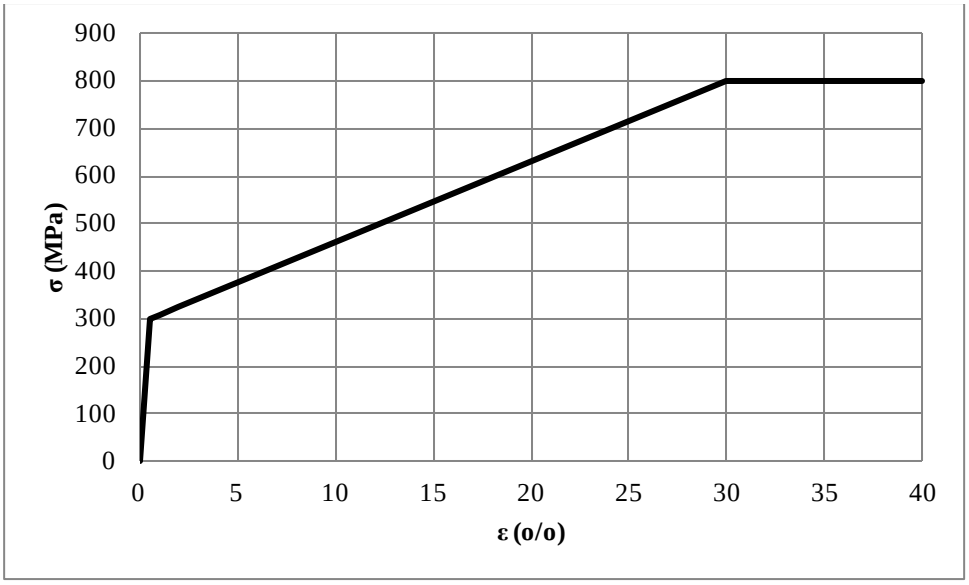

Figure 17: True stress-true strain data used for the analysis.

4.3.4 Axisymmetric Loading Conditions

The loading of the entire assembly is based on the bolt loads of the entire 3 dimensional engine. In order to obtain the required load on the axisymmetric head, a calculation must be completed. From [Popielas et al, 2000],

- Load = [Number of bolts/Cylinder * Bolt load per bolt] * 50 % for gasoline engines
- Load = [Number of bolts/Cylinder * Bolt load per bolt] * 75 % for heavy-duty engines

It was assumed that the engine is a heavy-duty engine of a high performance nature, so the75% of the bolt load option was chosen. The NASCAR engine uses different sized bolts with different corresponding bolt forces, so this must be taken into account while completing the loading. Also, for this loading case, it is assumed that the load is constant around the entire circumference of the cylinder bore. This is not the case for a real world engine, which typically will have higher forces near the bolts and lower forces in areas far from the bolts. Symmetry of the bolts was taken into account as well, which reduced the overall bolt force. The calculated force was found to be 180,000N and was located at the reference point of the rigid head.

The block was given full encastre boundary condition and the head was constrained so it is only able to displace in the vertical direction.

4.3.5 Convergence and Contact Controls

Convergence is generally a problem with highly non-linear problems in ABAQUS. There are certain techniques that can be applied in ABAQUS that will allow the simulation to reach convergence. Automatic stabilization should be activated within the Edit Step dialog box, under the basic tab. There are three stabilization options that can be used; Specify dissipated energy fraction, specify damping factor, use damping factors from previous general step. The Specify dissipated energy fraction was used with a value of 0.0002. Also, under the Other tab of the Edit Step dialog box, there are three options for Convert severe discontinuity iterations; Off, On and Propagate from previous step.

As a final resort, if the analysis still fails to converge, General Solution Controls can be used to alter various convergence criteria. If the simulation fails to converge with the default controls or uses an excessive number of increments and iterations, these parameters can be altered to "loosen" the ABAQUS convergence requirements. Under the Step module in ABAQUS, under Other, select General Solutions Controls and edit it for the appropriate step. Here, various step parameters can be edited from the default values. If the simulation is unable to converge due to many Severe Contact Iterations and chattering (points switching from open to closed during iterations). These numbers can be altered to force convergence.

For a nonlinear analysis in ABAQUS to be solved, the governing balance equations must be solved iteratively. In most analysis cases, ABAQUS /Standard uses Newton's method to solve nonlinear problems. In some cases it uses an exact implementation of Newton's method, in the sense that the Jacobian of the system is defined exactly, and quadratic convergence is obtained when the estimate of the solution is within the radius of convergence of the algorithm [Hibbit, et al, 2010]. A multi layer gasket being compressed will exhibit discontinuous behaviour, as the layers are coming into contact at varying points through the analysis. For contact, the contact is either present or absent. Also, there might exist strain reversal in plasticity a the gasket regions where the material is yielding.

A common warning in the message file for the gasket clamping case is regarding severe discontinuity iterations (SDIs). SDIs occur when abrupt changes in stiffness occur and are distinguished from regular, equilibrium iterations, in which the solution varies smoothly. During an analysis with default settings, ABAQUS /Standard will continue to iterate until the SDIs are sufficiently small (or completely eliminated) and the equilibrium (flux) tolerances are satisfied. This method can cause convergence difficulties where the contacts are only weakly determined,

and contact "chattering" occurs or if a large number of SDIs are required to settle the contact conditions.

From [Hibbit, et al, 2010], "By default, Abaqus applies sophisticated criteria involving changes in penetration, changes in the residual force, and the number of severe discontinuities from one iteration to the next to determine whether iteration should be continued or terminated. Hence, it is in principle not necessary to limit the number of severe discontinuity iterations. This makes it possible to run contact problems that require large numbers of contact changes without having to change the control parameters. It is still possible to set a limit, I_S^c, for the maximum number of severe discontinuity iterations; by default, $I_S^c = 50$, which in practice should always be more than the actual number of iterations in an increment."

4.4 Series 2: Single Cylinder Model with Varying Gasket Representation

Series 2 was dedicated to the study of a single cylinder of the engine using various gasket element types, element sizes and interaction properties. It's main purpose was to gain an understanding of the many ABAQUS parameters in a small scale test, before attempting the full bank analysis. The entire series was completed in three parts, all of which use Cylinder 5;

- Effects of the Interaction Properties at the engine head, block and gasket interfaces
- Effects of altering the deck interface mesh sizes and types
- Effects of using different elements types for the gasket assembly; Shell elements, 3D elements.

4.4.1 Procedure and Mesh

Using the original CAD of the engine, sections were cut such that only the solid section of Cylinder 5 remained. The studs along the axis of symmetry were cut in half as well. To reduce geometric complexity, the cam cover volume of the block was eliminated. Once altered, the individual parts were imported into the ABAQUS 6.10 software as solid step (.stp) parts and were assembled using the proper constraints.

Meshing of a complicated assembly in ABAQUS is not a simple process, especially for large, complex structures such as an engine. There are many tools available within ABAQUS that help the user apply a mesh, however the meshing of both the Quarter Model and Full Model was an extremely time consuming process. There was no direct procedure that was followed to mesh the assembly; it was simply a matter of trial and error using different procedures and techniques. Instances occurred in which ABAQUS would not allow a volume to be meshed and give no

explanation as to why the mesh had failed. There is no correct or incorrect procedure for meshing a complex part, rather individual techniques that can be applied to help simplify the process. Experience of the user is the greatest tool that can be applied during the meshing phase. An entire report could be written on the meshing techniques alone, thus only the major techniques will be discussed.

The first step before any meshing could take place was the simplification of the geometry in the Catia V5 program. Since the Single Cylinder Analysis was simply a test of the methods, much of the complicated geometry could be removed from the model. Areas such as the Block crankshaft area, camshaft tunnel and stiffening webs were eliminated. In order to simplify the analysis and reduce errors, the stud assemblies consisting of the stud, nut and washer/sleeve were combined into a single part, and further simplified to give a solid cylindrical volume. The studs were cut in half, lengthwise, in order to use symmetry in the assembly. Also, to eliminate the interference caused by thread overlap, the threaded sections of the bolts were reduced in diameter. Once complete, each part was exported as a step model. Within ABAQUS CAE, the Virtual Topology Combine/Ignore Entities tool was used on all parts. The entire surface was selected for each individual part, and the tool was applied. The purpose of this tool is to eliminate the majority of "soft" edges on a part. Since ABAQUS applies seeds to every edge that it finds, a part with a large amount of edges will result in meshing complications. This method greatly reduced meshing complications that initially arose due to the complexity of the Head and Block geometries. After the entities were ignored, a small group had to be restored using the Virtual Topology Restore Entities tool. The purpose of this was to restore certain flat surfaces that are required to apply the loads, boundary conditions, interactions and constraints. ABAQUS uses the geometric faces of the part to apply these features, where other FEA software will use the mesh. It was important to do all of the geometry simplification before the part was meshed, as any changes after the mesh was applied would result in an automatic deletion of the mesh.

The mesh of the single cylinder assembly is composed of varying sizes, shapes and types of elements. The main focus of the analysis is the interaction at the gasket-head and gasket-block interface. Thus, in order to reduce processing time, the elements are increased in size as they move away from the deck. The head and block are partitioned to yield 3 separate volumes for each component. The partition depth from the deck face is 1mm for Sections A and D. The partition depth from the deck face is 20mm from sections B and E. The remaining volumes are labeled C and F and contain the bulk of the geometry. Figure 5.2 shows the partition regions. On the right is the zoomed in deck surface. One factor that was explored in the following analyses is

the size and type of element and depth of partition at the deck. Various combinations were experimented with and the results compared. The interaction study used a single layer of 1mm elements, where the mesh study alters the size and number of layers. It is of importance to note that between partitioned regions of a solid, ABAQUS automatically introduces tied constraints between the adjacent elements. Before applying the 3D tetrahedral mesh to the full assembly, each partition was given a 2D triangular mesh by checking the "Preview Boundary Mesh." The purpose of this to check if there were any problems with the surfaces. If there were problems, they were eliminated by using the previously described Virtual Topology techniques. Once all of the partitions contained a boundary mesh, the tetrahedral mesh could be applied, one cell at a time. Often, attempting to apply the 3D mesh would result in errors at one or more elements. In order to fix the problems, the Edit Mesh command was used. The Edit Mesh command allows the user to edit various mesh parameters, such as node location, element edge deletion or addition, and the collapse edge feature, which was used extensively throughout the meshing process. In order to properly subject the bolts to pre-tension loads, partitions must be created at the mid-sections of the studs, shown in Figure 18. This must be completed before the meshing.

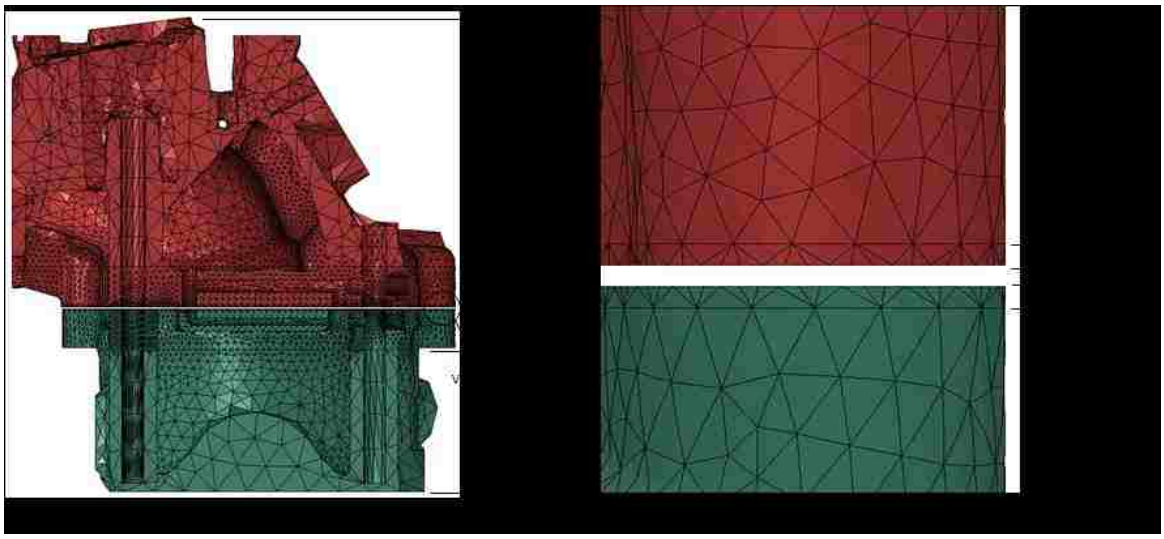

Figure 18: Partition Regions of single cylinder assembly

A summary of the mesh parameters that are used for the first section of the analysis are shown in Table 4. For these simulations, the mesh remained constant while only the interactions were altered. Note that the Assembly Node and Element totals are not equal to the sums of the rows, as there are 6 studs used in the assembly with varying sizes.

						Totals	
Part Name	**Partition**	**Element Name**	**Element Type**	**Size (mm)**	**No. of Elements**	**Nodes**	**Elements**
R6P8 Head	A	Quadratic Tet	C3D10	1	41848	276748	253440
	B	Quadratic Tet	C3D10	3	120634		
	C	Linear Tet	C3D4	14	90958		
R6P8 Block	D	Quadratic Tet	C3D10	1	25196	152618	108720
	E	Quadratic Tet	C3D10	3	63410		
	F	Linear Tet	C3D4	14	20114		
Stud, Long	All	Linear Tet	C3D4	5	1486	523	1486
Gasket	All	Linear Hex	GK3D8	1	6453	14814	6847
		Linear Wedge	GK3D6	1	394		
Assembly						**447134**	**378435**

Table 5: Mesh Information Summary for the Quarter Bank Analyses

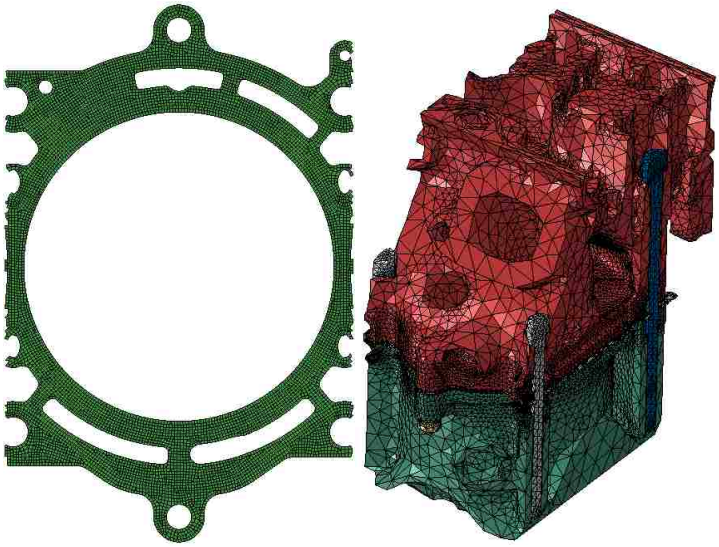

Figure 19: Mesh of the gasket (left) and mesh of the Quarter Bank Model (right).

4.4.2 Single Cylinder Materials

The Gasket Element single layer model is composed of different areas which represent different sections of the physical gasket. The input file for the entire gasket model is supplied by Fel-Pro, the gasket manufacturer. The main areas of concern for the analyses were with the Stop, Flexstop and Fullbead sections. These are shown in Figure 20 below.

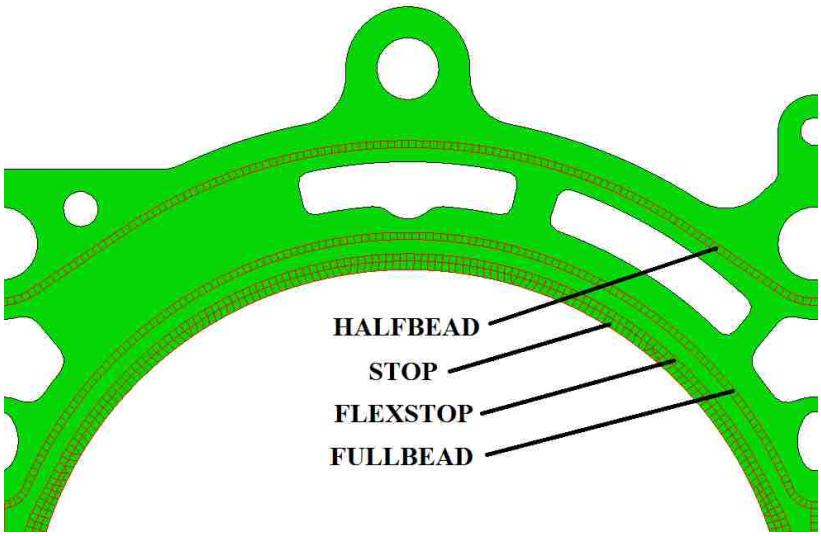

Figure 20: Location of Bead profiles in gasket composed of Gasket Elements

Each component had a material supplied, which is summarized in Table 5 below. Due to the complicated nature of a MLS gasket, the model supplied by FelPro has in depth properties such as thermal expansion, shear stiffness, loading/unloading behaviour, etc. These properties are contained within the input file of the gasket. The non-linear geometry of the gasket, along with material entering into plastic deformation during loading, results in non-linear loading and unloading curves. The curves are shown in Figure 21. Note that the peak for the Body and Stop curve is not shown, but has a value of 950MPa at 0.00889mm of closure.

Part Name	Material Name	Material Behaviours	Young's Modulus (MPa)	Poisson's Ratio
R6P8 Head	Aluminum	Elastic	71000	0.33
R6P8 Block	Grey Cast Iron		130000	0.26
Studs	Steel		200000	0.28
Gasket	BODY+ STOP	Gasket Membrane Elastic	1000	0.3
	FULLBEAD		1000	0.3
	HALF10		1000	0.3
	HALF15		1000	0.3

Table 6: Material Properties used in the Single Cylinder Model

Figure 21: Loading/Unloading curves of Gasket Sections. Note the high stiffness curve of the BODY + STOP which continues above the chart

4.4.3 Single Cylinder Steps

The Single Cylinder analysis included two Steps; Initial and Head Bolt Loading. The Initial Step (which is a default step required by ABAQUS CAE) applies the boundary constraints, interactions and contact constraints. The Head Bolt Loading Step applies the tightening force to each of the 6 studs.

4.4.4 Single Cylinder Constraints

There are 6 Tie constraints between the threads of the studs and their corresponding surfaces, as shown in Figure 5.4. The master surfaces are the tapped thread areas and the slave surfaces are the stud thread areas. There is a positional tolerance of 0.8mm for the short bolt threads. Also for the small studs, the head faces are tied to their corresponding counter bores. The reason for using tie constraints at the short stud heads was due to the detection of singularities in some of the early simulations, which caused the analysis to diverge.

4.4.5 Single Cylinder Loading Conditions

The pre-tension in the studs was created using the method outlined in the ABAQUS User's Manual Section 21.2. A partition was created during the meshing phase at each of the studs as is required by the Bolt Load command in ABAQUS. The pre-tension on each stud was set to 60,700N. Due to the symmetry of the Long and Medium studs, this amount was halved for these particular instances, resulting in a pre-tension of 30,350N. The direction of the load was applied along the axis of the studs and the side for the shell or internal faces was chosen to be towards the head of the stud. The Short Studs were given a full load of 33,360N. Figure 22 shows the naming convention for the three studs used throughout the analyses.

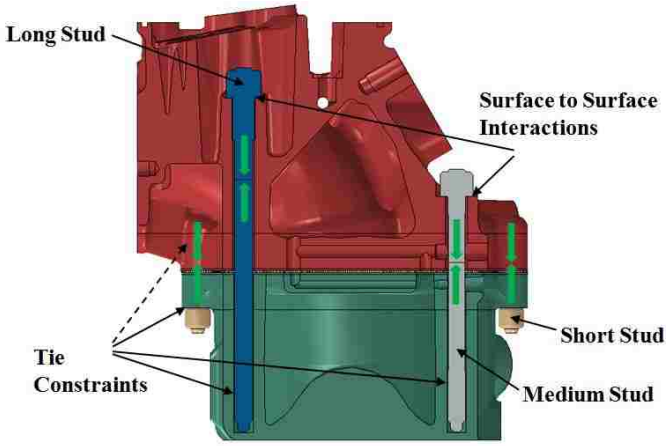

Figure 22: Stud Labels, Interactions, Constraints and Loading conditions. The bolt load tensions are shown by the green arrows.

4.4.6 Single Cylinder Boundary Conditions

The first Boundary condition was named "Fixed Block" and is of the type "Symmetry/Antisymmetry/Encastre." The bottom surface of the Block was constrained using the ENCASTRE option, which removes all 6 DoF from part Region. The second Boundary Condition was named "Symmetry" and uses the XASYMM option to create symmetry constraints on the Block, Heads, Studs, and Gasket at their cut surfaces.

4.4.7 Single Cylinder Field Output Requests

The following Field Output Requests were enabled for the analyses:

Stresses: S (Stress components and invariants)

Strains: E (Total strain components)

Displacement/Velocity/Acceleration: U (Translations and rotations)

Forces/Reactions: RF (Reaction forces and moments), NFORC (Nodal forces due to element stresses)

Contact: CSTRESS (Contact stresses), CDISP (Contact displacements), CFORCE (Contact force)

Energy: ENER, All energy magnitudes

It is important to note that E11 is not the Gasket Strain. Since a Gasket behavioral model is being used for the Analysis, the E11 value refers to the closure. A description is shown in the Three-Dimensional gasket element Library, Section 29.6.8 of the ABAQUS Manual.

4.4.8 Single Cylinder Interactions and Properties

Interactions at the contacting surfaces of an assembly analysis play an important role in the simulation. As the surfaces of the gasket, head and block come into contact under pressure, how the contacts interact with each other are based off of the Interactions and their properties. ABAQUS contains a large number of Interactions and properties, therefore many different combinations of the properties exist. The various Interactions and Interaction Properties were altered independently and the results compared with a basis model.

The major focus of the first set of analyses was to alter the Interactions and Interaction Properties at the Gasket/Head interface and the Gasket/Block interface in order to understand the consequences. Interactions at various surface interfaces are important to the full simulation and slight alterations can have major effects on how the analysis is handled by the Solver. This Section will give a brief description of each of the interaction parameters as discussed in the

ABAQUS Manual. The corresponding sections of the ABAQUS User's Manual are displayed in brackets.

4.4.8.1 Sliding Formulation (Tracking Approach)

The sliding formulation, also known as the tracking approach, has a considerable impact on how two surfaces in contact will interact during an analysis. ABAQUS /Standard uses two different tracking approaches to account for the relative motion of two interacting surfaces in a mechanical contact analysis; Finite Sliding and Small Sliding [34.1.1]. Finite Sliding is the most general tracking approach and allows for any arbitrary motion of the two interacting surfaces, including arbitrary rotation, sliding and finite amplitude. For this tracking approach, the contact connectivity of the currently active contact constraints changes upon relative tangential motion of the two contacting surfaces. Small Sliding assumes that although the overall assembly may undergo large deformations, there is relatively little sliding between the two surfaces in contact. It is based on linearized approximations of the master surface per constraint. For this tracking approach, the groups of nodes involved with the contact constraint are fixed throughout the analysis. The active/inactive status of the nodes can change during the analysis. This tracking approach should be used when approximations are reasonable, due to the computational savings and added robustness.

The ABAQUS Manual recommends that contacting surfaces of the gasket should be the Slave Surface and the corresponding contacting surfaces should be the Master Surfaces [29.6.3]. For the example problem entitled Coolant Manifold Cover Gasket Joint [5.1.4], the simulation uses the Small sliding contact condition for each of the contact pairs.

4.4.8.2 Contact Discretization Method

In order to simulate contact conditions, ABAQUS /Standard applies conditional constraints at various locations on two interacting surfaces. The conditions and locations of the constraints depend on the Contact Discretization Method used in the contact formulation. The two contact discretization methods used in ABAQUS /Standard are node-to-surface and surface-to-surface [34.1.1].

The Node-to-Surface discretization option establishes contact conditions in which each Slave node on one side of the contact interface interacts with a point of projection on the Master surface on the opposite side of the contact interface. Therefore, each contact condition uses a single Slave node and a group of nearby Master nodes from which the values are interpolated to the projection point. As a result, the node-to-surface discretization method ensures that the slave nodes are

constrained not to penetrate the master surface, however the nodes of the master surface can penetrate the slave surface. The contact direction is based on the normal of the master surface.

Surface-to-Surface discretization differs by considering the shape of both the master and slave surfaces in the region of contact constraints. The formulation enforces the contact conditions in an average sense over regions of nearby slave nodes instead of only at individual slave nodes. Since the averaging regions are approximately centered on the slave nodes, each contact constraint will predominantly consider one slave node, but also consider adjacent slave nodes. Although some penetration may occur at individual nodes, large penetrations of master nodes into the save surface do not occur. The contact direction is based on the average normal of the slave surface in the region surrounding a slave node.

According to the ABAQUS manual, if the surface geometry is reasonably well represented, the Surface-to-Surface discretization method provides more accurate pressure and stress results compared to the Node-to-Surface discretization method. Since the Surface-to-Surface discretization method resists penetrations in an average sense over the finite regions of the slave surface, there exists a smoothing effect of the pressure distribution. The ABAQUS Gasket example problem uses the Node-to-Surface discretization method [5.4.1].

4.4.8.3 Slave Adjustment

If there exists an initial interference or gap between two surfaces, the position of the surfaces can be adjusted for the contact pair. The adjustment is performed at the start of the analysis and cases ABAQUS /Standard to move the nodes of the slave surface such that they are precisely in contact with the master surface. This adjustment does not create strain in the model and can be used to eliminate small gaps or penetrations and thus, prevent possible convergence problems. The adjustment is necessary when two surfaces are tied together for the duration of an analysis [32.3.5].

It is recommended by the ABAQUS Manual that an adjustment be utilized when tying two surfaces together for the duration of an analysis and when using Small Sliding contact. The ABAQUS Gasket example problem uses an adjustment of 0.01mm for each of the contact pairs [5.4.1].

4.4.8.4 Friction Formulation

ABAQUS /Standard includes various friction models that define the force resisting the relative tangential motion of two surfaces in a mechanical analysis [15.14.1]. The stiffness Penalty

method permits some relative motion of the surfaces (an elastic slip) when the surfaces should be sticking. As the surfaces are sticking, the magnitude of sliding is limited to the value of elastic slip. ABAQUS continually adjusts the magnitude of the penalty constraint to enforce this condition.

The ABAQUS Gasket example problem uses the Penalty method with a value of 0.20 for each of the contact surfaces [5.4.1].

4.4.8.5 Pressure Overclosure

In ABAQUS there exists many different pressure-overclosure relationships that can be used to define the contact model. The most common is the Hard Contact relationship, which minimizes the penetration of the slave surface into the master surface at the constraint locations and does not allow the transfer of tensile stresses across the interface. When the two surfaces are in contact, any value of contact pressure can be transmitted between them. However, as soon as the surfaces separate from each other, the contact pressure reduces to zero [33.1.2].

The ABAQUS Gasket example problem uses the Hard Contact relationship for each of the contact surfaces [5.4.1].

4.4.8.6 Separation

The option to "glue" two surfaces together once they come into contact exists in ABAQUS /Standard by using the No Separation Contact option. The option can only be used for pure master-slave contact pairs and cannot be used with adaptive meshing or with the general contact algorithm. [33.1.2] To allow frictional slip to be transferred on both sides of the gasket, it is recommended to use the No Separation option on one side of the gasket. When membrane behaviour is defined for the gasket, this method will allow for the gasket membrane to stretch or contract as a result of frictional effects considered on both sides of the gasket. The technique will prevent rigid body modes of the gasket in its thickness direction. A regular contact pair that does allow separation should be used on the other side of the gasket [29.6.3].

The ABAQUS Gasket example problem uses the No Separation option at the bottom surface and allows for separation at the top surface [5.4.1].

4.4.8.7 Non-Linear Geometry Option

After a discussion with the ABAQUS Support Team regarding the analysis, it was advised to use the Non-Linear Geometry Option (NLGEOM) in the analysis. The default setting in an ABAQUS analysis is without the use of the NLGEOM command, and therefore must be enabled in the

ABAQUS CAE when defining the steps or added to the input file. According to the ABAQUS Manual (6.2.2), in a Nonlinear Static Analysis a large-displacement formulation should be used. Since the gasket structure contains material nonlinearity, this option should be considered. Due to the multiple layers and existence of beads in the gasket material, the gasket geometry is nonlinear in the real world. However, since the FEA input file uses 1mm cubed elements to give only a geometric representation of the gasket, the resulting geometry becomes linear. It is simply a 1mm thick plate with the thickness in the vertical direction. The nonlinearity of the assembly is given by the material definitions and the loading and unloading curves within the input file. Since the ABAQUS manual recommends using the NLGEOM option for nonlinear geometry, it was decided to try the simulations with the option enabled.

The NLGEOM option is not used in the ABAQUS Gasket example tutorial, even though the gasket does contain nonlinearity in the gasket loading curves.

4.4.8.8 Gasket Thickness Normal Directions

The gasket thickness directions were not included in the FelPro supplied gasket input file and do not propagate to the input file written by ABAQUS CAE. it was therefore necessary to add the thickness directions into the input file before the analysis was run. The 3 gasket thickness directions were added to the 5 locations within the *Gasket Section of the input file, shown in green below.

```
*Gasket Section, elset=FB, behavior=FULLBEAD
 , 0., 0., 1., 0.0, 0.0, -1.0
** Section: Section-5-FLEXSTOP
*Gasket Section, elset=FLEXSTOP, behavior=HALF10
 , 0.0776, 0., 1., 0.0, 0.0, -1.0
** Section: Section-4-STOP
*Gasket Section, elset=STOP, behavior=BODY
 , 0.4917, 0., 1., 0.0, 0.0, -1.0
** Section: Section-3-HB
*Gasket Section, elset=HB, behavior=HALF15
 , 0.0007, 0., 1., 0.0, 0.0, -1.0
** Section: Section-1-BODY
*Gasket Section, elset=BODY, behavior=BODY
 , 0.6167, 0., 1., 0.0, 0.0, -1.0
*End Part
```

4.4.9 Interactions and Properties Used

The purpose of the first Single Cylinder analysis was to alter the interaction properties at the block-gasket interface and the head-gasket interface and determine which had an effect on the results. A summary of the interaction properties used throughout the interaction study of the simulations are shown in Tables 6, 7 and 8 below.

BLOCK-GASKET							
Version	Interaction			Interaction Property			
	Sliding Formulation	Discretization Method	Slave Adjustment	Friction Formulation	Frictional Coeff	Pressure Overclosure	Separation
1.00	Finite	Node to Surf	ON=0.1	Penalty	0.15	Hard	Disallowed
1.01	Finite	Node to Surf	ON=0.1	Penalty	0.15	Hard	Allowed
1.02	Finite	Surf to Surf	ON=0.1	Penalty	0.15	Hard	Disallowed
1.03	Small Sliding	Surf to Surf	ON=0.1	Penalty	0.15	Hard	Disallowed
1.04	Small Sliding	Surf to Surf	ON=0.01	Penalty	0.15	Hard	Disallowed
1.05	Small Sliding	Surf to Surf	Only Overcloser	Penalty	0.15	Hard	Disallowed
1.06	Small Sliding	Surf to Surf	OFF	Penalty	0.15	Hard	Disallowed
1.07	Finite	Surf to Surf	ON=0.01	Penalty	0.15	Hard	Disallowed
1.08	Finite	Surf to Surf	Only Overcloser	Penalty	0.15	Hard	Disallowed
1.09	Finite	Surf to Surf	OFF	Penalty	0.15	Hard	Disallowed
1.10	Finite	Node to Surf	OFF	Penalty	0.15	Hard	Disallowed
1.11	Small Sliding	Node to Surf	ON=0.1	Penalty	0.15	Hard	Disallowed

Table 7: at the Block-Gasket interface for Series 2

HEAD-GASKET							
	Interaction			Interaction Property			
Version	Sliding Formulation	Discretization Method	Slave Adjustment	Friction Formulation	Frictional Coeff	Pressure Overclosure	Separation
1.00	Finite	Node to Surf	ON=0.1	Penalty	0.15	Hard	Allowed
1.01	Finite	Node to Surf	ON=0.1	Penalty	0.15	Hard	Disallowed
1.02	Finite	Surf to Surf	ON=0.1	Penalty	0.15	Hard	Allowed
1.03	Small Sliding	Surf to Surf	ON=0.1	Penalty	0.15	Hard	Allowed
1.04	Small Sliding	Surf to Surf	ON=0.01	Penalty	0.15	Hard	Allowed
1.05	Small Sliding	Surf to Surf	Only Ovrclsr	Penalty	0.15	Hard	Allowed
1.06	Small Sliding	Surf to Surf	OFF	Penalty	0.15	Hard	Allowed
1.07	Finite	Surf to Surf	ON=0.01	Penalty	0.15	Hard	Allowed
1.08	Finite	Surf to Surf	Only Ovrclsr	Penalty	0.15	Hard	Allowed
1.09	Finite	Surf to Surf	OFF	Penalty	0.15	Hard	Allowed
1.10	Finite	Node to Surf	OFF	Penalty	0.15	Hard	Allowed
1.11	Small Sliding	Node to Surf	ON=0.1	Penalty	0.15	Hard	Allowed

Table 8: Interactions at the Head-Gasket interface for Series 2

HEAD-STUDS (4 Normal)							
	Interaction			Interaction Property			
Version	Sliding Formulation	Discretization Method	Slave Adjustment	Friction Formulation	Frictional Coeff	Pressure Overclosure	Separation
ALL	Small Sliding	Surf to Surf	ON=0.01	Penalty	0.1	Hard	Allowed

Table 9: Interactions at the Stud Interfaces for Series 1

4.4.10 Single Cylinder with Mesh Refinement

The Quarter Bank Model with Varying Mesh Sizes and Types focused on the effects of mesh refinement and mesh type alteration at various areas of the assembly. Mesh sizes and types were changed at the Deck layer in order to gain insight into the effects of each of the analyses. The best results of the previous study were used as the Basis for comparison. The results of the mesh refinement were then compared against the base setup to discover which parameters have an effect on the analysis, positive or negative. One of the major concerns with the base setup was the large amount of processing time taken to complete the analysis. It is a goal of this analysis to discover a setup which can significantly offer a compromise between good solver times and dependable results.

The purpose of the mesh refinement was to use the same basic setup of the initial setup, but alter the mesh type and density at the gasket interfaces. Analysis 1.01 was used as the basis of the study, and any changes were compared with its numbers.

3.00: This is the same mesh used in all of the previous analyses. The thickness of the partition at the decks A and D for both the Head and Block was 1mm. In this volume, the mesh consists of 1mm tetrahedral elements (C3D10). The top section of both the block and head, C and F, contains linear tetrahedral elements (C3D4) with a size of approximately 12mm. The Midsection partition thickness is 20mm and contains quadratic tetrahedral elements (C3D10).with a varying size, as the elements must gradually change in size in order to connect the two surrounding volumes. The gasket uses linear hexagonal (GK3D8) and linear wedge (GK3D6) elements.

3.01: The thickness of the deck partitions, A and D, were changed from 1mm to 2mm and therefore, the size of the elements in this volume were increased from 1mm to 2mm. All mesh types remained the same.

3.02: The thickness of the deck partitions A and D, were changed from 1mm to 4mm and therefore, the size of the elements in this volume were increased from 1mm to 4mm. All mesh types remained constant.

3.03: The thickness of the deck partitions, A and D, were changed from 1mm to 6mm and therefore, the size of the elements in this volume were increased from 1mm to 6mm. All mesh types remained constant.

3.04: The thickness of the deck partitions, A and D, were changed from 1mm to 2mm. Instead of 1 layer of quadratic tetrahedral elements, 2 layers of elements were constructed with a size of 1mm. All mesh types remained constant.

3.05: The thickness of the deck partitions, A and D, remained at 1mm, however the tetrahedral elements at this volume were replaced with linear hexagonal elements (C3D8) of volume $1mm^3$. In order to complete this, a separate meshing technique had to be implemented; the "bottom-up" meshing technique. All other mesh types remained constant.

3.06: The thickness of the deck partitions, A and D, were changed to 2mm and the tetrahedral elements at this volume were replaced with two layers of quadratic hexagonal elements (C3D20) of size 1mm. In order to complete this, a separate meshing technique had to be implemented; the "bottom-up" meshing technique. All other mesh types remained constant.

3.07: The Meshing of the Head and Block remained the same as the basis. The Gasket elements were all changed from Linear Tetrahedral and Wedge to quadratic tetrahedral (GK3D18) and wedge (GK3D12). This was accomplished by opening the original gasket input file in Abaqus, changing the gasket element types, and then exporting as another input file.

A summary of the element and node totals in comparison with the 3.00 base analysis is shown in Table 9 below, with the percentages representing the increase or decrease in amounts. Figure 23 shows the 4 different mesh sizes at a section of the block.

Mesh Refinement Totals				
Trial	**All Nodes**	**All Elements**	**% Nodes**	**% Elements**
3.00	447134	378435	100.0%	100.0%
3.01	222131	248190	49.7%	65.6%
3.02	112070	157546	25.1%	41.6%
3.03	104333	152442	23.3%	40.3%
3.04	899099	624167	201.1%	164.9%
3.05	904807	628255	202.4%	166.0%
3.06	930342	581962	208.1%	153.8%
3.07	488562	378435	109.3%	100.0%

Table 10: Mesh Refinement increases for Nodes and Elements.

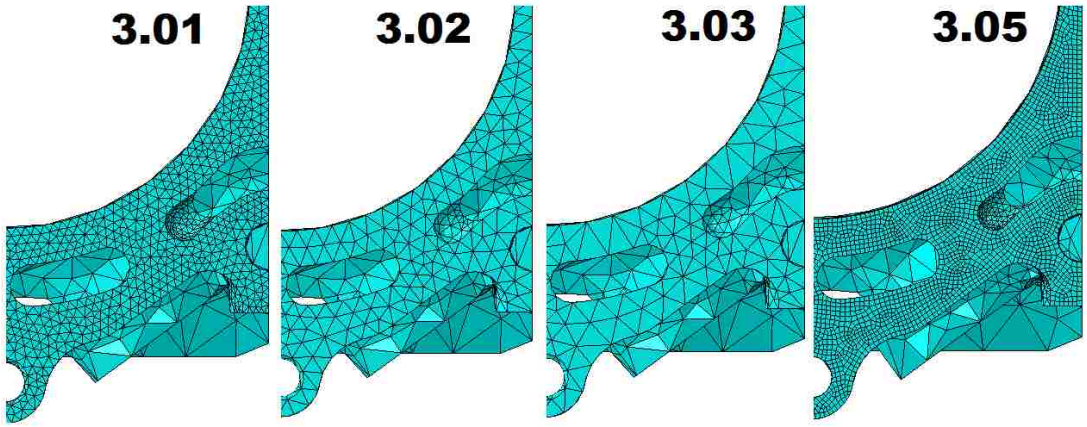

Figure 23: From left to right, on the block deck face, the meshes of 3.01, 3.02, 3.03 and 3.05. The hexagonal elements can be seen in Analysis 3.05.

4.4.11 Gasket Model using Conventional Shell, Continuum Shell and 3D Elements

The use of gasket elements is satisfactory for determining the behaviour of the gasket as a single piece and its effect on the head and block. However, if one requires information regarding each individual gasket layer or the fire ring, a more in depth analysis must be performed. The purpose of the shell method is to analyze the 3D representation of the head, block and gasket using all layers of the physical gasket. It is similar to the 2D axisymmetric analysis discussed previously, however the assembly is now in 3D, which allows for the stiffness of the head, block and studs to play an important role. Since the gasket layers are extremely thin sheets of metal, shell elements are appropriate to model the entire assembly. However, shell elements do not transfer force in their thickness direction, which results in discrepancies between the FEA results and the physical

results. A 3D gasket element was also tried. The following is a discussion on the method used for analysis of the full shell gasket and 3D gasket. Although this method has been used before, the exact method used by other companies is proprietary. Therefore, the method discussed was a result of trial and error by the author. The analysis continues the use of cylinder 5 for the simulation and uses the same parameters of the Single cylinder model used previously. The only changes to the ABAQUS assembly/model was regarding the gasket and it's physical representation.

4.4.12 Varying Gasket Element Type Procedure

The most time consuming aspect of the method is the alteration of the gasket geometry in the CAD program. It is helpful to have a solid model of the gasket, however, when imported as a .step or .iges file, the assembly consists of thousands of separate surfaces. There are a few approaches that can be taken if this is the case, but the end goal is to have each gasket layer appropriately separated. From this, the layers can be shown or hidden, thus allowing individual layers to be imported into ABAQUS. The end goal is to have just the top or bottom surface of each layer present in ABAQUS. The top and bottom surface should be identical, so it does not matter which. Each particular surface can be used as the mid surface of a group of shell elements. This surface can also be used to create bottom-up meshes for the continuum shell elements and the 3D elements.

If the CAD model of the gasket contains solid geometry, each layer should be imported into ABAQUS individually to keep proper organization. The CAD file can simply be saved with the appropriate layer shown, and the rest of the layers hidden. ABAQUS only imports what is visible in the Catia space. During the import process, the Topology of the part should be changed to "Shell." If it is missed in this step, it can be completed in the Parts module. After the full layer is imported into ABAQUS as a shell, it is necessary to delete the unnecessary faces from the geometry. An efficient way to do this is to hide the faces which will be used as the shell surface. Under Create Display Group, select Faces under the item list. When prompted to make a selection, change the drop down box at the bottom of the screen from "individually" to by face angle. Enter a face angle of 45 degrees and select a face on the top surface of the gasket. This should select all faces on the top of the gasket. If it does not, enter a higher value, such as 60 degrees. Unless there are severely sharp edges along the top surface, the selection should encompass all of the faces. Do not enter a value equal to or greater than 90 degrees, as this will select all of the faces that are within 90 degrees of each other, which will be all of the faces. When the full surface is selected, it can be hidden using "Remove" button for the Display Group. Back

in the Parts module, under "Edit Geometry," the visible faces can be deleted by selecting all of them in a single selection box. Now, the remaining top surface can be shown by selecting "Replace All" under the display group module. If done correctly, the top surface of the gasket layer should remain. This will be used as the middle surface of the shell elements for the gasket assembly. The same procedure should now be repeated for each layer of the gasket, including the fire ring(s).

The sections used for each gasket layer and fire ring depended on the type of analysis. Conventional and continuum shell elements require shell sections, where 3D elements use homogeneous sections. A single section can be created for all of the gasket layers if all of the layers have the exact same thickness. If one layer has a different thickness than the rest, it must use a different Section. The thicknesses of the gasket can be measured from the CAD program and might be different for each layer. The material specifications used are based off of data provided by [Olsson, 2001] from Figure 17. Figure 24 shows the layers as surfaces before and after being meshed.

Figure 24: Surface model of the gasket assembly (Left) and meshed shells of gasket assembly (right)

The mesh for each type of analysis used linear, quad elements with reduced integration. Element sizes were set to 1mm. The conventional shell elements have their thickness defined in the property sections. The continuum and 3D elements used bottom-up meshing to create the extruded geometry of the mesh. Each layer can be inserted into the full assembly between the head and the block. The distance between the head and block deck faces is determined by the largest distance between the top surface of Layer 1 and the bottom surface of Layer 2. Each layer must be positioned such that it's located at its mid surface position. This is accomplished by using the Face to Face Offset constraint and then specifying the appropriate distance between the surfaces. The CAD program should be used to determine the position of the mid-surfaces of the layers.

The Fire Ring is usually welded to one of the gasket layers and therefore a Tie Constraint should be used be used between the two. The master surface is the gasket layer and the slave surface is the fire ring.

4.5 Series 3: Full Bank Analysis at Varying Engine Operating Conditions

Series 3 used a complete Full Bank Model (or half engine) with pre-load of the studs applied at various engine conditions, while using the FelPro supplied gasket element model. Both of the Left and Right banks of the engine were meshed and use the same Gasket input model, supplied by FelPro. The focus was on the Right Bank of the engine, as this is where the gasket has failed during testing. The block was simply split directly at its plane of symmetry leaving the left or right side, depending on the analysis. The parameters used are based off of the best results found in the previous three studies, specifically, Analysis 1.01.

A thermal map of the engine was provided and applied to the assembly. The conditions in which the engine are studied are as follows:

- Cold Clamping (CC)
- Cold Firing (CF)
- Hot Clamping (HC)
- Hot Firing (HF)

4.5.1 Full Bank Materials

Series 3 used the same materials as Series 2. The full Material Table and gasket loading curves are described in Section 4.4.2 above.

4.5.2 Full Bank Mesh

It was apparent after the Quarter Model analyses were completed that the number of elements and nodes of a full bank model would have to be kept to a minimum, while still being fine enough at the deck interface to capture the highly varying values of pressure. A similar method to that of the Quarter Bank Analysis was utilized, which involved partitioning the block and the head into separate regions. The meshes of head and block were partitioned into 4 separate sections for each part; A, B, C, D, E, F, G, H as shown in Figure 25. Note that sections D and H are not fully shown, but do extend to the remainder of the parts (the top of the head and the bottom of the cylinder). The reason for the change from 3 regions of the Quarter model to 4 for the Full Bank was ensure that mesh was propagated correctly from one region to another. It was important to have a solid layer of pure 1mm tetrahedral elements at the gasket interface. Also, there are areas

of the head that do not come into contact with the gasket or the block. These areas correspond to the bores of the block. Thus, 4 circular areas were partitioned so that the size of the elements could be increased in the areas of less importance. Figure 26 shows the partitioned regions with different sized meshes for the first two valve areas.

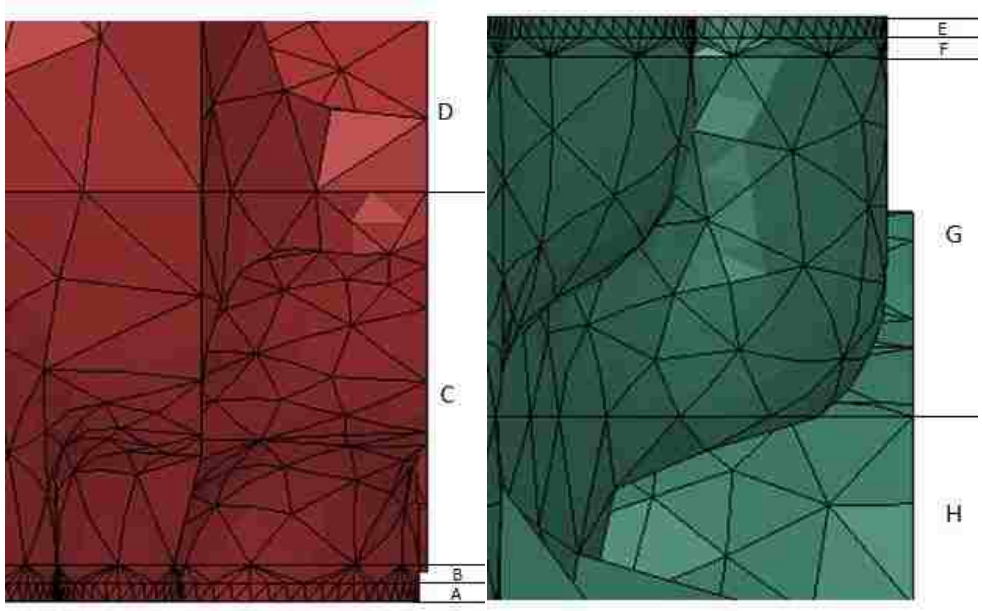

Figure 25: Mesh Regions of the Head (left) and Block (right)

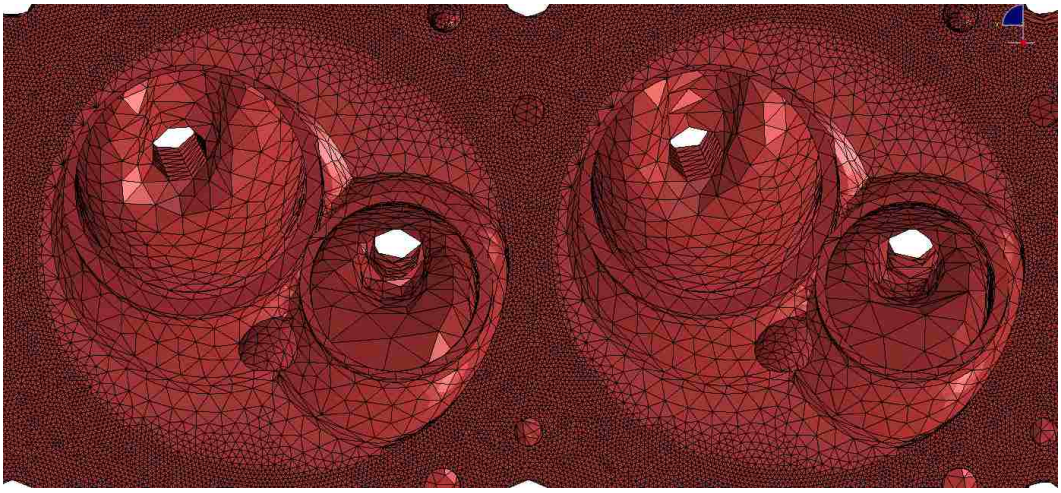

Figure 26: The regions of the head with larger elements

Table 10 below summarizes the mesh numbers for the Right Bank analysis used in Series 3. The left bank contains similar numbers as well. Figure 27 shows the entire meshed right bank. The left bank looks identical.

							Totals	
Part Name	**Region**	**Element Name**	**Element Type**	**Element Size (mm)**	**No. of Elements**	**No. of Nodes**	**Elements**	**Nodes**
R6P8 Head	A	Quadratic Tet	C3D10	1	301765	582687	997921	989418
	B	Quadratic Tet	C3D10	6	111300	253579		
	C	Quadratic Tet	C3D10	6	153938	244887		
	D	Linear Tet	C3D4	20	430918	95491		
R6P8 Block	E	Quadratic Tet	C3D10	1	244634	478946	684931	707214
	F	Quadratic Tet	C3D10	6	87712	205305		
	G	Quadratic Tet	C3D10	6	59481	101957		
	H	Linear Tet	C3D4	20	293104	71951		
Stud, Long	All	Quadratic Tet	C3D10	4	4976	8097	4976	8097
Gasket	All	Linear Hex	GK3D8	1	29375	66954	31309	66954
		Linear Wedge	GK3D6	1	1934			
Assembly							**1764760**	**1848904**

Table 11: Right Bank Element Totals

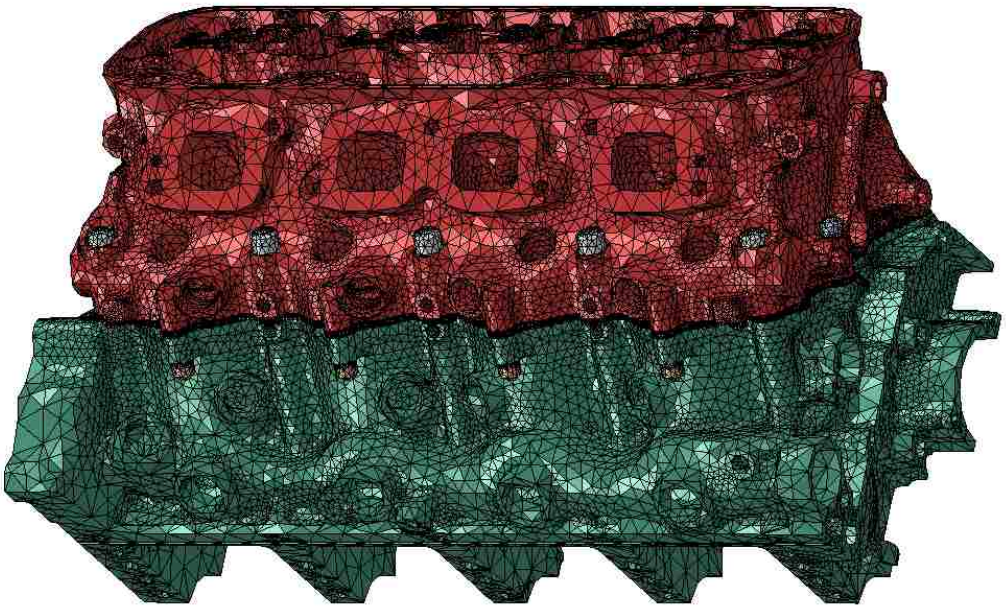

Figure 27: The entire meshed Right Bank Engine Assembly

4.5.3 Full Bank Steps

The full bank analysis must be performed by uses of various steps in ABAQUS. The following steps shown in Table 11 were used for the thermal analysis of the right engine bank.

Step No.	Name	Conditions
Initial	Initial	Apply all Boundary conditions to block.
1	Cold Clamping	Apply bolt loads to all studs.
2	Stud Fixing	Fix all studs to current length.
3	Thermal Map Addition	Apply temperatures to nodes of head and block.
4	Peak Pressure- Cyl 1	Apply peak pressure to Cylinder 1.
5	Peak Pressure- Cyl 3	Apply peak pressure to Cylinder 3. Remove pressure from Cylinder 1.
6	Peak Pressure- Cyl 5	Apply peak pressure to Cylinder 5. Remove pressure from Cylinder 3.
7	Peak Pressure- Cyl 7	Apply peak pressure to Cylinder 7. Remove pressure from Cylinder 5.

Table 12: Steps used for Series 3

4.5.4 Full Bank Constraints

Series 3 used tie constraints at every stud surface. The heads of the studs were tied to the engine block and head bearing surfaces and the threads were tied to the engine block and head bores. The bearing surfaces were the counter bore areas where the heads of the studs contact their respective surfaces. Also, at the gasket and head interface, a equation constraint was used between two sets of gasket and block nodes to ensure that the gasket could not be subject to rigid body motions. The areas of constraints are represented by the pink and red areas in Figure 28.

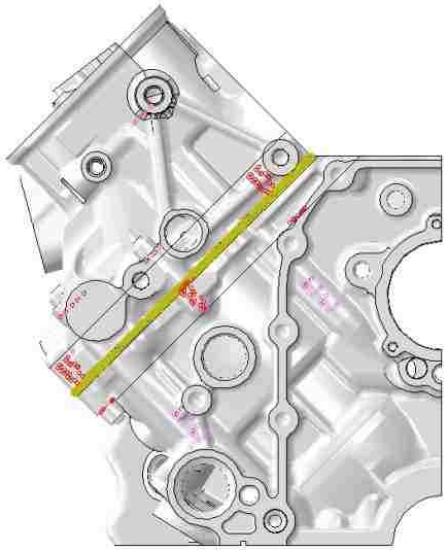

Figure 28: Areas of constraints used for the Studs (pink and red colors)

4.5.5 Full Bank Loads

The pre-tension in the studs was created using the method outlined in the ABAQUS User's Manual Section 21.2. A partition was created during the meshing phase at each of the studs. The

pre-tension on the Long and medium length studs was set to 60,700N. The short length studs were given a full load of 33,360N. The studs being loaded are shown in Figure 29.

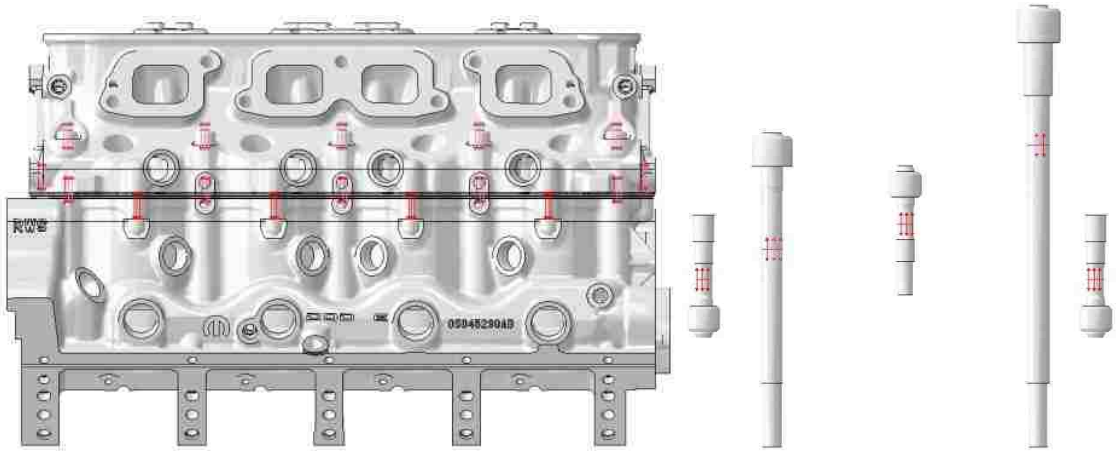

Figure 29: Bolt loading conditions for full bank. Full engine view (left) and end view with engine hidden (right)

4.5.6 Varying Bolt Loads

Under normal engine conditions, as the engine heats up, the head studs heat up as well. During the thermal loading of the head and the block, the engine studs tend to relax their forces. An analysis was completed using these values for the bolt forces. It is suggested by [Popielas, et al, 2003] that the resulting magnitude of bolt tensions are 70-80% of the original, cold clamping values. Therefore, for the analysis, 3 separate cases were studied; the 100%, 80% and 70% bolt tension cases. The values of force used are shown in Table 12.

	Tensile Force (N)		
Part	100%	80%	70%
Long, Medium Studs	60700	48560	42490
Short Studs	33360	26688	23352

Table 13: Reduced Bolt Forces

Also, due to the deformation of the head during the previous analyses, it was decided to do a study on the influence of the small length studs in the 180° locations. For the cold clamping case, the studs were given loads of 0%, 50%, 100% and 150%. Figure 30 shows the location of the stud loads being altered. All other studs loads remained constant.

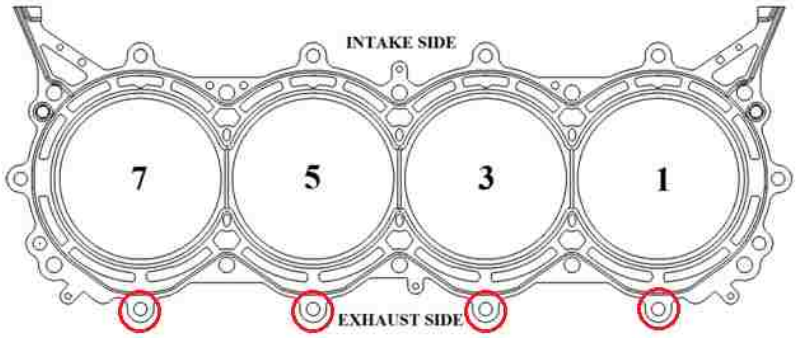

Figure 30: Locations of altered bolt loads

4.5.7 Peak Pressure Addition

The second stage of the full bank analysis is the pressure addition to the cylinder. The maximum pressure can be provided by the powertrain engineer or by physical testing results. The peak pressures were taken from data provided by Penske and are listed in Appendix B. Under peak pressure conditions, the major components that the pressure will act on are the piston face, cylinder walls, head deck face, and valve faces. If the analysis does not include the valves, an alteration to the pressure must be completed in order to ensure the proper force on the deck face. The values that are needed are the cylinder radius, intake valve face radius and exhaust valve face radius. Using the formula, the altered pressure is given. This is the value that should be applied to the deck face when the valves are not in the simulation. The areas of pressure addition are shown in red in Figure 31. P_{MOD} is the modified pressure to be applied to the Head Deck Face, using

$$P_{MOD} = P_{MAX} \times \left[\frac{R_C^2}{R_C^2 - (R_I^2 + R_E^2)}\right] \qquad \text{(Equation 9)}$$

where PMAX is the maximum cylinder pressure, R_C is the Cylinder Radius, R_I is the Intake Valve Radius and R_E is the Exhaust Valve Radius.

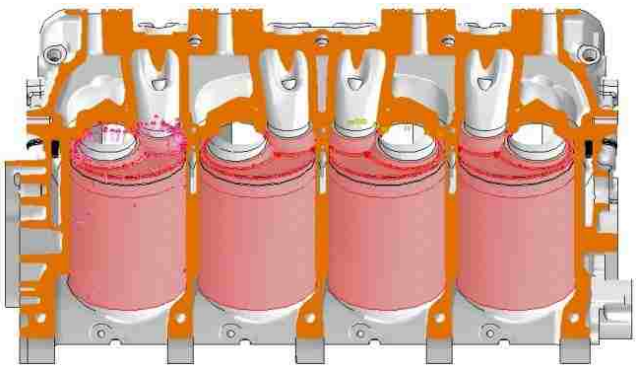

Figure 31: Locations of cylinder pressure (red surfaces)

4.5.8 Full Bank Boundary Conditions

The Boundary Conditions used for Series 3 were similar to those used in the previous Series. The base of the Block was constrained using an Encastre Constraint. A symmetry constraint was used for the cut faces of the block along the centre plane of the engine. Since there is a 90° angle between the cylinders, when the assembly is cut down its middle, the resulting plane is not aligned with the Global Axis of the assembly. In order to properly apply the Symmetry constraint, a local axis was created that was aligned with the plane of symmetry. There were two options regarding the location of the encastre boundary condition. Early attempts used a full encastre on the entire bottom face of the engine block. However, after observing the stress results due to the effect of the temperature map addition, it was decided to change the location of the encastre to a different location. The encastre was moved to the crankshaft journal locations of the block. This resulted in a less "stiff" boundary condition, as shown in Figure 32 (right).

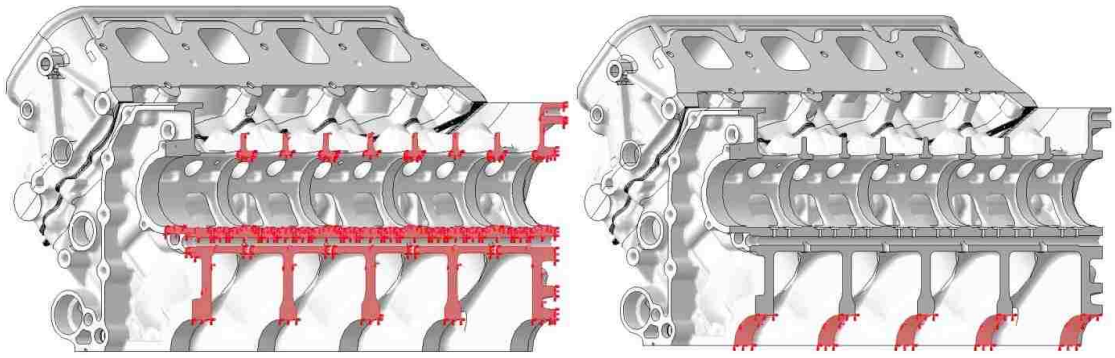

Figure 32: Symmetric boundary locations (left) and Encastre boundary conditions (right)

4.5.9 Full Bank Output Requests

The following Field Output Requests were enabled for the Series 4.

Stresses: S (Stress components and invariants)

Strains: E (Total strain components)

S11: Pressure in the gasket element.

S22: Direct membrane stress.

S33: Direct membrane stress.

S12: Transverse shear stress.

S13: Transverse shear stress.

S23: Membrane shear stress.

E11: Gasket closure if the gasket response is defined directly using a gasket behaviour model; strain if the gasket response is defined using a material model.

E22: Direct membrane strain.

E33: Direct membrane strain.

E12: Transverse shear motion if the gasket response is defined directly using a gasket behaviour model; strain if the gasket response is defined using a material model.

E13: Transverse shear motion if the gasket response is defined directly using a gasket behaviour model; strain if the gasket response is defined using a material model.

E23: Membrane shear strain

Displacement/Velocity/Acceleration: U (Translations and rotations)

Forces/Reactions: RF (Reaction forces and moments), NFORC (Nodal forces due to element stresses)

Contact: CSTRESS (Contact stresses), CDISP (Contact displacements), CFORCE (Contact force)

Energy: ENER, All energy magnitudes

4.5.10 Full Bank Interactions

The Quarter Model Analyses of Series 2 completed earlier in the thesis project gave insight into what interaction parameters would be used for the full bank model. It was decided that at the gasket interface, the following interactions be used for the Full Bank Analysis:

Sliding Formulation: Small Sliding

Contact Discretization Method: Surface to Surface

Slave Adjustment: 0.1

Friction Formulation: Penalty

Pressure Overclosure: Hard

Separation: No separation allowed at the Block interface. Separation allowed at the Head

Friction Coefficient of 0.15 for both interfaces

4.5.11 Application of Thermal Map

In order to properly define the proper temperature map to the engine block and head, it was necessary to position the engine parts according to how the CFD simulation was completed. Basically, the global positioning of the FEA assembly must overlap the global positioning of the CFD assembly. Once completed, the thermal temperature map was supplied as two separate input

files, one for the head and one for the block. The format of the input file consisted of a list in the following format:

```
*TEMPERATURE
Head-2.1,392.061
Head-2.2,389.867
Head-2.3,394.113
...
*TEMPERATURE
P05045291AB_B01_CYLINDER_BLOCK_M-1.1,367.785
P05045291AB_B01_CYLINDER_BLOCK_M-1.2,367.046
P05045291AB_B01_CYLINDER_BLOCK_M-1.3,393.969
...
```

There are three components to the input file; the name of the part, the node number and the temperature. The name of the part must exactly correspond to the name of the part in the ABAQUS assembly, or the simulation will not run. Each input file consisted of the same number of values as nodes of the parts.

In order to apply the temperature map to the assembly, an addition Step and a predefined field was created in ABAQUS CAE. This field was a Temperature Field with Direct Specification, Constant through region and a magnitude of 100. The temperature value was arbitrary, as it is deleted in the next procedure. After writing the master input file to be used for the analysis, the temperature map input files were copied and pasted into the master input file, in place of the arbitrary value created previously in the temperature map addition step. This increased the size of the input file by approximately 100mb.

During a CFD analysis, rarely are the studs and gasket included. Therefore, when the temperature maps are provided, the temperature map does not include the studs or gasket. There are two options if a temperature needs to be provided to the other components; Complete a full heat transfer simulation or simply apply temperatures to the components. The former was out of the scope of the research. In order to apply temperatures to these components, some assumptions had to be made. Since it would be extremely time consuming to perfectly match the elemental temperatures to their contacted element, single temperatures were added to the parts. The temperature map was viewed for the head and the block. It was assumed that the areas at the bolt bores would correspond to the same temperatures at the studs. The temperature profiles at these areas are relatively steady, therefore, a single temperature was applied to all of the studs. At the deck face, the temperatures vary significantly from the inner edges of the cylinder to the outer edges of the block and head. Therefore, temperatures were applied to the gasket in three regions;

- High temperature at the inner beads of the gasket
- Mid temperature at the middle beads of the gasket
- Low temperatures at the outer beads of the gasket

The temperatures at the head and block decks are shown in Figure 33.

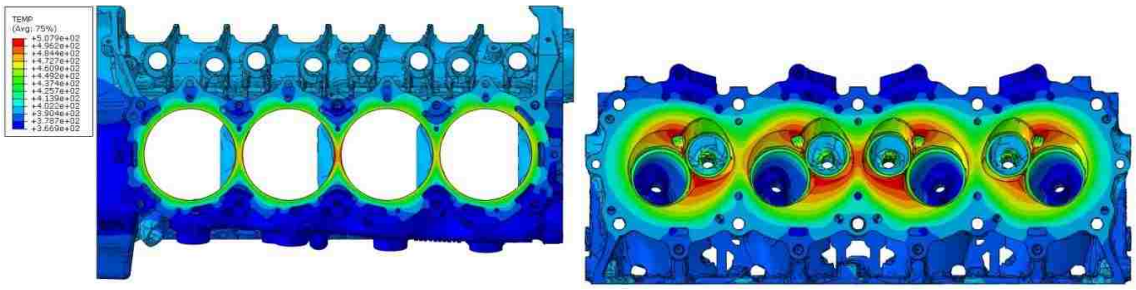

Figure 33: Temperature map of block in °C.

Chapter 5: Results and Discussion

5.1 Series 1: Axisymmetric Results

The following section is devoted to the results and discussion of the Axisymmetric Analyses.

5.1.1 Axisymmetric Stresses and Strains

The results of the two-dimensional axisymmetric analyses are shown in the Figures below. The values that are of interest are the Von Mises combined stress, the S11 normal stresses and the S12 shear stresses. These values are shown in Figure 34, 35 and 36 for each cut section of the gasket. It should be noted that the S11 normal stress in this case does not correspond to the S11 normal stresses in the gasket element case.

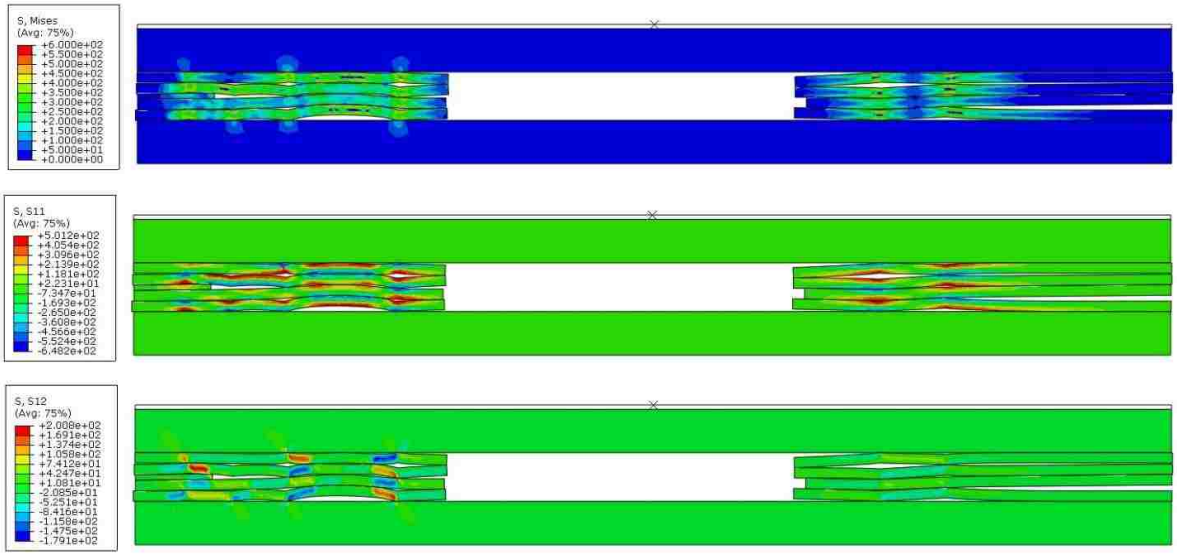

Figure 34: Axisymmetric VM (top), vertical pressure (middle) and shear stresses (bottom) for 0° Section

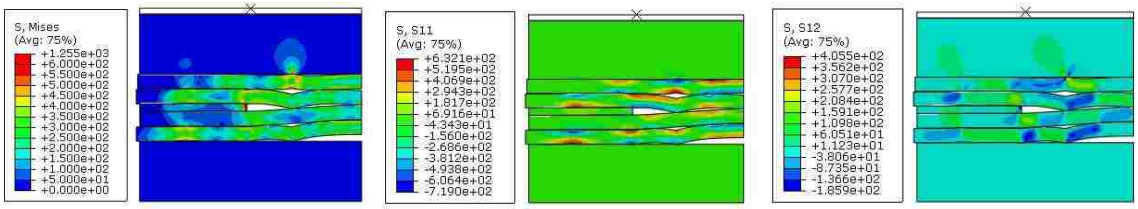

Figure 35: Axisymmetric VM (left), vertical pressure (middle) and shear stresses (right) for 90° Section

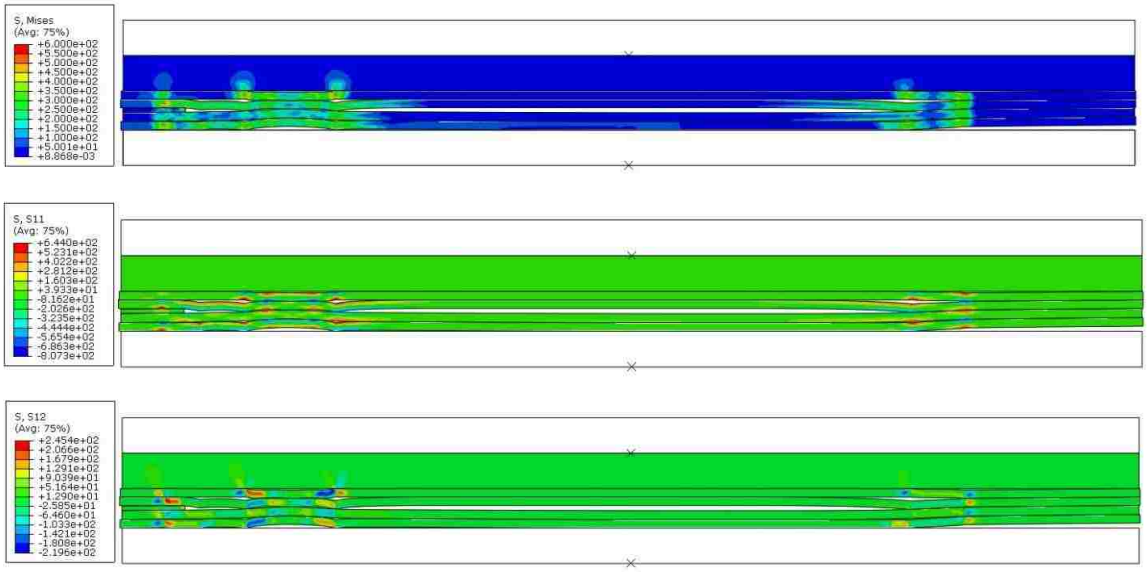

Figure 36: Axisymmetric VM (top), vertical pressure (middle) and shear stresses (bottom) for 180° Section

The Von Mises stress values give an indication to the areas in the gasket layers that are under the highest stress. In the actual gasket, there have been cases of the fire ring separating from the third gasket layer to which it is laser welded to. The stress values at the firing ring give no indication that there are abnormally high stresses causing this to occur. The S11 normal stresses show the area in which the gasket layers are in compression and tension. As the beads are compressed during clamping, the valleys of the gasket are stretched, thus causing tensile forces and the peaks of the gasket are compressed, thus causing compressive forces. In a typical gasket forming process, residual stresses would be present in these areas due to the forming process on the gasket layers. In order to fully understand the interaction of the residual stresses, the stresses must be included in the FE simulation. The shear stresses show the areas of maximum positive and negative shear in the gasket as it is compressed.

5.1.2 Axisymmetric Fuji Pressure Film Comparison

The Pressure distribution on the top layer of the gasket is compared to the Fuji Pressure film analysis. The resolution of the Fuji Paper is low when zoomed, so the qualitative results are quite fuzzy. In order to increase the visibility of the 2D axisymmetric cases, the options to revolve the section was used, giving a "3D" representation of the layers.. This gave a third dimension to the results and allowed for the contact pressures to be compared with the Fuji Film analysis. The Pressures of the gasket sections are compared against their Fuji paper counterparts and shown in Figures 37, 38 and 39 below.

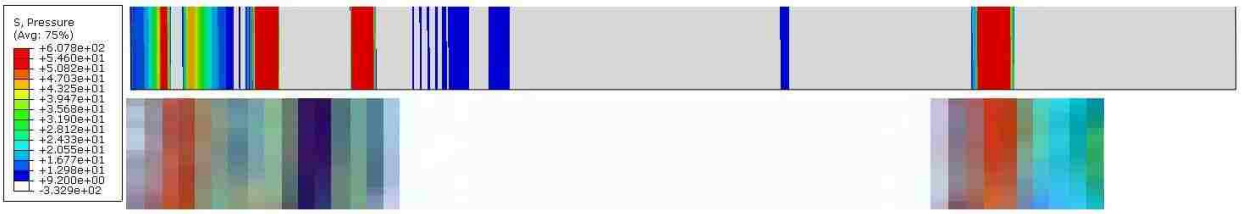

Figure 37: Comparison of 0° Section (top) with Fuji Film (bottom)

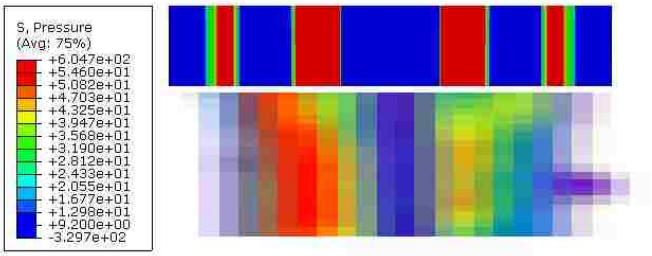

Figure 38: Comparison of 90° Section (top) with Fuji Film (bottom)

Figure 39: Comparison of 180° Section (top) with Fuji Film (bottom)

In order to increase the visibility of the Fuji paper, the jpeg picture had to be zoomed in quite substantially. The comparison with the Fuji film shows that the locations of pressure tend to correlate. It is difficult to perfectly match the FEA result to the Fuji film, as the Fuji film resolution is quite low. Also, the comparison is mostly done through visual comparison, with no exact numbers to compare. However, from a qualitative standpoint, the areas of maximum pressure tend to match. The values of the FEA results tend to be higher than that of the Fuji Film.

5.1.3 Axisymmetric Bead Stiffness

For each of the sections, the Force was plotted compared to the closure of the gasket. These are shown in Figure 40.

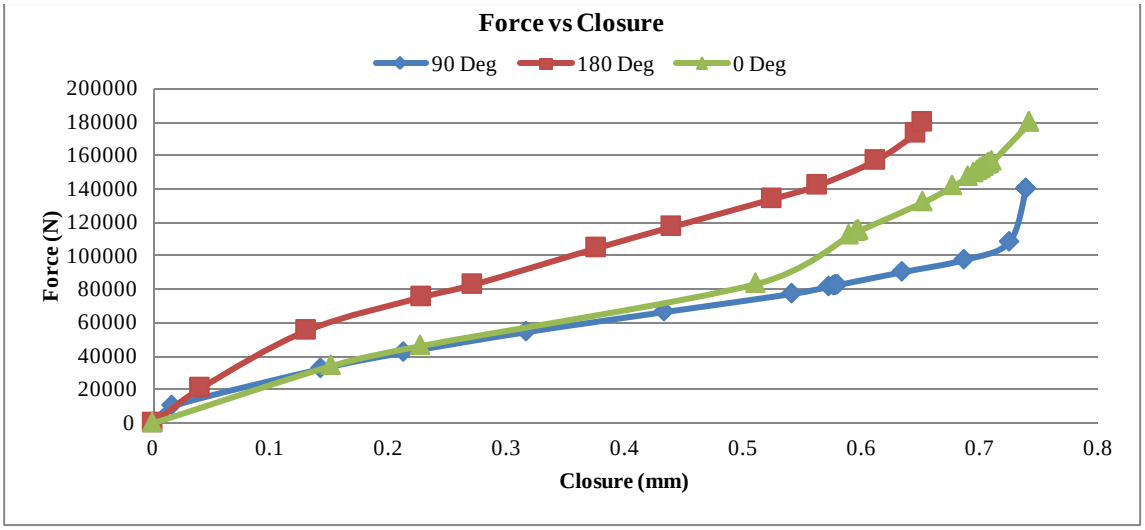

Figure 40: Force vs Closure curves for all Axisymmetric Sections

The Force Vs closure graph gives an indication of the stiffness of the gasket at the different cross sections. The stiffness of the gasket is represented by the slope of the curve and tends to increase significantly as the closure is increased. The section at 180° has the highest stiffness, followed by the 0deg area, and finally the 90° area with the lowest stiffness. The difference in stiffness between the 0° and 180° locations is most likely due to the coolant passage that is present in the 0° location. The absence of material is causing the stiffness reduction. Increasing the clamp loads could give more insight into the stiffness of the gasket at the higher closure values. The values are difficult to compare to the given values in the gasket input file, as those are relative to pressure and not force.

5.1.4 Axisymmetric Discussion

All of these analyses are assuming that the head and block can only deform in the vertical direction. In the real world case, the head is able to deform in all directions. An important strength of the axisymmetric analysis is the ability to include the geometry of the full gasket with all layers and fire rings, while being very computationally efficient. The interactions between the layers can be studied during cold clamping and the corresponding contact pressure between the head and gasket can be observed. Regarding the contact pressure during cold clamping, the axisymmetric analyses gave moderate correlation to the Fuji pressure film results. The locations of the maximum pressures were similar for the two cases. However, the magnitude of the FE results tended to be higher than the real world results. It is difficult to fully compare the FE result with the Fuji Film, as the resolution Fuji .jpeg is relatively low. A higher resolution picture should be requested from the company who does the laser scanning. A typical axisymmetric analysis

assumes that the load is distributed equally around the entire circumference of the assembly. However, for the physical results, the aluminum head is able to deform over the gasket at different areas. Also, the locations nearest to the studs have higher clamping forces than compared to the areas away from the studs. It is difficult to accurately predict how the stresses fluctuate around the cylinder bore.

Knowing how the gasket is compressed in the real world case is important to fully understand the gasket behaviour. As the gasket layers are compressed and come into physical contact with each other, stresses are introduced into the each gasket layer. The Von Mises stress, normal stresses and shear stresses were compared against each other for each of the three locations. These values are informative, however the assumption is made that there is zero stress in the layers before the analysis begins. This is an incorrect assumption, as residual stresses are produced during the forming process of the gasket layers. The gasket residual stresses can be determined with the Proteus® software and then exported to an input file to be used in the FEA. Neither Chrysler nor FIAT have access to this program. In order to fully understand the forming process, more investigation must be completed. This is a crucial aspect of the gasket stress and a full project could be dedicated to this topic alone. [Popielas, 2003] gives a brief overview of the procedure used to develop the Proteus® program. The equations given could be used to help determine residual stresses in the beads of the gasket. Regarding the gasket forming process, as the flat sheet of metal is formed into its beaded shape, tensile and compressive stresses are formed. The magnitude and type of stress is determined by a number of parameters, such as bead height, tool radius, tool material, etc. If the stresses are high enough, local cracking can occur in the material. When the gasket is compressed during cold clamping, the gasket is deformed back into its natural, flat state. This would decrease some of the stresses that were imposed during the forming process. The assumption can be made that the stresses in the gasket layers of the 2D axisymmetric analyses is less than that of the real world case. There had been observation of the real world fire ring separating from the layer to which it is welded to. The analysis did not show any reasons to conclude a cause for this.

The axisymmetric analysis gave information regarding the stiffness of the gasket at the different locations. This could be helpful in determining why the head is deforming more or less at the varying locations. However, one would expect that the head would deform less if it is being compressed against a higher stiffness area of the gasket. When looking at the full bank analysis, this is not the case, as the head area at the exhaust (180°) location is deforming the most. It can be

concluded that the different stiffness's of the gasket areas are not a significant source of the head deformation.

5.2 Series 2: Single Cylinder Results

The purpose of Series 2 Interaction study was to determine the best combination of Interaction properties by methodically changing single parameters for each analysis. The logic for the changes as the analyses were completed are explained below. Refer to the Tables 6, 7 and 8 above for reference to the iteration changes.

- **1.00:** The first analysis run was used as the base scenario. All preceding analyses would be compared to this analysis, until a new basis was discovered. The interaction properties were chosen by following the ABAQUS Coolant Gasket Tutorial (5.4.1). 4 Numerical Singularity Warnings were present on 4 gasket nodes.
- **1.01:** The separation options were switched at the gasket and the head interfaces. Separation was allowed at the block interface but disallowed at the head interface. The differences in the results were negligible. 4 Numerical Singularity Warnings were present, on the same 4 gasket nodes as in the previous analysis. The Separations would be switched back to 1.00 status for the next analysis.
- **1.02:** The Descritization Method was changed from Node to Surface to Surface to Surface at both of the Head and Block Gasket interfaces. The Analysis was able to complete in approximately 50% of the time of Analysis 1.00 with a similar number of iterations. The pressure results were identical. 4 Numerical Singularity Warnings were present, on the same 4 gasket nodes as in the previous analysis. Due to the reduced processing time, 1.02 was changed to the new basis.
- **1.03:** The Sliding Formulation was changed from Finite Sliding to Small Sliding at both interfaces. The difference in processing time and iteration numbers was drastic. Analysis 1.03 was able to complete in 1155 seconds while requiring only 1 iteration. The pressure results were identical to the previous values, however strange spiking occurred, which is discussed in Section 2.10. Due to the reduced processing time, reduced iteration numbers and absence of Warnings, 1.03 was changed to the new basis.
- **1.04:** Analyses 1.04, 1.05 and 1.06 focused on the alteration of the Slave Adjustment at the deck interfaces. The slave adjustment value was changed from 0.1mm to 0.01mm for both interfaces. The results were identical to the 1.03 basis.

- **1.05:** The slave adjustment value was changed from 0.1mm to Only Overclosure for both interfaces. The results were identical to the 1.03 basis, except Numerical Singularity Error was present.
- **1.06:** The slave adjustment value was turned off for both interfaces. The results were identical to the 1.03 basis, except the pressure spikes and spotting disappeared. 1343 Numerical Singularity Errors was present, all on gasket nodes.
- **1.07:** The next three analyses (1.07, 1.08 and 1.09) focused on reverting back to using the Finite Sliding Formulation while altering the Slave adjustment distances, as was done in the previous three analyses. Analysis 1.07 uses a Slave Adjustment of 0.01mm. The processing time and iteration numbers increased drastically to the values of Analysis 1.02. The pressure distribution remained the same. 4 Numerical Singularity Warnings were present, on the same 4 gasket nodes as in the earlier analyses. Analysis 1.07 was changed to the new basis, for comparisons sake.
- **1.08:** The Slave Adjustment was changed from 0.01 to Only Overclosure. The processing time and iteration numbers remained high. The pressure distribution remained the same. Zero Warnings were present.
- **1.09:** The Slave Adjustment was changed from 0.01 to Off. The processing time and iteration numbers remained high. The pressure distribution remained the same. Zero Warnings were present.
- **1.10:** The purpose of Analysis 1.10 was to investigate the alteration of the Discretization Method compared to the previous Analysis 1.09. The Slave Adjustment remained Off and the Discretization method was changed to Node to Surface. The processing time and iteration numbers remained high. The pressure distribution remained the same. Zero Warnings were present.
- **1.11:** The Small sliding Formulation was used with Node to Surface Discretization Method. The processing time and iteration numbers decreased drastically to the values of Analysis 1.03. The spikes and spotting was present with the pressure distribution remaining the same. Zero Warnings were present.

The results obtained for Series 2 show the consequences of altering the Interactions. The focus of the comparisons is on the S11 Pressure of the 3 major sections of the gasket by use of a graphical representation of the pressures along the circumference of the cylinders at every 10°. The Stop, Flexstop and Fullbead gasket beads were all analyzed. The 0° point corresponds to the intake side of the engine. Other outputs that are discussed are the Shear Stress E11, Gasket Displacement U3

and Von Mises Stresses. The method used for creating the graphs is outlined in Appendix A. The Series 2 interaction property simulations were able to complete with varying increment totals, CPU times, wallclock times and warning messages. The values of the simulation parameters are summarized in Table 13. An interesting result regards the warnings on the gasket. Usually, if the warning was of the Numerical Singularity type, the 4 nodes that were affected were Gasket Nodes 190856, 190906, 190941, 190923. These nodes are on one of the tabs of the gasket, in an area that is in direct contact with the head and block. There appeared to be nothing special about these nodes that could cause the issues.

Single Cylinder Interaction Study Results				
Version	**CPU Time (s)**	**Wallclock Time (s)**	**Total Increments**	**WARNINGS**
1.00	5.05E+05	100523	172	4- Numerical Singularities (Gasket Nodes 190856, 190906, 190941, 190923)
1.01	5.39E+05	110590	174	4- Numerical Singularities (Gasket Nodes 190856, 190906, 190941, 190923)
1.02	4.06E+05	57760	168	4- Numerical Singularities (Gasket Nodes 190856, 190906, 190941, 190923)
1.03	7959	1155	1	ZERO
1.04	8644	1543	1	ZERO
1.05	10028	1441	1	1- SOLVER PROBLEM. NUMERICAL SINGULARITY WHEN PROCESSING NODE GASKET.157278 D.O.F. 3 RATIO = 5.55947E+09.
1.06	9348	1456	1	1343- Numerical Singularities (All on Gasket Nodes)
1.07	4.48E+05	62817	185	4- Numerical Singularities (Gasket Nodes 190856, 190906, 190941, 190923)
1.08	3.96E+05	55422	158	ZERO
1.09	4.01E+05	56331	173	ZERO
1.10	3.63E+05	51294	161	ZERO
1.11	7.94E+03	1152	1	ZERO

Table 14: Summary of Series 1 Results

The S11 pressures along the circumference of the Stop, Flexstop and Full Beads of the gasket are shown in Figures 44, 45 and 46 for the Cold clamping condition. For the analysis, the 0° corresponds to the intake side of the engine assembly and follows a clockwise path around the circumference of the bore. The highest pressures occur on the Flexstop and the lowest occur on the Stops. For each analysis, at the 90° and 270° circumference points, there exists a sharp decline in the S11 Pressure. Figure 41 shows the typical gasket pressures and closures at the gasket. There are areas of extremely high pressure at the upper and lower tabs that contain the small, upside-

down studs. These can be attributed to the cutting of the head, which significantly decreases the bending stiffness at the tab areas.

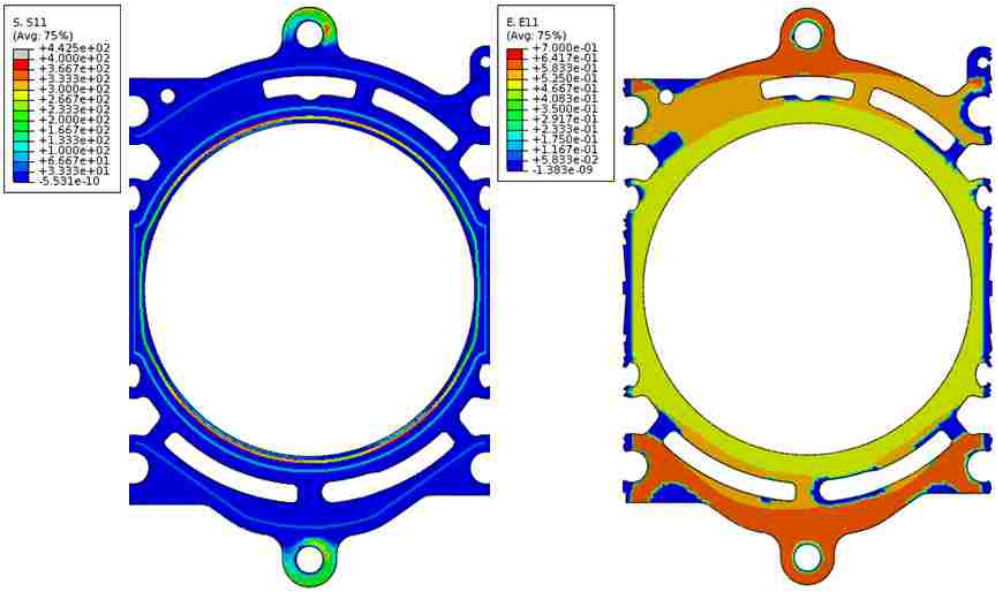

Figure 41: S11 pressure (left) and E11 Gasket Closure (right)

The first change of the analysis was to switch which surface contained the No Separation option, the Head or the Block. The corresponding results were nearly identical, as was the amount of time and number of iterations taken to complete the simulation. Also, the 4 Numerical Singularity warnings on the Gasket Nodes were still present.

The next analysis changed the Discretization Method from Node to Surface to Surface to Surface. The results corresponding results were almost identical, however the wallclock time was reduced to approximately one half and the number of iterations required were only slightly reduced. Also, the 4 Numerical Singularity warnings on the Gasket Nodes were still present.

Subsequently, the Sliding Formulation was altered. It was discovered that a major consequence of changing from Finite to Small Sliding is the massive reduction in computational cost required. The total number of increments reduces from approximately 170 to 1 when the change is made. However, when the sliding formulation is changed from Finite Sliding to Small Sliding, an interesting effect occurs for the Displacement U3 and the Gasket Closure E11. Within areas of the gasket that are not in direct contact with the Head and Block, the Displacement U3 "spikes" to unrealistic values. These spikes are also present for the E11, S11 and Von Mises values in areas that are in normal contact with the head and block. For the Gasket Closure E11, there exists random spotting on the gasket for area in contact with the head. Figure 42 below shows a typical result. The results for analysis' 1.03, 1.04 and 1.05 are all identical, with the presence of the spikes

and spotting. However, it was found that by completely turning off the Slave Adjusmtent option for Analysis 1.06, the spikes were significantly reduced for U3, E11 and S11. Also, the change resulted in 1343 Numerical Singularities, all on gasket nodes. The remaining Analyses show identical results to the previous, with the only differences being in the spiking and spotting.

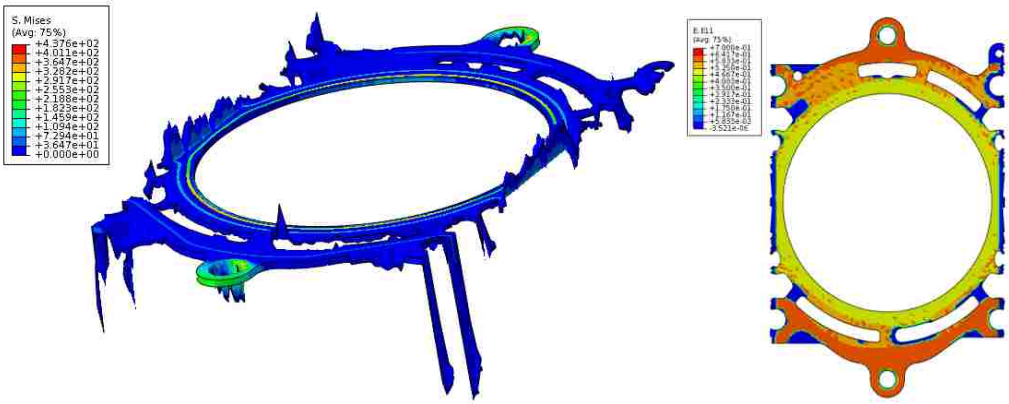

Figure 42: Areas of Von Mises Spiking (left) and E11Gasket Closure spotting (right) with a scale factor of 5

A major discovery of the analyses was the complete elimination of the spiking of the gasket seen in the interaction study. This was accomplished by adding normal values to the input file prior to analysis. A typical result is shown in Figure 43, in which the large displacements and spotting of Figure 42 were eliminated.

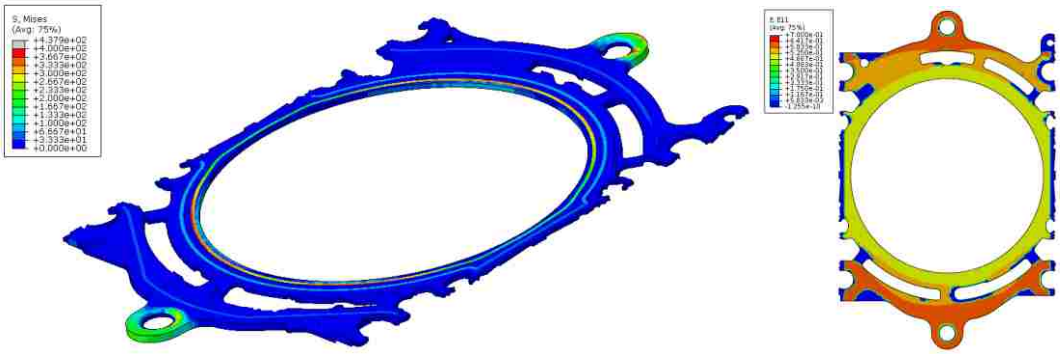

Figure 43: Typical results of Series 2 showing no Spiking and Spotting, as seen in Series 1.

The values of the Pressure in the Gasket Elements, S11, stress are identical for all of the analyses of the interaction study. Figures 44, 45 and 46 below show that for the simulations, at the beads, the pressure curves completely overlap each other.

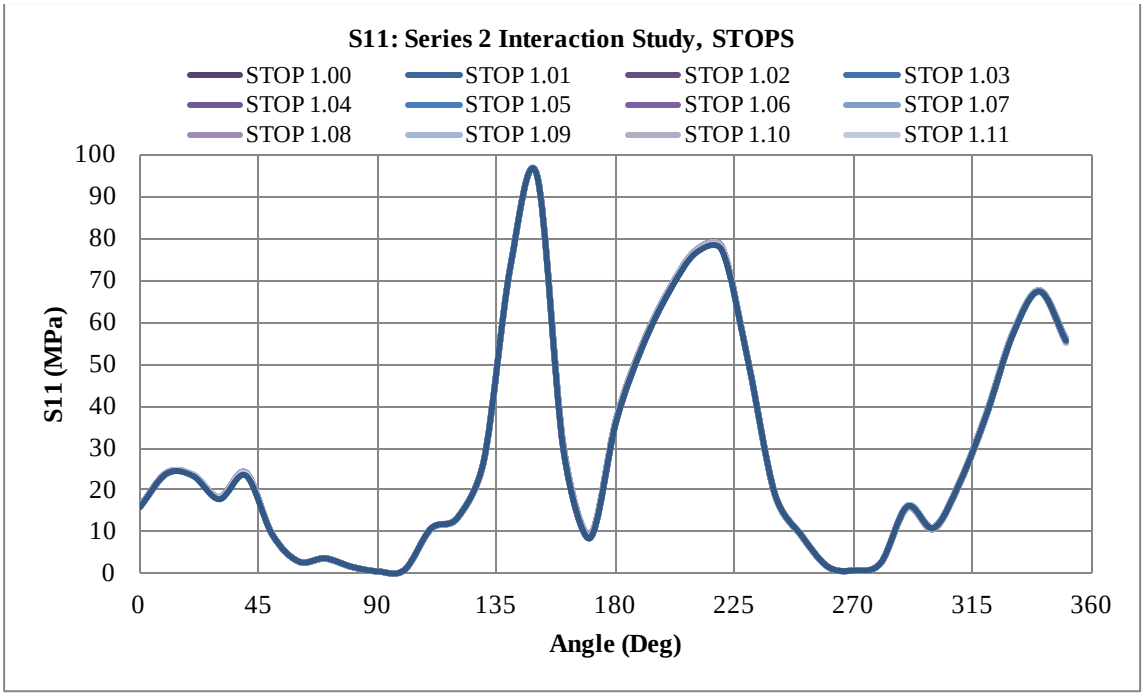

Figure 44: Circumferential S11 Pressures on all of the Series 1 Stops

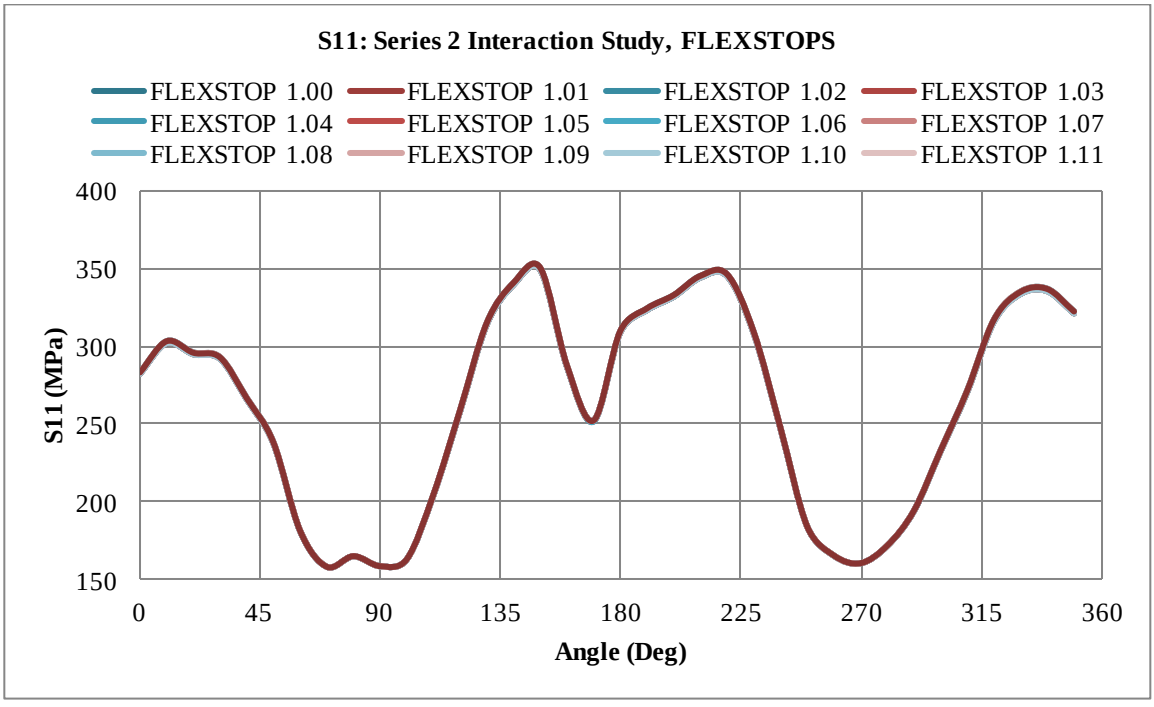

Figure 45: Circumferential S11 Pressures on all of the Series 1 Flexstops

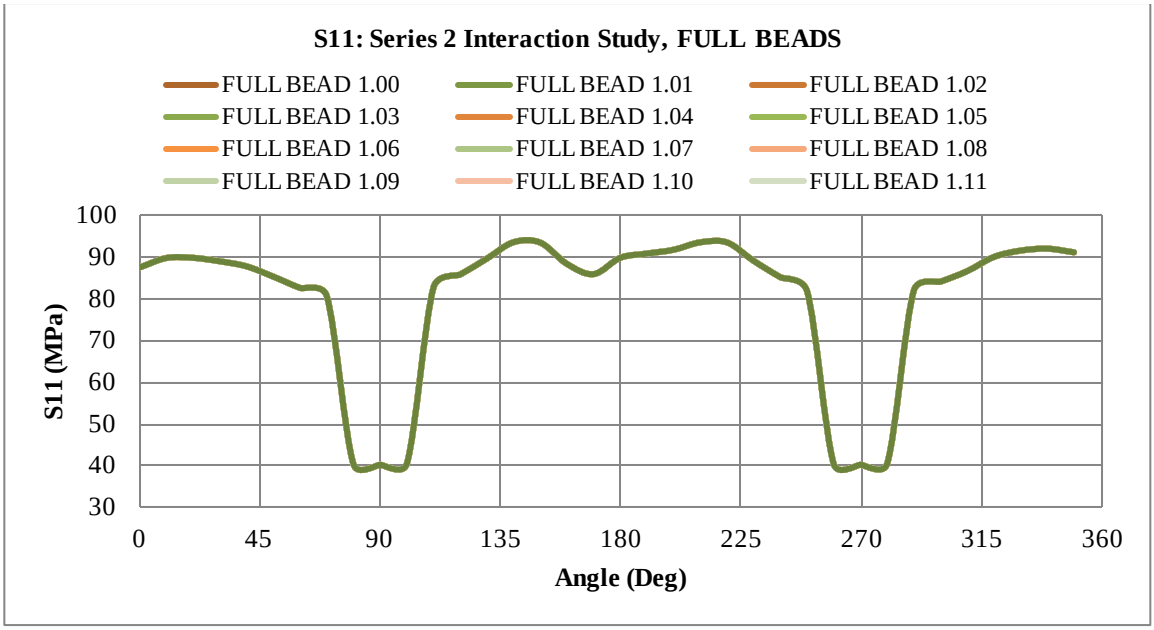

Figure 46: Circumferential S11 Pressures on all of the Series 1 Full Beads

5.2.1 Areas of Incompatibility

Figure 47 shows a Series 2 Interaction Study Analysis case with the Von Mises stresses applied. The black arrows are pointing to areas of significant stress peaks, which can be seen in around the entire assembly. These high stresses occur at the partition planes where the elements in contact are of different orders; quadratic elements are used closer to the deck face and linear elements are used for the remainder of the head and block volumes. Where the elements meet, there are free nodes that cannot be shared between the elements. This results in incompatibility between the elements. It is common for pressure spikes to exist in these areas. Since the area of interest is directly at the deck surfaces, the pressure spiking does not affect the analysis requirements.

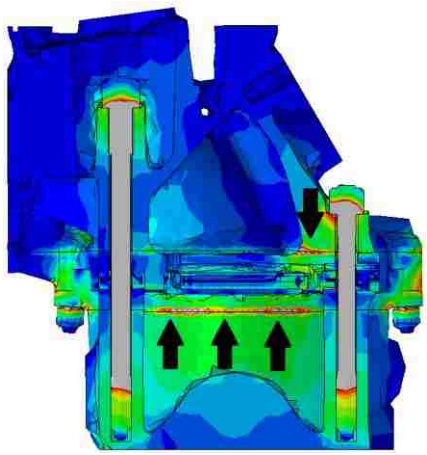

Figure 47: Areas of incompatibility at varying element types

5.2.2 ABAQUS Interactions and Settings Discussion

It is apparent that altering the Interactions does not have a significant effect on the pressure distributions at the gasket beads. The main consequence of changing the Interactions appears to be the speed of the simulation and amount of increments needed for convergence. It is obvious that the largest influence on the quality and speed of the analysis is caused by the alteration of Sliding Formulation. When the Finite Sliding Formulation is used, the analyses require a large amount of time and iterations to complete successfully. However, the results are acceptable and do not contain the inaccurate peaks. When the Small Sliding Formulation is used, the total time and iterations requires are significantly reduced, however there exists the strange spikes and spotting in the results.

If a gasket analysis must be completed with the absolute smallest amount of time or CPU power, the user is able to accomplish this by using a certain combination of interactions and options. Since it was found that the using the Small sliding formulation gave acceptable results, one can use this method for a very fast simulation. It must be taken into account, however, that the results will contain large, inaccurate displacements in areas of non-contact. The interaction study gave good insight into the effects of the Interactions and their properties at the deck interfaces. For the proceeding Series of analyses, regarding Interactions and their properties, separation would be allowed at only the Head and Gasket interface. The remaining interactions would use Small Sliding formulation, Surface to Surface discretization, a slave adjustment of 0.1mm, a penalty friction formulation, a hard contact and a friction coefficient of 0.15.

The simulations ran in Interaction study also gave a good indication of the consequences of altering the Sliding formulation and Discretization Method options, while adding the gasket normals to the input file and using the NLGEOM option. The major discovery of the these analyses was the elimination of the spiking and spotting on the gasket that was present on the gasket results of previous studies. This was attributed to the addition of the gasket normals to the input file. It was also confirmed that changing the Sliding Formulation from Small Sliding to Finite Sliding has a major effect on the amount of time and number of increments that are required to complete the simulation. If the Small Sliding Formulation is used, the time required for completion of the simulation is reduced by a factor of 8, which is a substantial gain. The changes do not have an effect on the physical results the simulations.

It was decided that the Small Sliding Formulation and the Surface to Surface options were the best options to use for the preceding simulations. The NLGEOM option and the gasket normal

definitions would be used, as the spiking of the previous Series was eliminated. Analysis 2.01, which used the preceding contact interactions and options, would be used as the basis for comparison in the following analyses.

The Analyses completed in Series 2 Interaction Study gave good insight into the many different options used in the Analysis of a simple Cold Clamped engine case. It was concluded that although the Interaction Properties do not have a significant effect on the physical results of the Cold Clamping Pressures, they do greatly affect the total CPU time and amount of iterations needed for completion of the analysis. The pressure distribution results of Series 1 and 2 are almost identical, but the times and iteration amounts vary significantly. It was shown that the greatest contribution to the change in CPU time was the Sliding Formulation; a Finite Sliding Formulation resulted in a large processing time and a Small Sliding Formulation resulted in a relatively small amount of processing time. However, if the Small Sliding Formulation was used without the gasket normal definitions included in the input file, strange spikes and valleys are manifested on the gasket. When the gasket normal definitions were added to the input file before the analysis was run, the spikes and valleys disappeared. The addition of the Nonlinear Geometry option (NLGEOM) did not have an effect on the pressure distributions on the gasket, but did increase the amount of iterations needed for convergence and CPU time by approximately a factor of 10. It was decided to continue using the NLGEOM option, as the complexity of the Analyses would be increasing with the addition of multiple Steps, temperatures and pressures.

5.2.3 Single Cylinder Mesh Refinement Results

The analyses completed in Series 2: Mesh Refinement dealt with the alteration of the mesh at the head/gasket and block/gasket interfaces. The processing time needed for convergence is directly related to the amount of nodes and elements in the assembly. As the total amount of nodes and elements was decreased, the processing time decreased as well. The opposite occurs for an increase in nodes and elements. This is a typical result of any finite element analysis, as computational time is highly dependent on the mesh size. The summary of the results is shown in Table 14.

Mesh Refinement Results						
Trial	**Successful**	**CPU Time (s)**	**Wallclock Time (s)**	**% WallClock Time**	**Total Increments**	**WARNINGS**
3.00	YES	4.75E+04	7186	100%	18	4- 2 Negative Eigenvalue, 2 Distortion
3.01	YES	4.09E+04	7042	98%	16	5- 4 Negative EV, 1 Excessive distortion
3.02	YES	9314	1462	20%	16	2- 1 Negative EV, 1 Excessive Distortion
3.03	YES	14251	2595	36%	16	2- 1 Negative Eigenvalue, 1 Excessive Distortion
3.04	YES	3.34E+05	45296	630%	9	3- 1 Negative Eigenvalue, 2 Excessive Distortion
3.05	YES	2.88E+05	47171	3240%	13	4- 2 Negative Eigenvalue, 2 Distortion
3.06	YES	4.63E+05	84998	1183%	6	8- 3 Negative Eigenvalue, 2 Numerical Singularities, 3 Excessive Distortion
3.07	YES	84703	11675	802%	9	5- 4 Negative Eigenvalue, 1 Excessive distortion

Table 15: Mesh Refinement Results

The S11 Pressure values at the Stop, Flexstop and Full bead were overlaid for each analysis and are shown in Figures 48, 49 and 50 below. It is evident that each analysis results in a different distribution of pressure along the beads of the gasket. Analyses 3.01, 3.02, 3.03, 3.04 and 3.06 tend to relate closely with each other, with only minor differences along the paths. The major area of difference occurs at the 0-45° areas, but then tend to converge for the remainder of the circumference. Major differences of Analyses 3.05 and 3.07 can be seen along the entire angular pressure maps. The Full Bead curve for Analysis 3.07 contains a large valley at 90° and then only a slight dip at 270°. This does not correspond with the other analyses, which contain equal, medium valleys at both of these locations. The reason for the differences can be attributed to the extra nodes on the gasket of 3.07, due to the change from linear to quadratic elements, which add additional nodes at the midsurfaces of the element. Differences in pressure could be caused by the method which ABAQUS uses to determine the average element pressure at the centroid, depending on if the element is linear or quadratic. The hexagonal element analyses of 3.05 and 3.06 seem to follow the trends of the other analyses, but do show areas of difference. This is prevalent at the 90° and 270° areas of the Flexstop, where 3.05 does not reach the low values of the other analyses. All other results at the different beads tend to correlate with the others, with only minor differences.

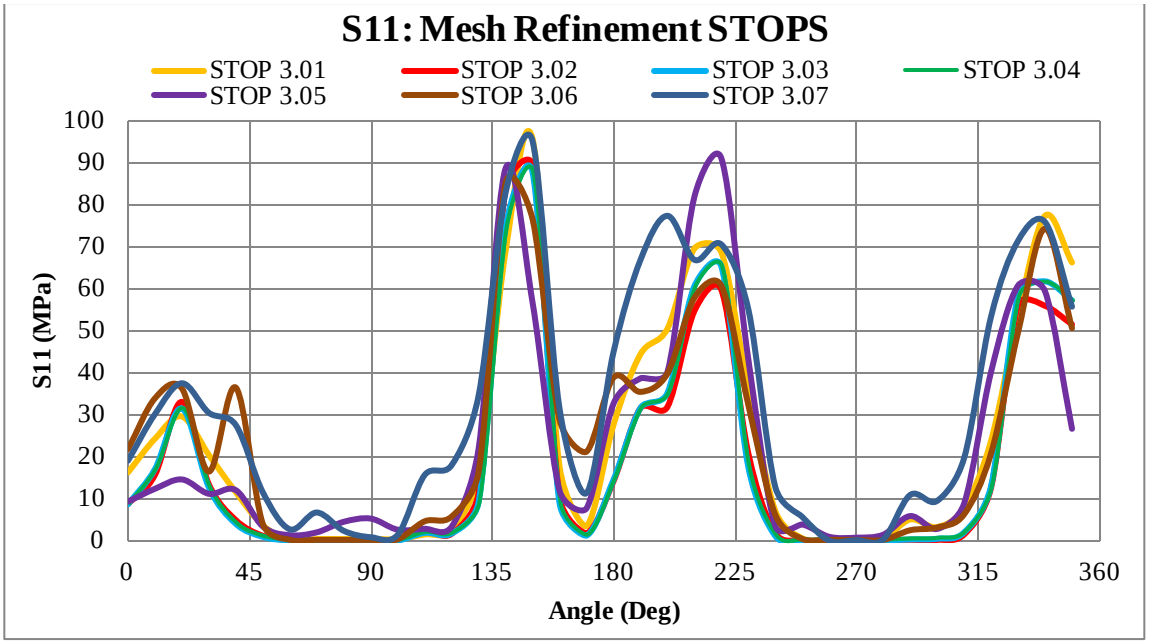

Figure 48: Circumferential S11 Pressures on all of the Mesh Refinement Study STOP bead

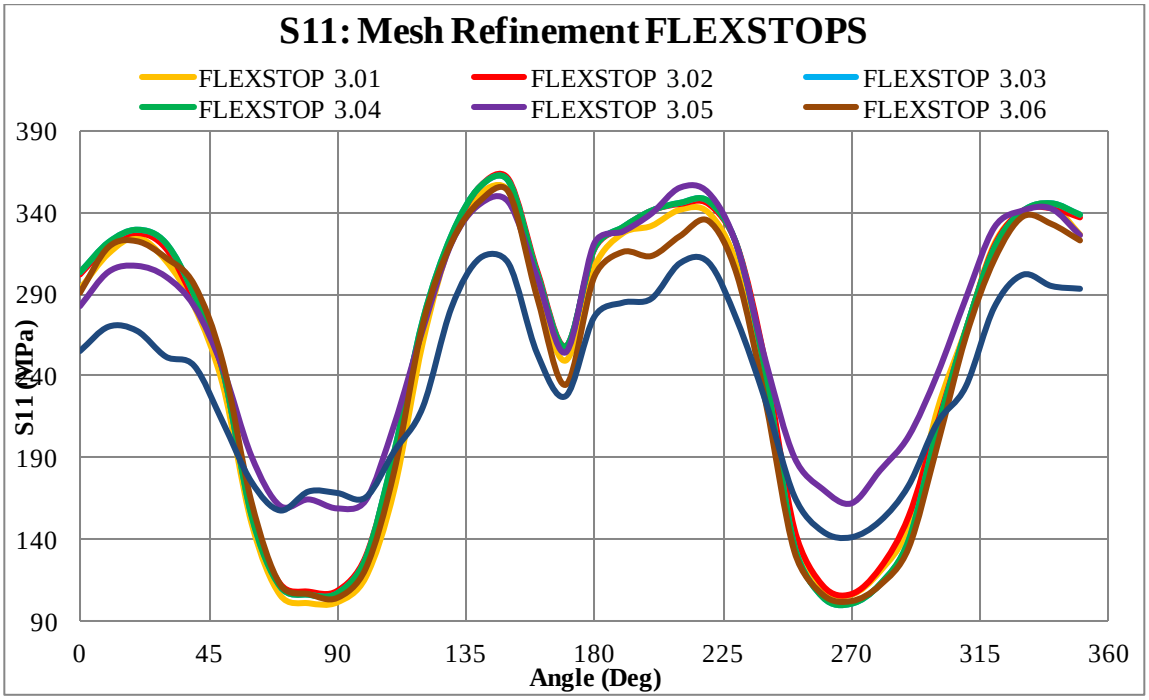

Figure 49: Circumferential S11 Pressures on all of the Mesh Refinement Study FLEXSTOP

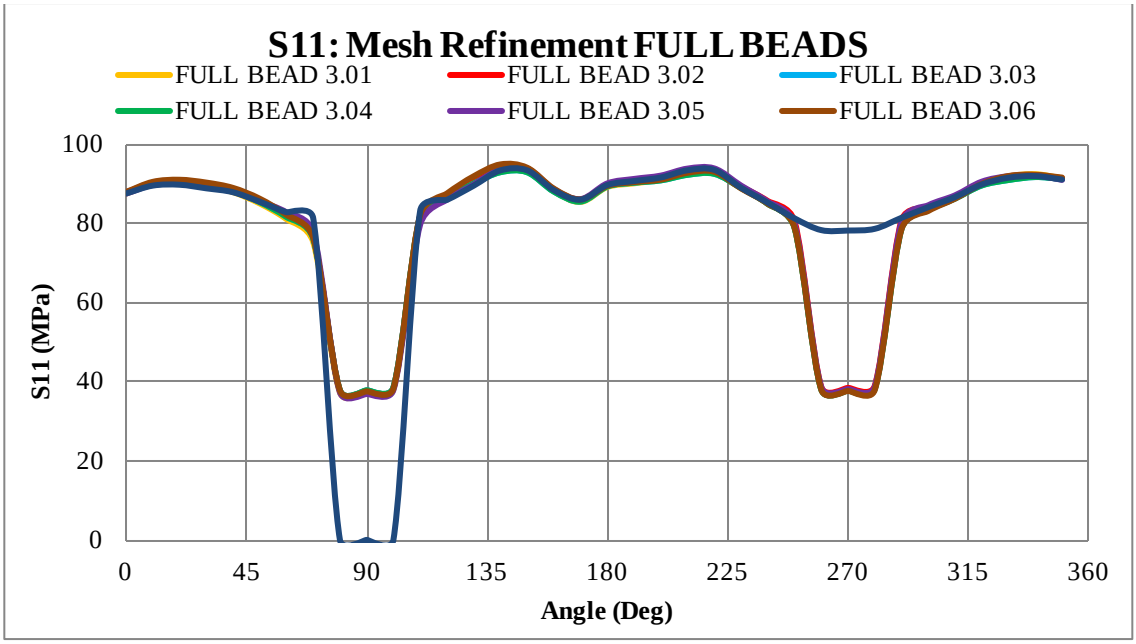

Figure 50: Circumferential S11 Pressures on all of the Mesh Refinement Study FULLBEAD

An apparent result of changing the mesh density at the engine head and block is the distribution of pressures at the deck surfaces themselves. As the density of the mesh at the deck faces decreased, the pressures at the faces tended to be become less detailed. Using Baseline Analysis 2.01 as a comparison, as the size of the mesh increased from 1mm of Analysis 2.01 to 6mm of Analysis 3.03, there is a significant reduction of pressure resolution. The areas of pressure in contact with the gasket beads can clearly be seen with the 1mm meshes, however disappear completely with the larger mesh size. The finest resolution of pressure occurs at the head deck face of Analysis 3.06. This is due to the large number of nodes of the quadratic hexagonal mesh on the engine block and head. The trends can be seen below in Figure 51.

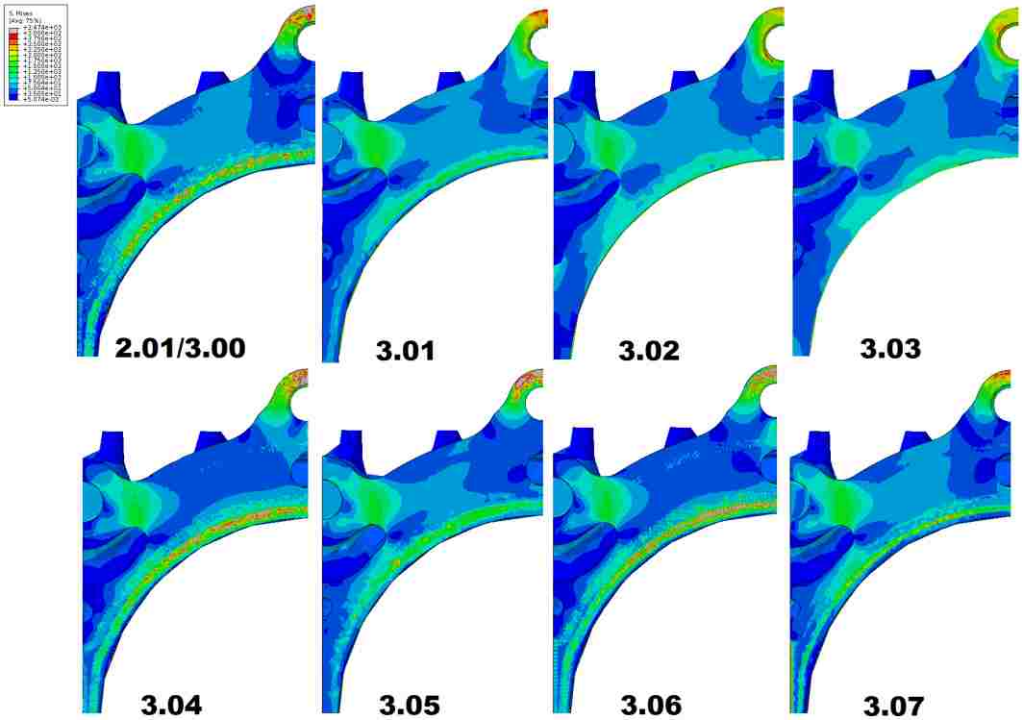

Figure 51: Pressure Distributions at the Engine Block deck faces of Mesh Refinement Study.

5.2.4 Mesh Refinement Discussion

Mesh densities and types at the deck surfaces do alter the circumferential distribution of the gasket pressure. Every different mesh used resulted in a different pressure profile, however the paths do follow the same relative shape. The greatest effect that the element sizes and densities have, however, is at the deck faces themselves. If a high resolution of pressure distribution at the deck face is needed, a smaller quadratic element must be used.

The results of Mesh Study indicate that the mesh types and sizes have a major effect on the results of an analysis. Simple alterations of size or type result in the pressure distributions along the entire circumferential path along the gasket beads. Not only are the gasket pressures altered, it was shown that the head and block deck pressures were affected as well. Therefore, if detailed information is needed at the deck surfaces, it is advised to use a element size of 2mm or smaller. The decreased number of nodes and elements resulted in decreased processing time and iterations, which is a simple result of the computer having to solve less equations for convergence.

The bottom-up meshing technique used for Analyses 3.05 and 3.06 is cumbersome and time consuming. The resulting mesh does not perfectly match the geometry of the engine, as the bottom-up technique can only follow a straight path in one direction. It also introduces an incompatibility between the meshes of adjoining regions close to the areas of interest near the

deck faces. For these reasons, this meshing technique was not considered for the proceeding analyses. The alteration of the gasket input file of 3.07 to be composed of quadratic elements instead of linear elements was not a difficult or time consuming process. The results tend to follow the same trends, but visually are much more refined due to the increased number of nodes. Since the input file is supplied in the state of linear elements and the simulation was more time consuming with very little difference of pressure distribution, there was no reason to apply the change to quadratic elements for the proceeding analyses.

For the proceeding analyses, it was decided that the head and block deck would consist of one layer of 1mm Quadratic Tetrahedral elements. The gasket element type would remain linear, as is supplied in the input file.

5.2.5 Varying Gasket Element Types

A major strength of completing an analysis using the entire geometry of the gasket is the ability to visualize parameters at each layer of the gasket assembly. The first studies using various gasket elements focused on Conventional Shell Elements. The Von Mises stress values were determined for the 4 gasket layers and fire ring and are shown below in Figure 52.

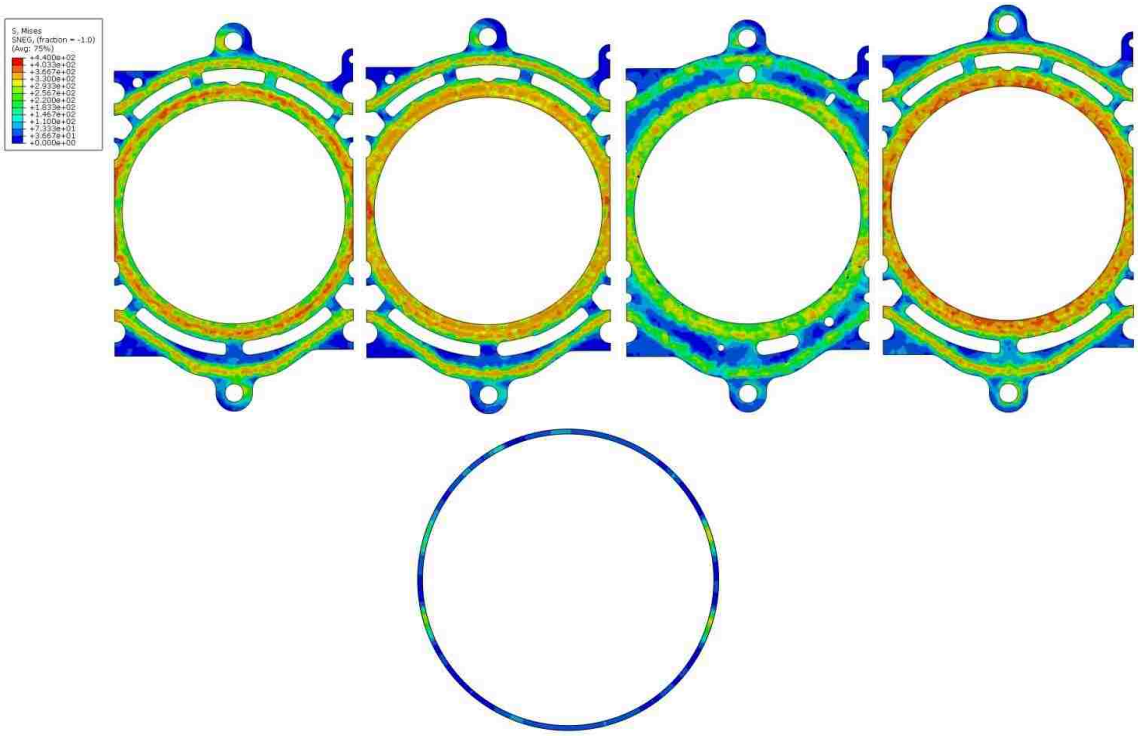

Figure 52: Von Mises stress at each gasket layer and Fire Ring. Clockwise from Top Left; Layer 1, Layer 2, Layer 3, Fire Ring, Layer 4

It is important to be able to visualize the stress patterns on the head due to the compression of the gasket, as these should be the most similar values to the real world Fuji Film results. The contact pressure values at the head and on layer 1 as a result of the cold clamping of the gasket is shown below in Figure 53. On the far right is the Fuji Film results for comparison.

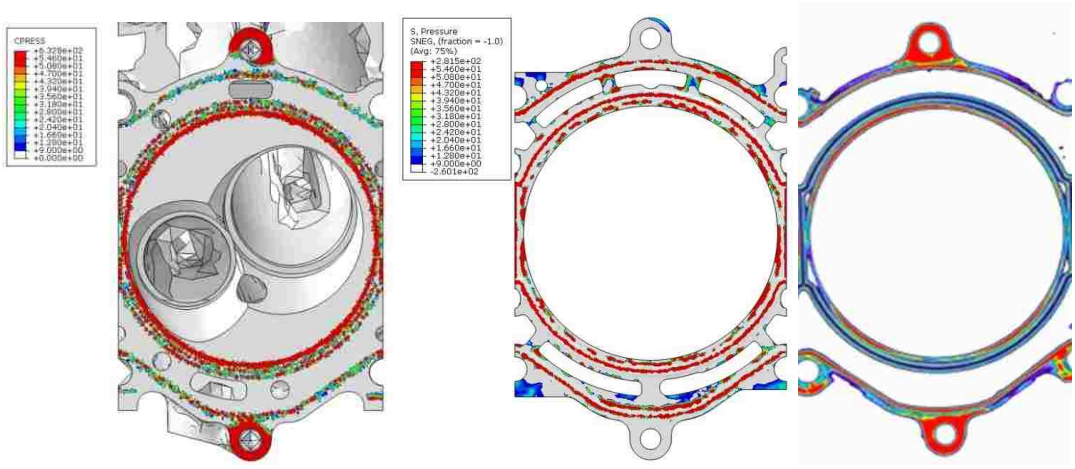

Figure 53: Contact pressure on head face and pressure at gasket layer 1 compared to the Fuji Film results (right)

The pressure values for the virtual case appear to be much higher than that of the Fuji Film case. However, there are similarities with the contact pressure patterns around the circumference of the cylinder. The bead stress profiles are able to be distinguished from the non pressured areas of the gaskets, but the resolution is much less than the Fuji Film.

5.2.6 Varying Gasket Element Discussion

The analyses using continuum Shell elements and 3D elements were unsuccessful, for two different reasons. The continuum shell simulations were unable to converge. The 3D Gasket element simulations were able to converge, however the results unusable. Regarding CPU time, the 3D analysis took approximately 800 iterations and 257000 seconds of CPU time.

Using continuum elements and 3D, the analyses were unable to converge, but using conventional shell elements, the analyses were able to converge. Even using a single cylinder model caused the analyses to require much CPU time. Conventional shell elements do not transmit forces in their thickness direction, which ensures that the results will not be completely accurate to real world results. The results obtained from the shell elements were similar to the results found in the 2D axisymmetric analyses. As the gasket layers are compressed, the beads of the layers are compressed as well, which causes areas of tension and compression in the layers. Due to the

behaviour of Shell elements, which do not transmit forces in the normal directions, these stresses are occurring due to shear loading of the beads. The resulting contact pressures on the head show minor correlation.

Before any analysis is completed, it is important for the analyst to determine what the goal of the simulation is. The analysis using gasket elements to represent the overall structure of the gasket, but not the internal layers and their behaviours, is appropriate when the information regarding the behaviour of the head and block are required. This type of analysis is relatively computationally inexpensive and gives satisfactory results. The type of results that can be achieved are;

- Head and Block deformation
- Uncoupled stresses and strains on the gasket elements
- Gasket bead closures
- Thermal expansion values of the head and block
- Dynamic motion of block head and gasket (with dynamic analysis)

When an analysis on the behaviour of the gasket layers is required, the analyst must perform a simulation in which all of the layers of the gasket and their fire rings are included. As a relatively simple and inexpensive analysis, the 2D axisymmetric can give useful information as to what occurs as the gasket is compressed. The interactions of all of the layers can be quantitatively and qualitatively studied. The 3D studies using all of the gasket layers should be completed if information regarding the stress in all of the gasket layers or fire rings is required.

When compared with the Fuji film analysis, the FEA pressure values were always higher than the Fuji Film. For all types of analysis, it is apparent that the finite element pressure results are always higher than the real world pressure numbers.

The knowledge gained through results and modeling experience of Series 2 was crucial in the creation of the Full Bank Models of the proceeding sections. Using a small quarter model gave the ability to make changes very quickly and obtain results in a short period of time, in most cases. The proceeding full bank model uses the best configuration found from the Quarter Bank Analyses in terms of contact interactions and mesh modeling techniques.

5.3 Series 3: Full Bank Results

The Series 3 Analyses were completed for both the left and right banks of the engine. Both bank assemblies use the same gasket input model. The left bank completed with a Total CPU time of $4.5x10^5$ seconds and 22 Total Iterations. The right bank completed with a Total CPU time of

$4.6x10^5$ seconds and 23 Total Iterations. Figure 8.4 below shows the pressure distribution on the left and right bank gaskets, along with the directions that were followed for the pressure graphs. The results are that the pressures of the left and right banks are symmetrical, which allows for an easier comparison between the two.

5.3.1 Fuji Pressure Film Comparison

Fuji Paper is a powerful technology that allows the pressure distribution to be found between two contacted surfaces. Procedure wise, it is as simple as placing the special paper between the head and the gasket, and tightening the head to the block using the standard stud torques. The Fuji paper results supplied by Dodge are shown in Figure 54 and have a maximum pressure value of approximately 55 MPa and a minimum value of approximately 9 MPa. This is due to the scale that Fuji paper is able to measure, and does not correspond to the actual maximum pressures on the gasket. The maximum pressure values of the Series 3 Analyses were approximately 380 MPa. Figure 54 also shows the FEA analysis of the right engine bank with the same limits of the pressure legend. The color scale is approximately the same as well. Both analyses show that the body of the gasket generally does not contain any areas of pressure, except at the stud bearing surfaces. The dark blue areas of the Fuji Paper results correspond to areas of negligible pressures and can be considered to be zero for the Comparison. Figure 55 shows the comparison of the pressure values with a high pressure Fuji Film.

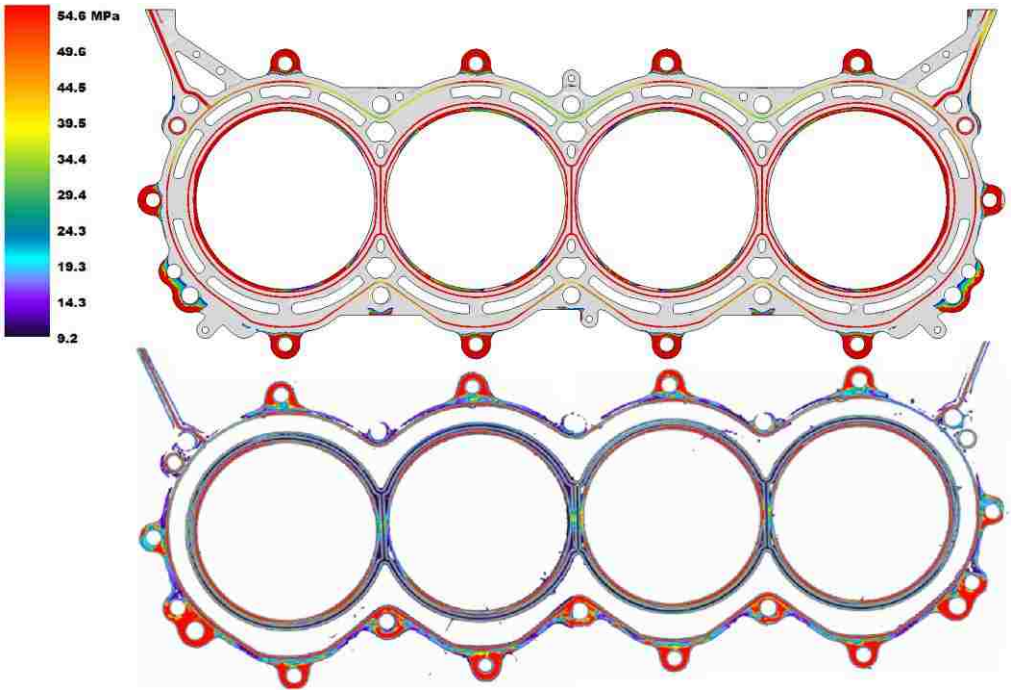

Figure 54: FEA Analysis of the Right Bank Gasket elements (Top) and Medium Fuji Paper results as supplied by Dodge (Bottom)

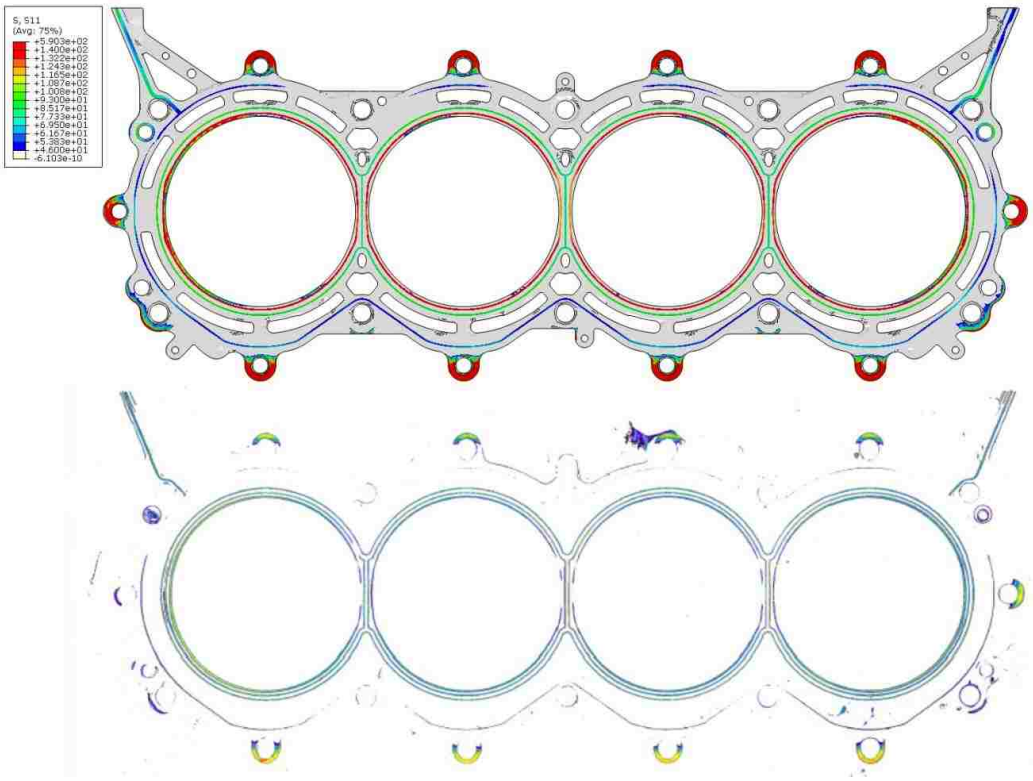

Figure 55: FEA Analysis of the Right Bank Gasket elements (Top) and High Fuji Paper results as supplied by Dodge (Bottom)

The pressure maps of the FEA and Fuji film for Cylinder 7 are shown below in Figure 56. Visually, the Halfbeads at the very outer edge of the gasket tend to correlate. The location of the Halfbead is shown in Figure 20, and is the bead closest to the outer edge of the gasket. Unlike the Stop, Flexstop and Fullbeads, the Halfbeads do not follow a distinct path around each cylinder, rather only a single path around the entire gasket. Thus, the bead is difficult to analysis using the pressure map method. There are peaks at the 0° and 135°-270° areas, with a minimum pressure from 270°-360°.

The pressure maps of the Fullbeads do not correlate, as the pressure values of the FEA map are much higher than the Fuji map. The entire circumference of the FEA Fullbead map is much higher than the maximum value of 55MPa, where the entire circumference of the Fuji Map holds at approximately 35MPa. The Fuji map appears to have two separate Fullbead sections, very close to each other, which could explain the major difference. An investigation into the material properties provided by FelPro is suggested for future analyses.

In the Fuji paper maps, it is very difficult to distinguish the Stop and the FlexStop as they appear to be combined. The pressures of the FEA Flexstop are significantly above the limits of the Fuji

map, but the FEA Stop bead tends to correlate. Regarding the Stop/Flexstop of Cylinder 7 gasket, starting at the 0° point for both maps and following the circumference around in a clockwise manner, many similarities can be seen using Figure 8.8.

- **0° - 45° :** The pressures start at approximately 35 MPa for both maps. The FEA map tends to decrease slightly towards 45°, where the Fuji map slightly increases and peaks at 45°.
- **45° - 90° :** Both maps decrease to minimum values until the 90° area. The FEA map quickly drops to a pressure of below 9 MPa, while the Fuji map drops to a minimum of approximately 20MPa.
- **90° - 135° :** The pressures both rise significantly and peak at the maximum value. The FEA map peaks slightly after 135°, while the Fuji Map peaks at 135°.
- **135° - 180° :** The pressures both reduce to a much lower value. At 170°, the pressure of the FEA map is approximately 10MPa and the Fuji map is approximately 35MPa.
- **180° - 360° :** Both pressure maps rise to the maximum value of 55Mpa and remain above this value up to the starting point.

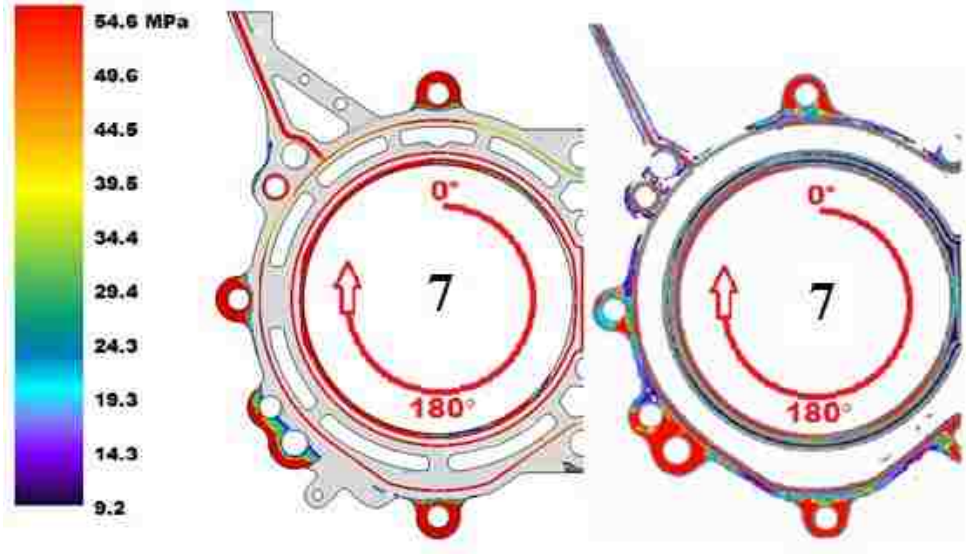

Figure 56: FEA Result (left) and Fuji Paper Result (right) of Cylinder 7

The Pressure Maps of the FEA and Fuji paper for Cylinder 5 are shown below in Figure 57. As was the case with Cylinder 7, the Halfbeads at the top and bottoms edges of the gaskets tend to correlate. There are peaks at the 0° and 180° areas, and decreasing values while moving further away. Similarly to Cylinder 7, the pressures maps of the Fullbead to not correlate. The entire circumference of the FEA Fullbead map is higher than the maximum value of 55MPa, where the

entire circumference of the Fuji Map holds at approximately 35MPa. The Fuji map appears to have two separate Fullbead areas, which could explain the major difference.

Regarding the gasket Stop and Flextop of the Cylinder 5 gaskets, starting at the 0° point for both maps and following the circumference around in a clockwise manner, many similarities can be seen.

- **0° - 45° :** The FEA map starts at a value of approximately 20Mpa where the Fuji map starts at almost 55MPa. The FEA map increases slightly to 40MPa and then reduces to the minimum. The Fuji map steadily reduces to a value of 45MPa.
- **45° - 90° :** Both maps decrease to minimum values until the 90° area. The FEA map quickly drops to a pressure of below 9 MPa, while the Fuji map drops to a minimum of approximately 20MPa.
- **90° - 135° :** The pressures both rise significantly and peak at the maximum value. The FEA map peaks slightly after 135°, while the Fuji Map peaks at 135°.
- **135° - 180° :** The pressures both reduce to a much lower value. At 170°, the pressure of the FEA map drops below 9MPa and the Fuji map is approximately 30MPa.
- **180° - 225° :** Both pressure maps rise to the maximum value of 55Mpa .
- **225° - 270° :** Both pressure maps drop significantly and reach minimum values of below 9MPa at 270°.
- **270° - 360° :** The pressures rise again to the maximum value and hold this value until 360°.

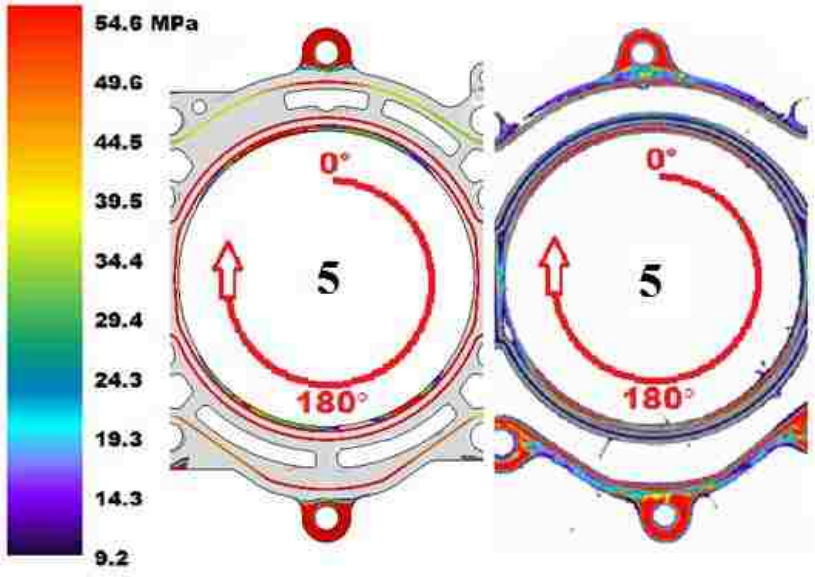

Figure 57: FEA Result (left) and Fuji Paper Result (right) of Cylinder 5

The results of the Full Bank Cold Clamping tests are similar to those of the previous Quarter Model Analyses for the cold clamping case. A major difference occurs at Cylinders 1, 2, 7 and 8 at the front and rear of the engine, where there are additional studs applying a clamping force. The S11 pressures in these areas do not decrease as the Quarter Models do. The FEA and Fuji paper The maps seem to correlate very well in the Halfbead areas, fairly in the Stop/Flexstop areas, and not at all in the Fullbead areas. The Stop and Flexstop pressure results tend to follow the same patterns, with maximum pressures occurring in the stud areas where clamping forces are applied. The minimum areas of pressure always occur at the adjoining region between two cylinder, where the area is far from the stud clamping force. Both pressure maps indicate that the body of the gasket experiences zero pressure for a cold clamping case. As was discussed earlier, the Fuji paper results seem to show a double Fullbead, which might be the source of the inaccuracy. An apparent difference between the Stop and the Flexstop of the FEA model and physical gasket is the placement of each; the FEA model places the 2 beads next to each other, following two distinct paths, where the physical gasket has the Stop overtop of the Flexstop. This makes the pressure distributions for each difficult to determine using only a visual of the Fuji map. Further investigation must be completed in order to determine the cause of these differences. It would be beneficial to work with the gasket supplier, FelPro, in order to gain further understanding into their methods in creating the gasket input file.

5.3.2 Contact Pressure on Deck Faces

The contact pressure on the deck faces were displayed in the results and are shown in Figure 58. The pressures tend to follow a similar pattern of the gasket pressures.

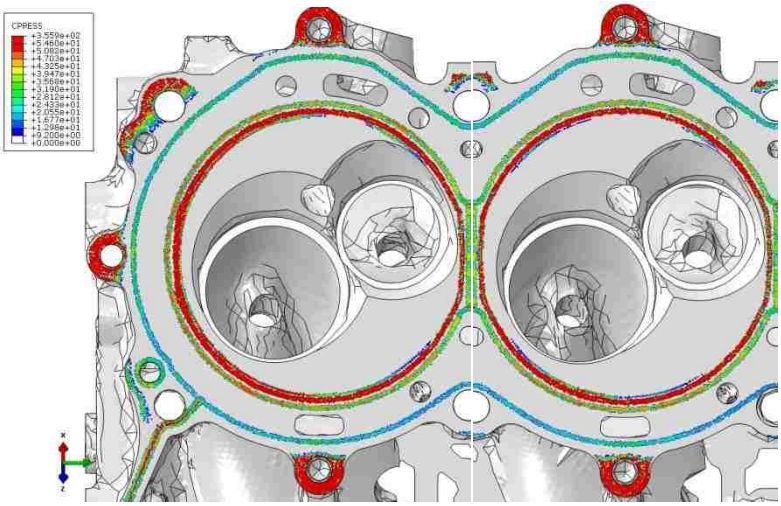

Figure 58: Contact Pressure on Cylinder 5 and 7 Deck Faces

5.3.3 Cold Firing Normal Pressure Comparison

The S11 Pressures at the three main bead areas for all of the engine cylinders were assembled using the methods discussed in Appendix A and are shown in Appendix C. The pressure distributions for the cold clamping and cold firing cases for the right bank are displayed in Figures 59-62. Areas of peak pressure tend to occur at locations close to the studs, where the clamping for is at a maximum. The drastic dips in pressure at the 90° and 270° at the Stop and Flexstop circumferences are apparent in Cylinder 5, as they were in the Quarter Model Analyses completed above. This dip occurs at the 90° of Cylinder 7, however, there is difference at the 270° area. Since there are no studs at the inner areas of the cylinders to apply force, the dips in pressure exist at these areas. As was the case with all of the previous simulations, the FullBead pressure remains relatively steady at just under 100MPa. As the peak pressure of the cylinder pushes the head in the vertical direction, the pressures on the gasket tend to be reduced. This reduction in pressure tends to be even more prominent at the 180° location.

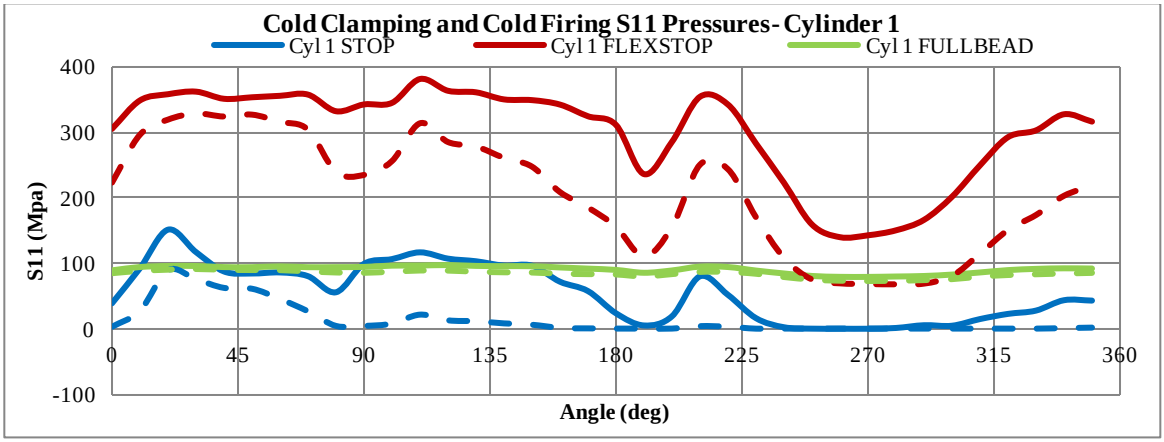

Figure 59: S11 Pressure values at Cylinder 1for Cold Clamping and Cold Firing

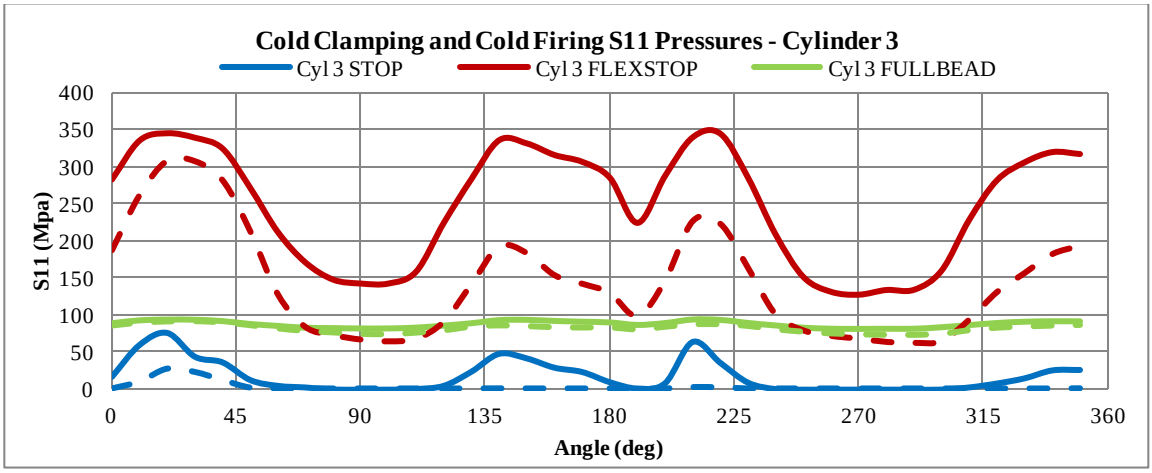

Figure 60: S11 Pressure values at Cylinder 3 for Cold Clamping and Cold Firing

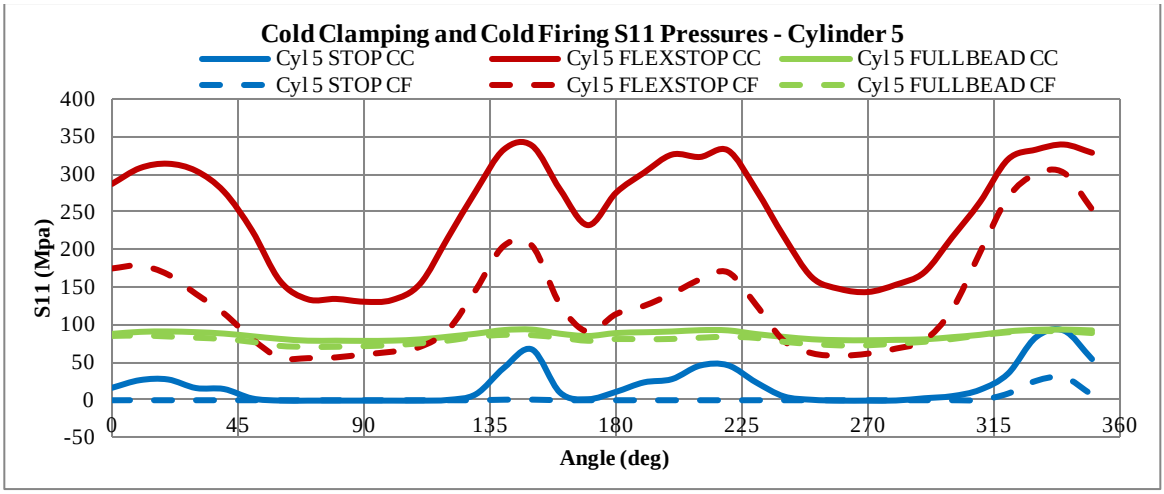

Figure 61: S11 Pressure values at Cylinder 5 for Cold Clamping and Cold Firing

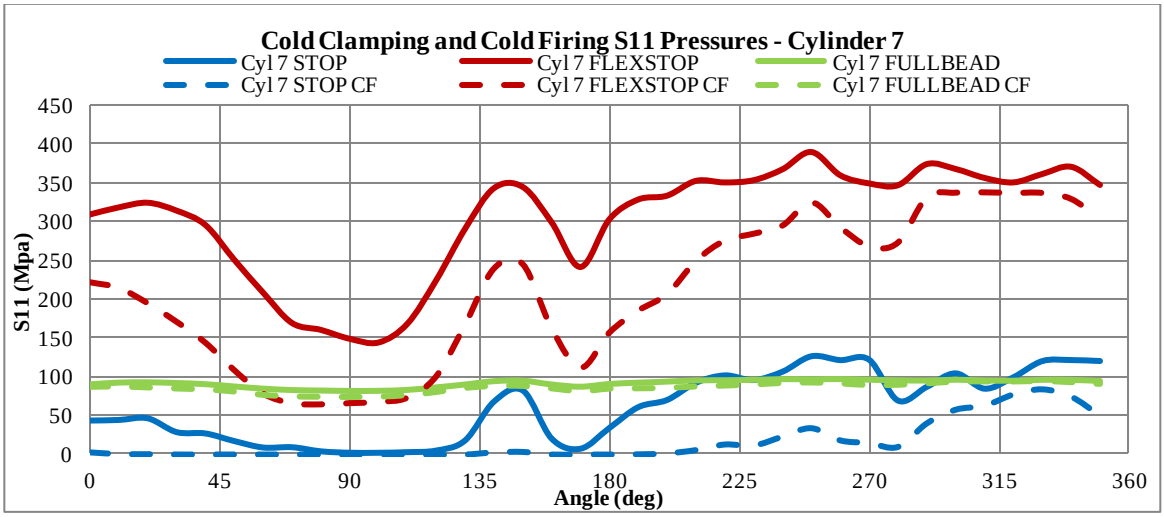

Figure 62: S11 Pressure values at Cylinder 7 for Cold Clamping and Cold Firing

5.3.4 Head and Head Gasket Deformation

As the head is clamped over the gasket and onto the block, it exhibits a cupping behaviour in which the outer edges of the head displace much more than the inner areas of the head. This is shown in Figure 63. Correspondingly, the gasket displacement map also shows this cupping behaviour, as the areas around the edges of the gasket tend to be more compressed than the areas on the inner areas of the gasket. The gasket closures are shown in Figure 64.

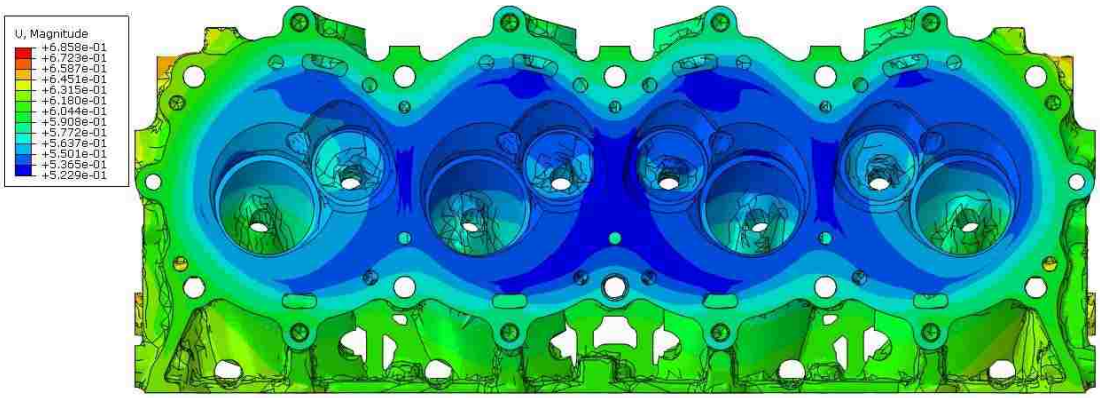

Figure 63: Areas of cupping on the Head deck surface

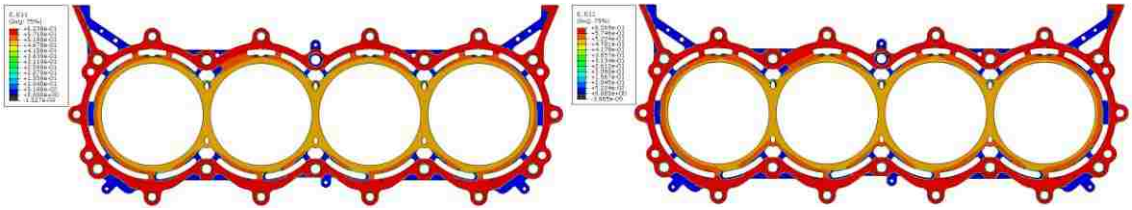

Figure 64: Gasket closure for Cold Clamping (left) and hot Clamping (right)

As the head is bolted to the block with the gasket in between the deck faces, the head deforms around the gasket. This flexure can be attributed to the stiffness of the head. The head geometry is much longer than it is wide, so it is able to flex about the transverse axis of the engine. At the intake side of the head, corresponding to the 0° location currently discussed, the stiffness is much greater than the adjacent location at the 180° location on the exhaust side. This can be attributed to the geometry of the head, which is much bulkier at the intake side. The reduced stiffness at the exhaust side causes has a interesting effect on the contact pressure of the gasket. The cupping phenomena is much less severe at the exhaust side of the head. From the top view in the above pictures, the cupping of the head can be seen in the color scale of the magnitude U. The deformation follows the bolt pattern around the edges of the head. The figures below show the deformation of the head in the cold clamping and hot clamping conditions. The sections are taken at 3 different locations through the head and the deformations are magnified by 100X. When comparing the Figure 66 to Figure 68, (the 180° location vs the 0° location) it can be seen that the head deformation is much greater at the 180 deg location. The geometry of the head at exhaust location an appears to be deform much more than at the intake location, where there is much more material.

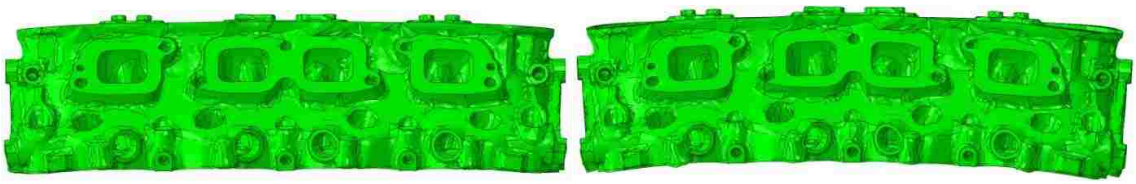

Figure 65: Head Deformation for Cold Clamping (left) and hot Clamping (right) at 100X, No Section

Figure 66: Deformation for Cold Clamping (left) and hot Clamping (right) at 100X, Section cut at Medium Length Studs

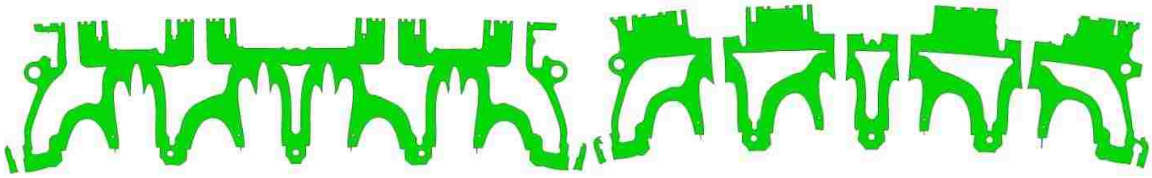

Figure 67: Deformation for Cold Clamping (left) and hot Clamping (right) at 100X, Section cut at Cylinder Centre

Figure 68: Deformation for Cold Clamping (left) and hot Clamping (right) at 100X, Section cut at Long Length Studs

5.3.5 Boundary Conditions with Thermal Map

When adding the thermal analysis, the initial stress distribution on the block after the thermal map had been applied was much too great. The stresses were caused by the block being over constrained along the bottom face. As the material is trying to expand due to heating, it was being held by the constrained, thus causing unrealistic areas of high stress values. The encastre boundary condition was "relaxed" such that only the crankshaft journal faces were constrained. The comparison of the two cases is shown in Figure 69. The result is on the right and indicated that the high stressed area have been greatly reduced.

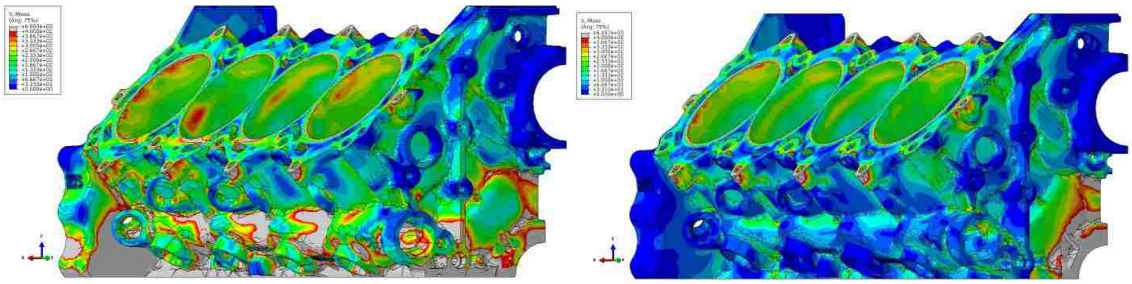

Figure 69: Von Mises Stress values after application of Thermal map. Original BCs (left) and improved BCs (right)

The temperature map addition to the block is shown in Figure 70 below. The section is cut at the cylinder to show that the highest magnitudes of temperature occur at the top of the cylinders.

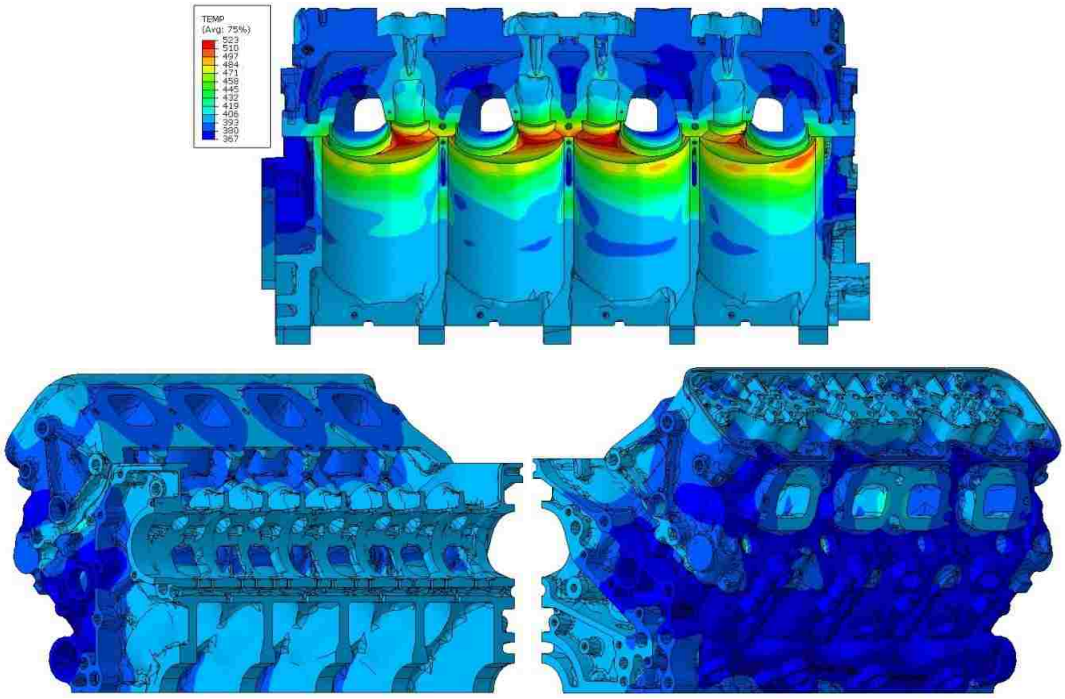

Figure 70: Temperature Map addition on Engine Assembly

5.3.6 Reduced Bolt Loading for All Studs

The S11 pressures on the three bead areas of the gasket during hot firing were determined for 3 cases; 100% bolt load, 80% bolt load and 70% bolt load. The results for the cylinders 1 and 5 hot firing case are shown in Figure 71 and Figure 72 below. For each of the bolt load cases, there exists a dip in pressure at the 170deg locations. Comparing the 100%, 80% and 70% bolt loads, it is seen that, after the thermal map has been applied to the block and head, the reduction in S11 pressures is very minimal. The pressure patterns follow the same shape around the cylinder circumference for all bolt loading cases. The Stop pressure curves tend to fluctuate and approach

zero pressure at the 170deg locations. The Fullbead curve is relatively flat, with a small reduction in pressure at the 170deg location.

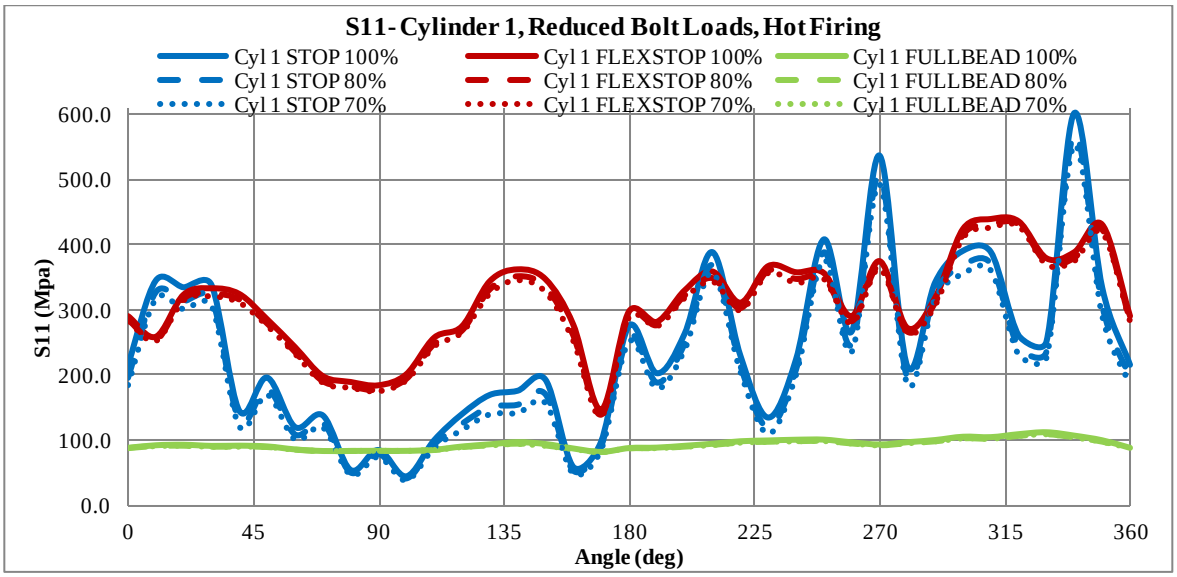

Figure 71: S11 Pressures during reduced Bolt Loads, Cylinder 1

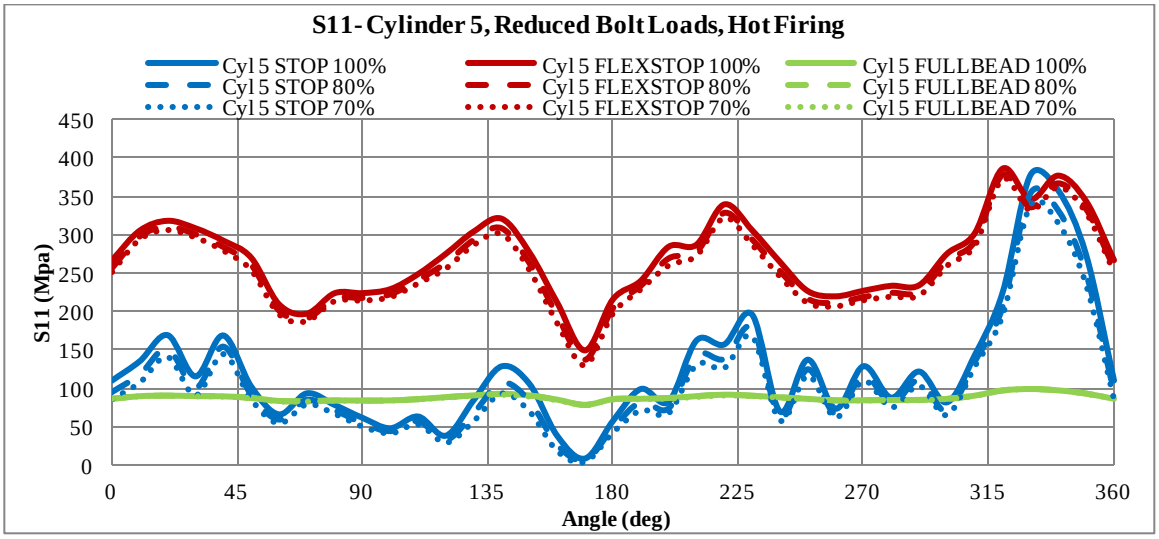

Figure 72: S11 Pressures during reduced Bolt Loads, Cylinder 5

It was shown that the reduction in bolt clamping forces for the long, medium and short length studs caused by the heating of the stud material, did not significantly reduce the S11 pressure on the gasket beads. For the Stop and Flexstop gasket layers, there are only minor reductions in S11 pressures. For the Fullbead layer, there is negligible pressure reduction. After the pressure map is applied, the major contributing factor of pressure on the gasket is the expansion of the head and block. Regardless of the bolt tension magnitude, there always exists dips in the gasket pressure at the 170 deg location. The addition of the thermal map caused the head and the block to expand

quite substantially. This expansion created more clamping force on the gasket and thus resulted in extremely high peaks in pressure of the STOP beads. The fluctuating pressures at these locations is most likely unrealistic, but is due to the high stiffness of the STOP bead. For all of the analysis cases, there were dips in gasket pressure and closure at the 170-190° locations.

5.3.7 Varying Bolt Loading for the 180° Studs

The 180° bolt loads were varied to determine if these locations had a significant influence on the gasket pressures and closure. The results are shown for cylinder 5 only. The results of the E11 closures are shown in Figures 73-78. It is apparent that with 0% bolt load at these locations, there exists a noticeable dip in closure and pressure at all beads of the gasket. As the load is increased to 50% of normal bolt load, the closure and pressure is increased significantly. However, as the load is increased to 100%, although there is an increase in the closure and pressure, the difference is less substantial. The increase in pressure and closure from 100% to 150% is even less significant. The only areas that are affected by the varying bolt loads are from 135° to 225°. The only area that does not follow this trend is the Pressure of the Beads at the 170° locations. The S11 pressure at the STOP not affected by the increase in bolt load of the 180° studs. For the FLEXSTOP and FULLBEAD, the increases are less severe in these areas as well.

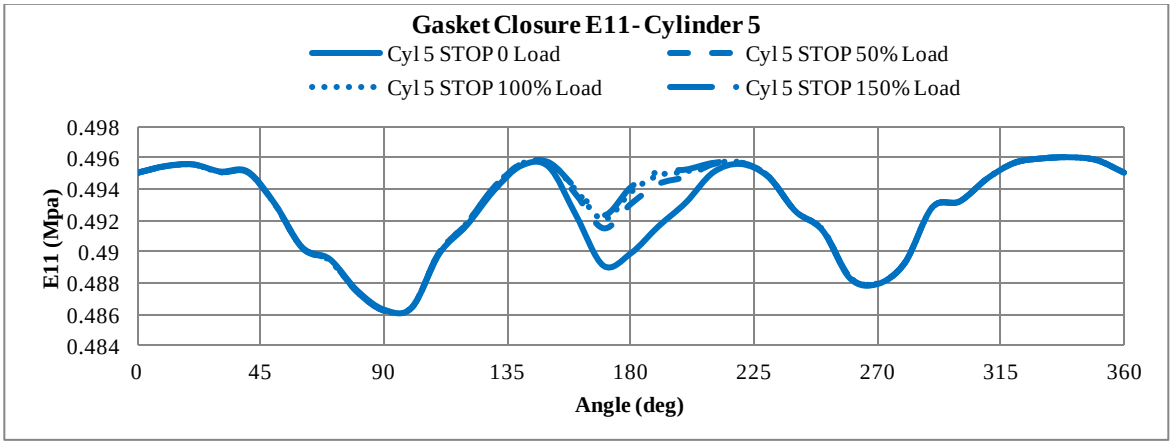

Figure 73: E11 Gasket Closure of the STOP of Cylinder 5, varying stud loads at the 180° studs

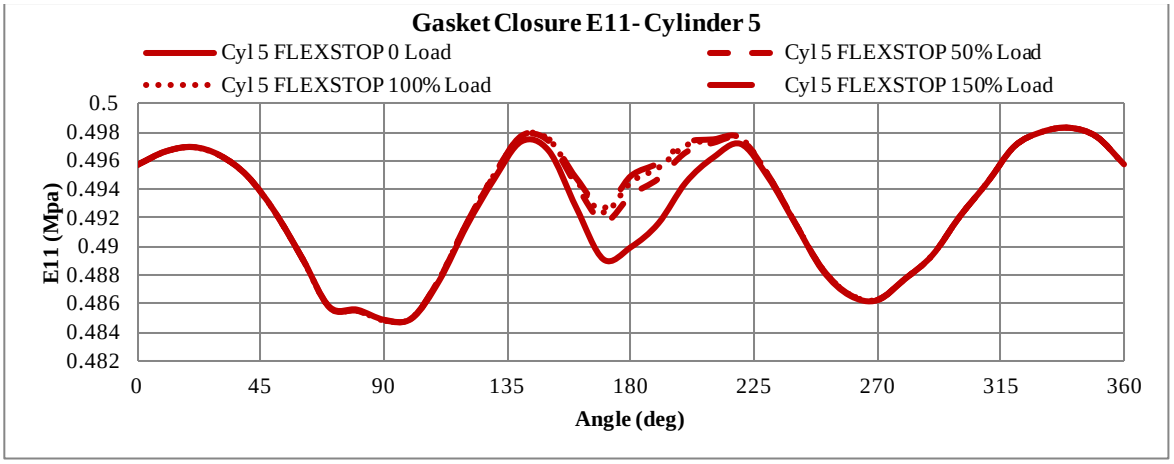

Figure 74: E11 Gasket Closure of the FLEXSTOP of Cylinder 5, varying stud loads at the 180° studs

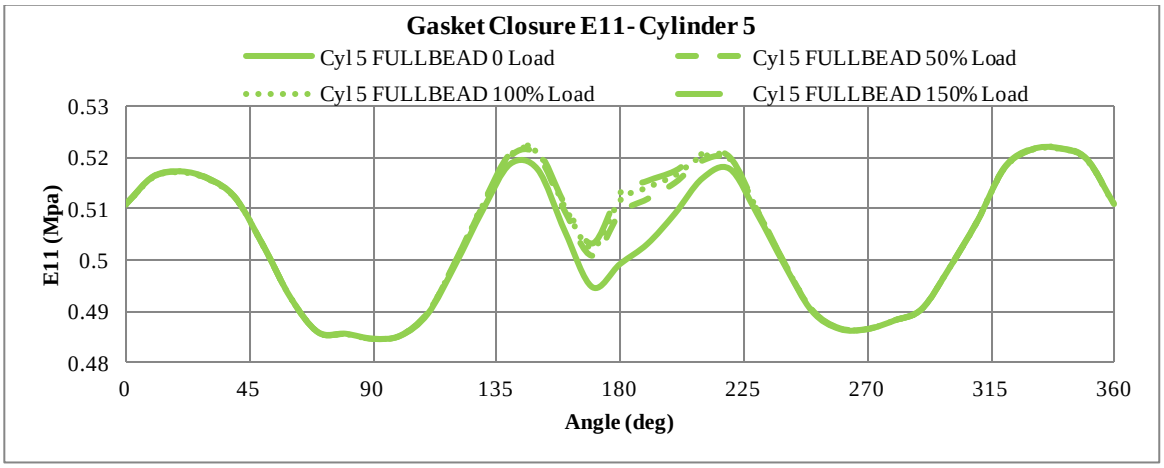

Figure 75: E11 Gasket Closure of the FULLBEAD of Cyl 5, varying stud loads at the 180° stud

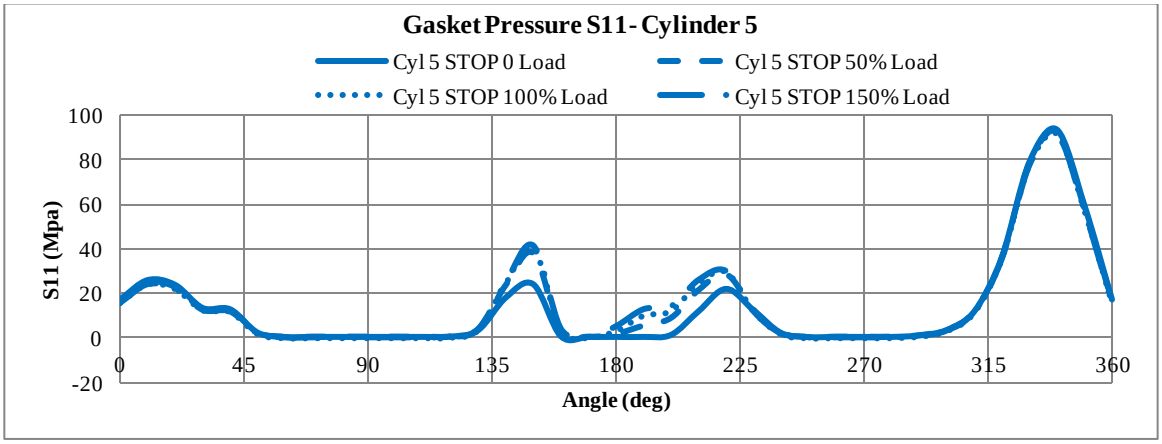

Figure 76: S11 Gasket Pressure of the STOP of Cylinder 5, varying stud loads at the 180° stud

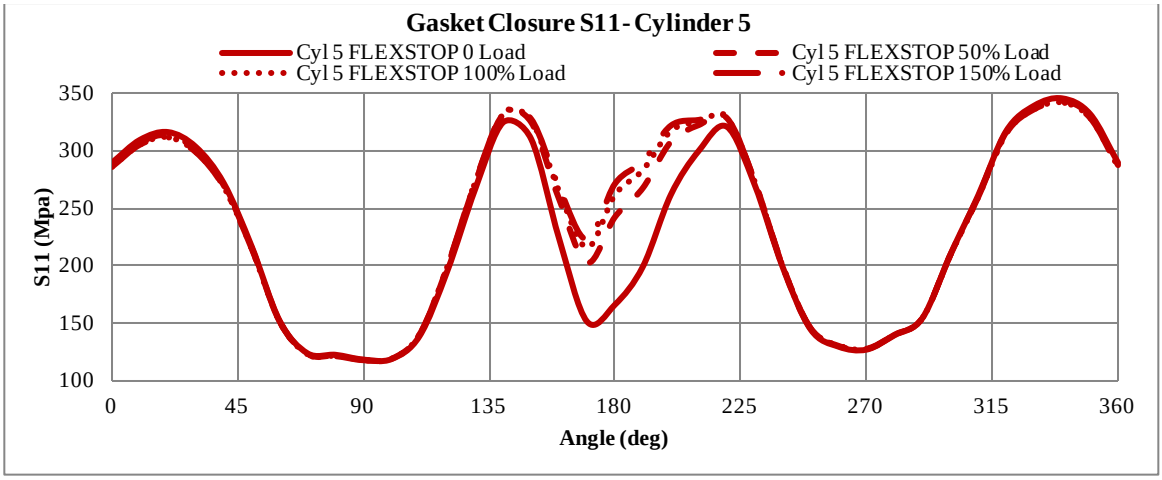

Figure 77: S11 Gasket Pressure of the FLEXSTOP of Cyl 5, varying stud loads at the 180° studs

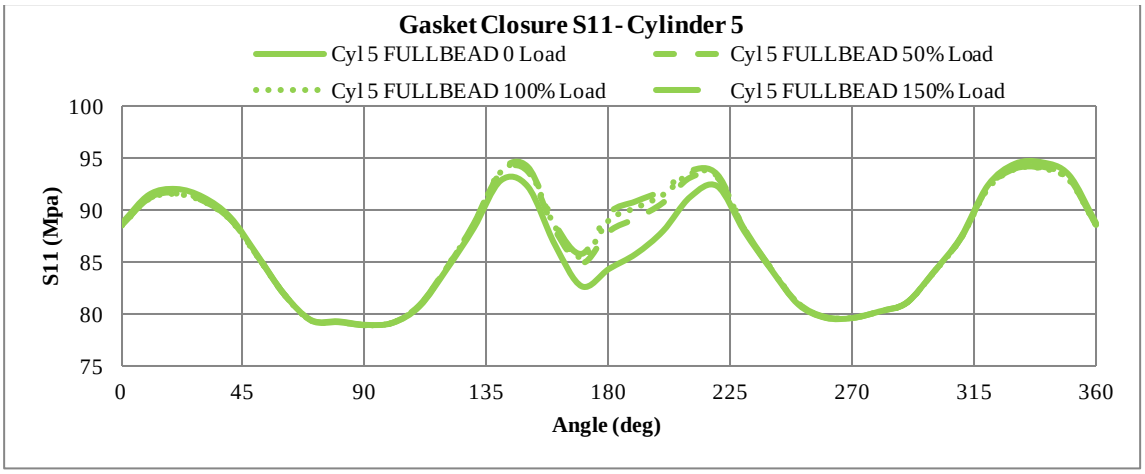

Figure 78: S11 Gasket Pressure of the FULLBEAD of Cyl 5, varying stud loads at the 180° studs

5.3.8 Gasket Closure for Cold Clamping, Hot Clamping and Hot Firing Conditions

The gasket closures at each bead area are compared for the cold clamping, hot clamping and hot firing cases. The results are shown in Figures 79-82 for all cylinders. The general trend is that after the thermal map is applied, the closure of the gasket beads increases. This is due to the expansion of the materials causing greater pressure on the gasket. However, where this doesn't occur is approximately at the 170° area of the beads, where the gasket closure decreases. The major dips occur at the 180° locations. There also are decreases in closure at the 90 and 270° locations, where the beads are further away from the studs.

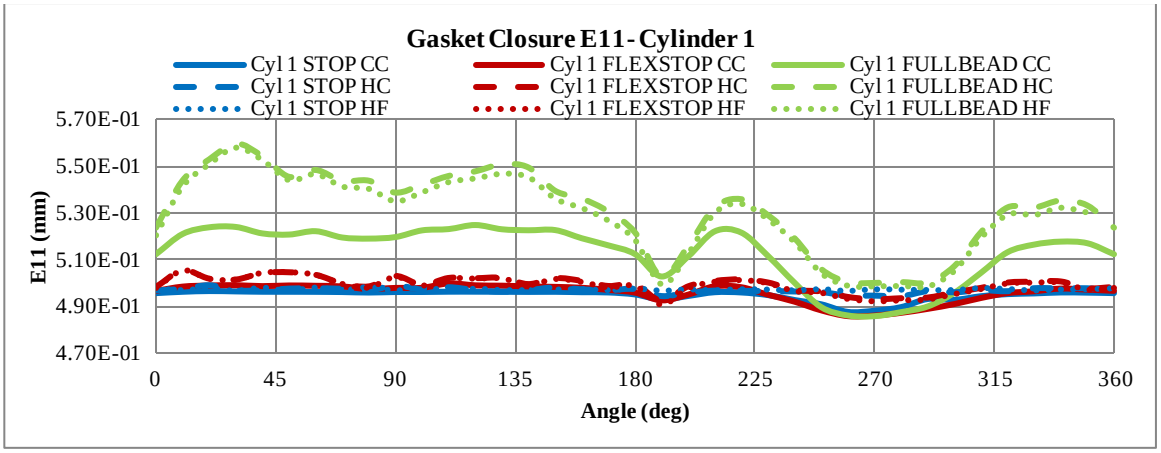

Figure 79: E11 Gasket Closure values at Cylinder 1 for Cold Clamping, Hot Clamping and Hot Firing

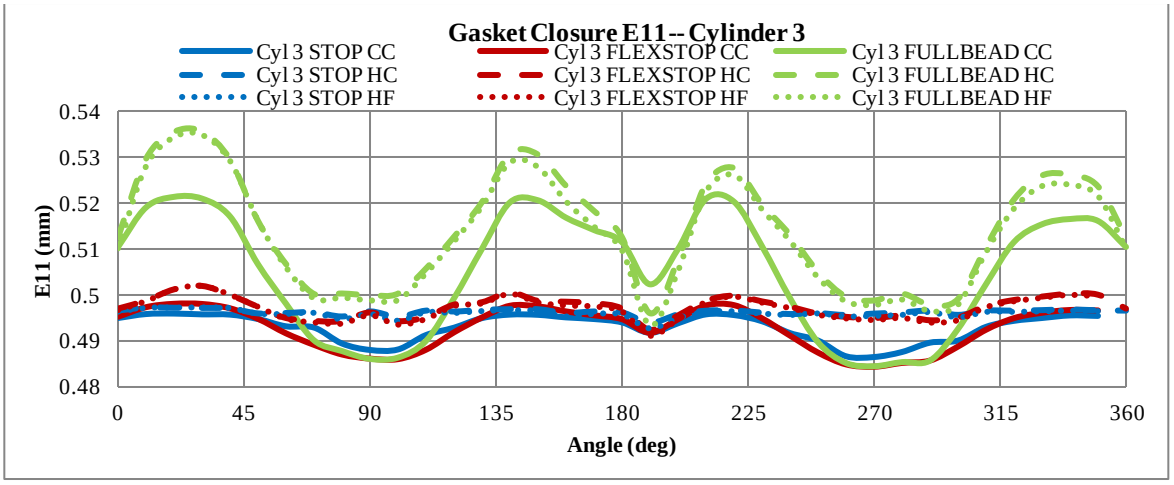

Figure 80: E11 Gasket Closure values at Cylinder 3 for Cold Clamping, Hot Clamping and Hot Firing

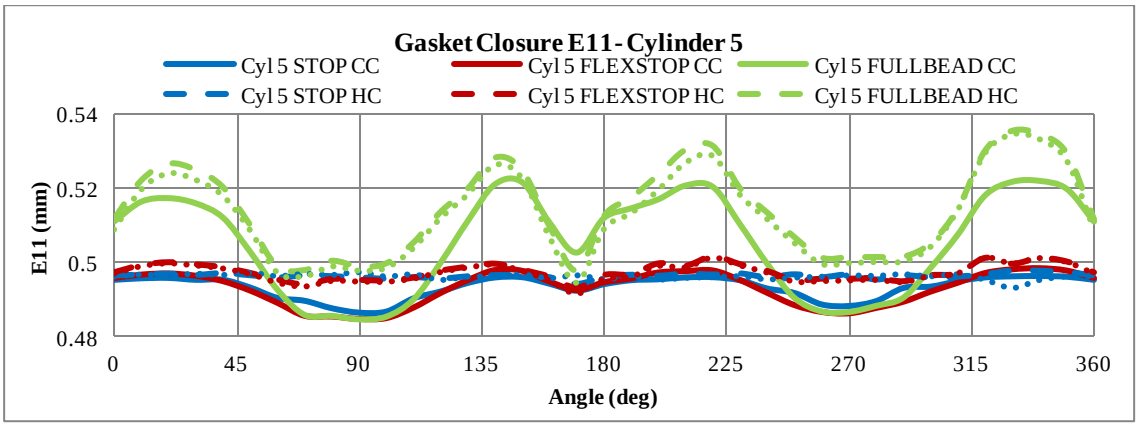

Figure 81: E11 Gasket Closure values at Cylinder 5 for Cold Clamping, Hot Clamping and Hot Firing

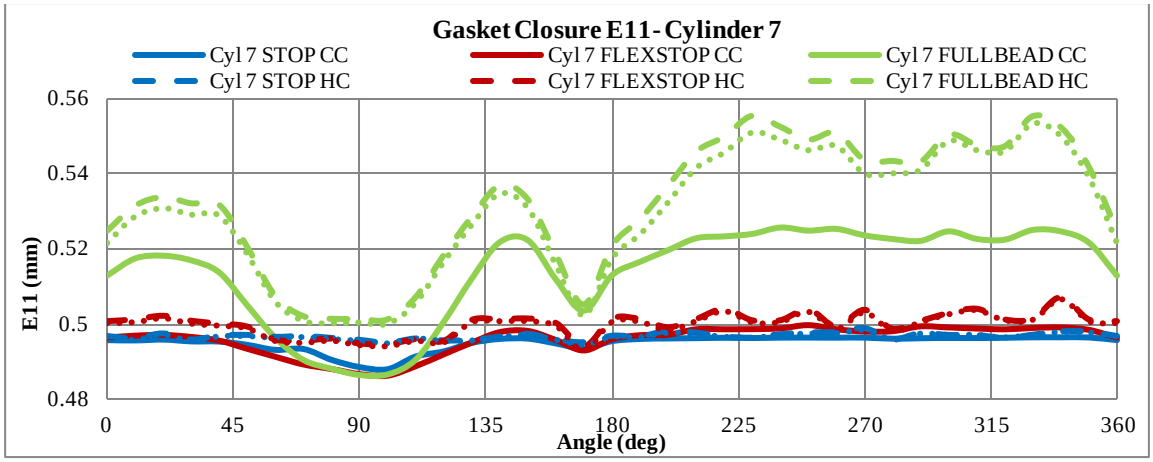

Figure 82: E11 Gasket Closure values at Cylinder 7 for Cold Clamping, Hot Clamping and Hot Firing

5.3.9 Reduction in Normal Pressure from Cold Clamping to Hot Firing and from Hot Clamping to Hot Firing Conditions

Figures 83-90 below show the percentage comparisons of the S11 pressures at the three different beads of the gasket in different situations. The cold clamping case was compared to the Hot Firing case. Also, the Hot clamping case was compared to the Hot Firing case. These were completed for each cylinder on the right bank. The percentage changes at the 180deg locations tend to be the highest. There are significant drops in the STOP bead at these locations for all of the cases. The pressure values reach approximately -80% at cylinders 3 and 5.

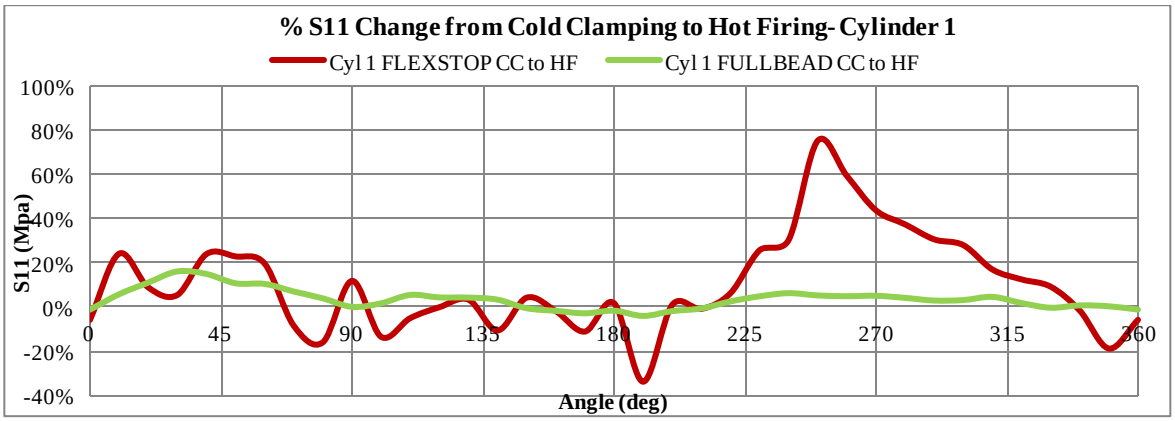

Figure 83: S11 Pressure % change from Cold Clamping to Hot Firing for Cylinder 1. Note that STOP values are not shown.

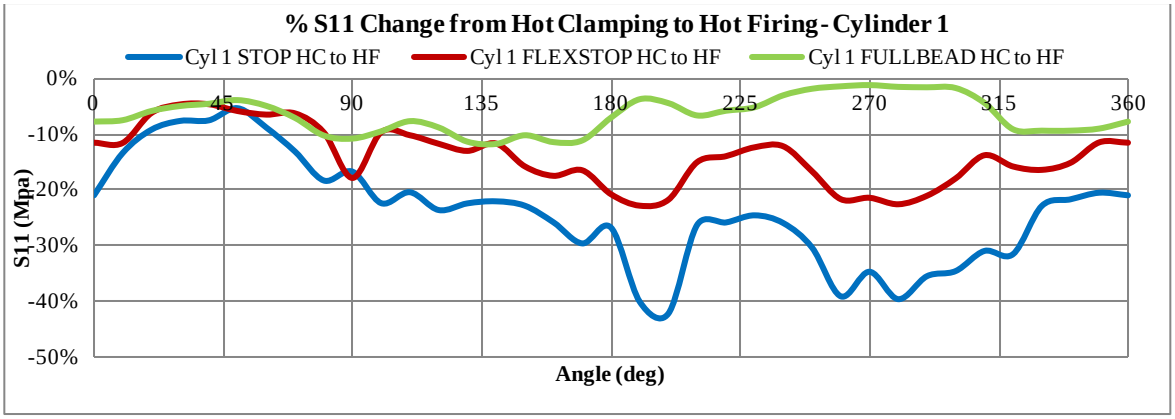

Figure 84: S11 Pressure % change from Hot Clamping to Hot Firing for Cylinder 1

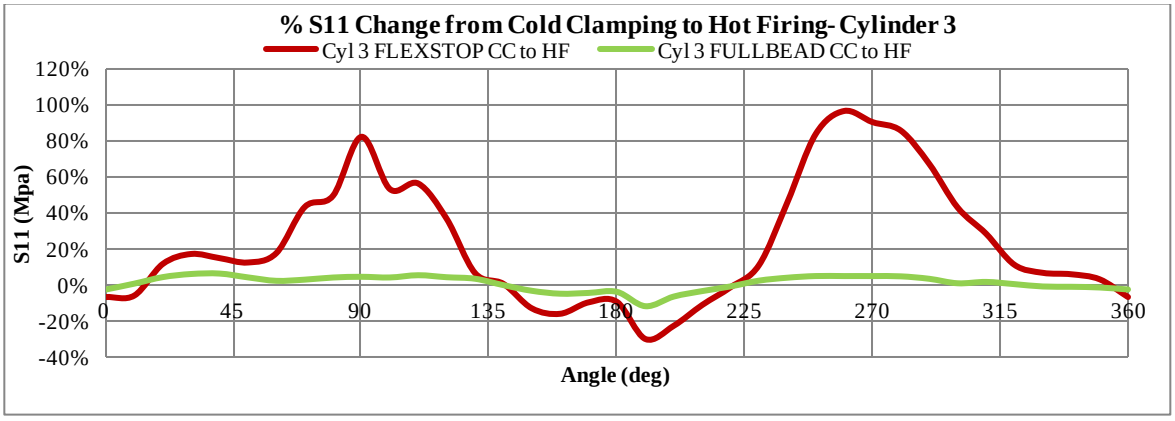

Figure 85: S11 Pressure % change from Cold Clamping to Hot Firing for Cylinder 3. Note that STOP values are not shown.

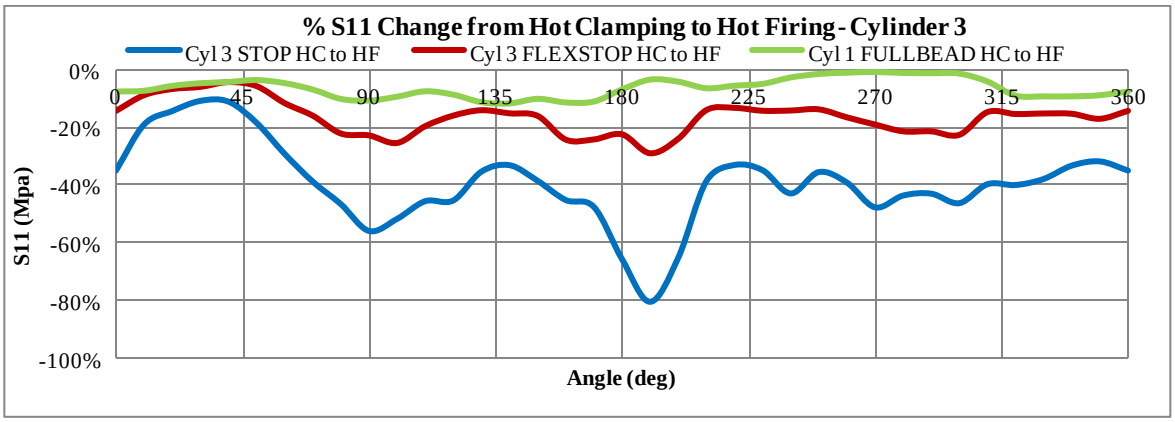

Figure 86: S11 Pressure % change from Hot Clamping to Hot Firing for Cylinder 3

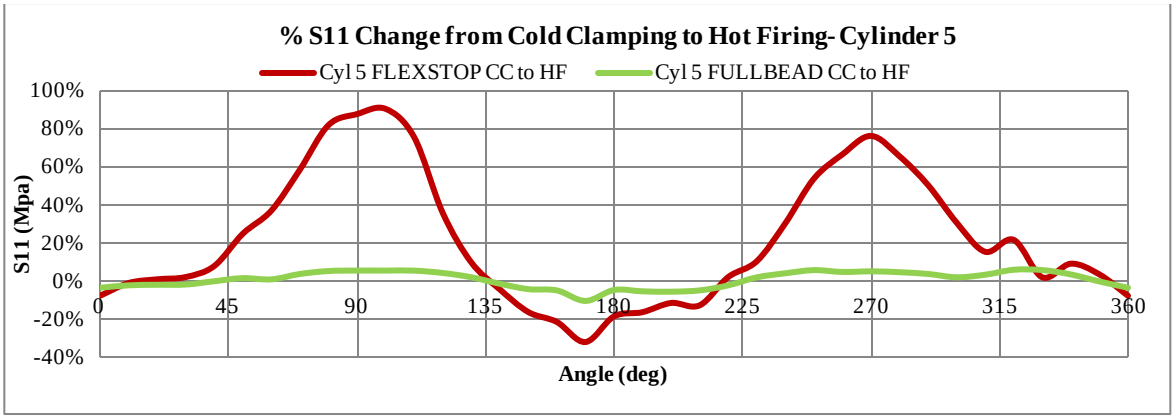

Figure 87: S11 Pressure % change from Cold Clamping to Hot Firing for Cylinder 5. Note that STOP values are not shown.

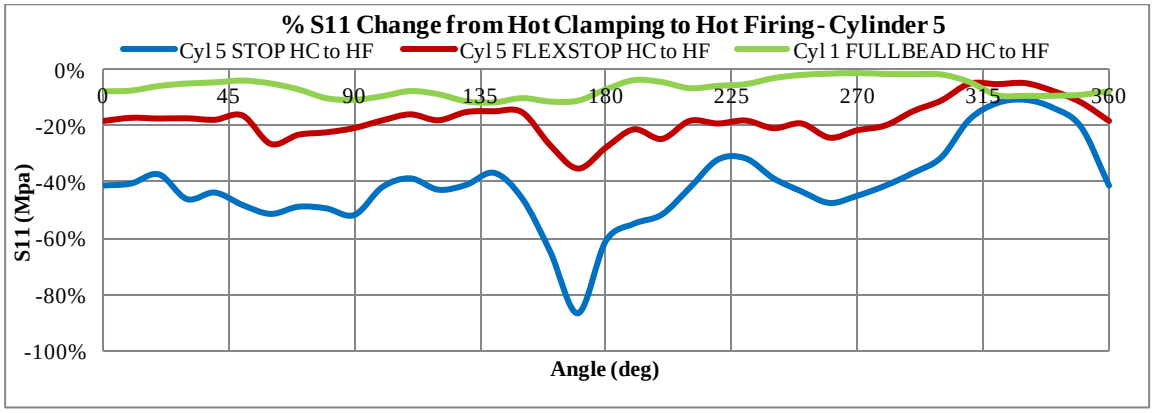

Figure 88: S11 Pressure % change from Hot Clamping to Hot Firing for Cylinder 5

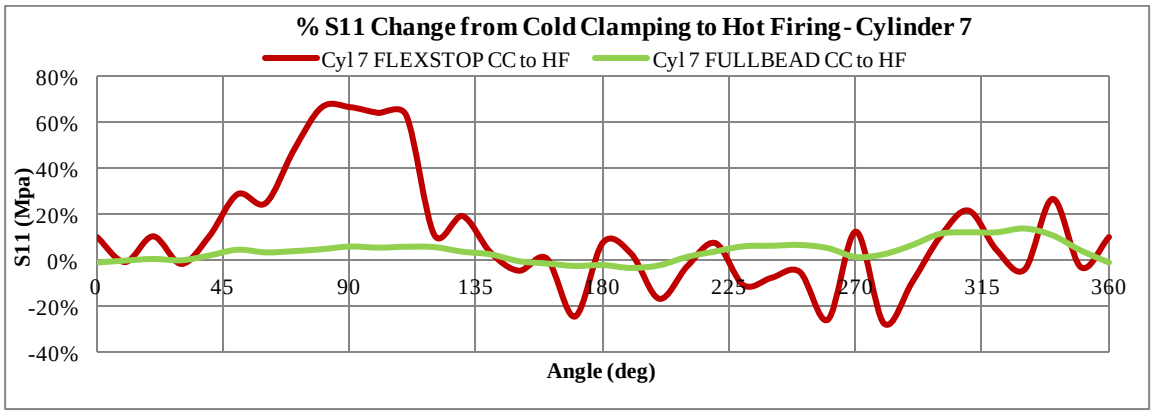

Figure 89: S11 Pressure % change from Cold Clamping to Hot Firing for Cylinder 7. Note that STOP values are not shown.

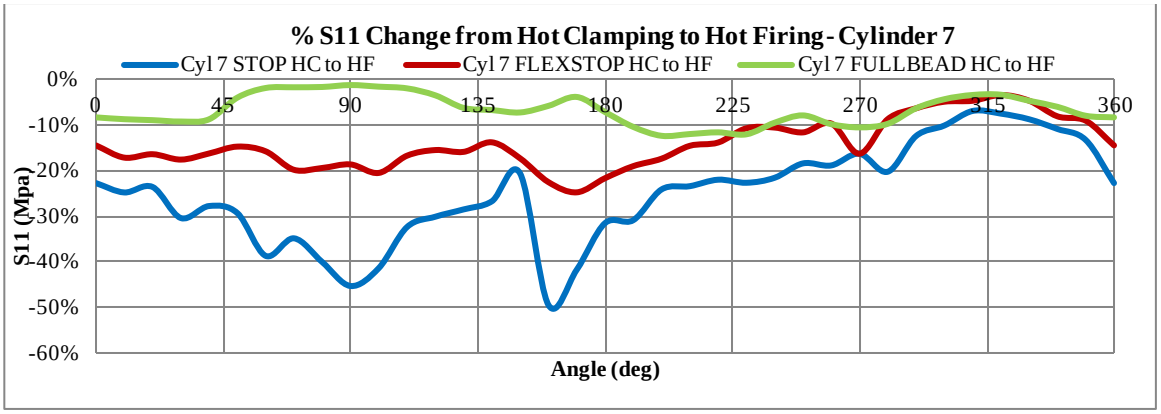

Figure 90: S11 Pressure % change from Hot Clamping to Hot Firing for Cylinder 7

5.3.10 Gasket Normal Stresses For the Cold Clamping, Hot Clamping and Hot Firing Conditions

The S11 gasket normal stresses are compared for the Cold clamping, Hot clamping and Hot firing conditions and are shown in Figures 91-94. The addition of the thermal map to the engine causes fluctuating peaks on the FLEXSTOP and STOP beads areas, but not the FULLBEAD. The severe fluctuations on the STOP are most likely caused by its high stiffness and therefore, sensitivity to gasket closure and pressure.

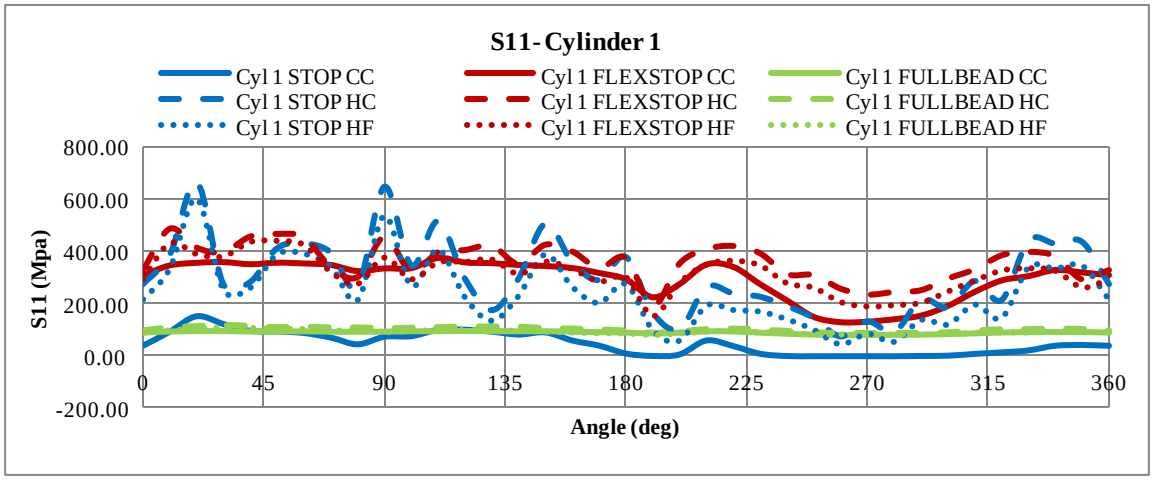

Figure 91: S11 Pressure values at Cylinder 1 for all Conditions

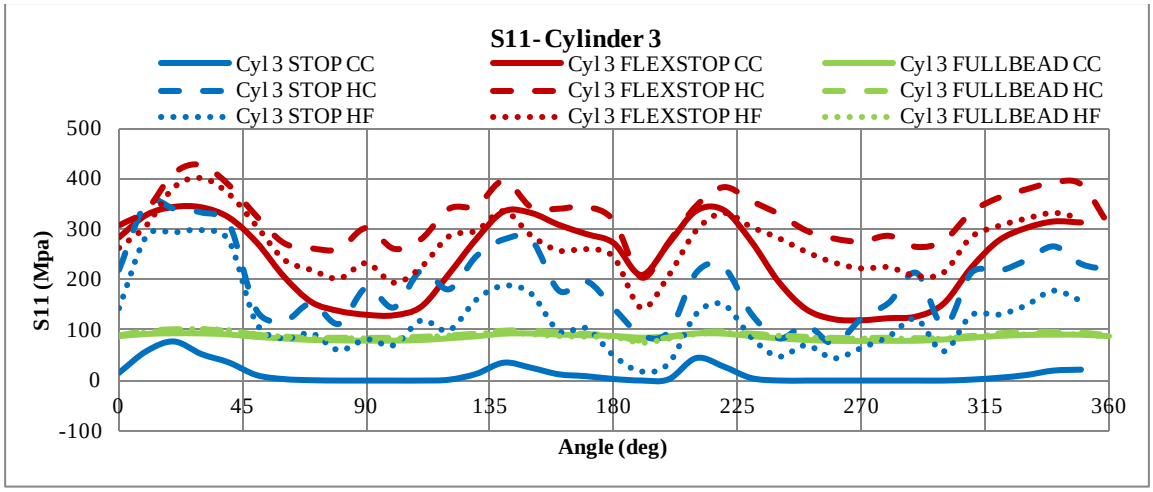

Figure 92: S11 Pressure values at Cylinder 3 for all Conditions

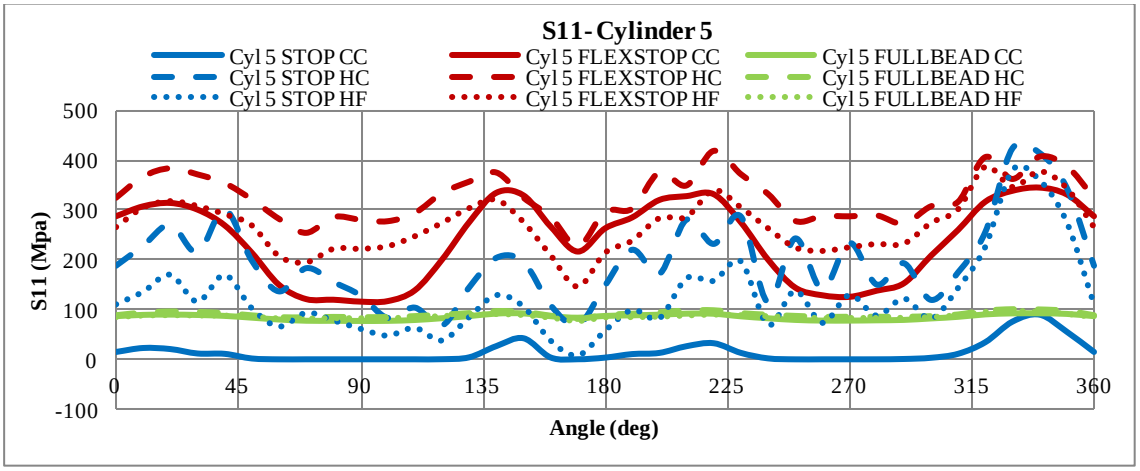

Figure 93: S11 Pressure values at Cylinder 5 for all Conditions

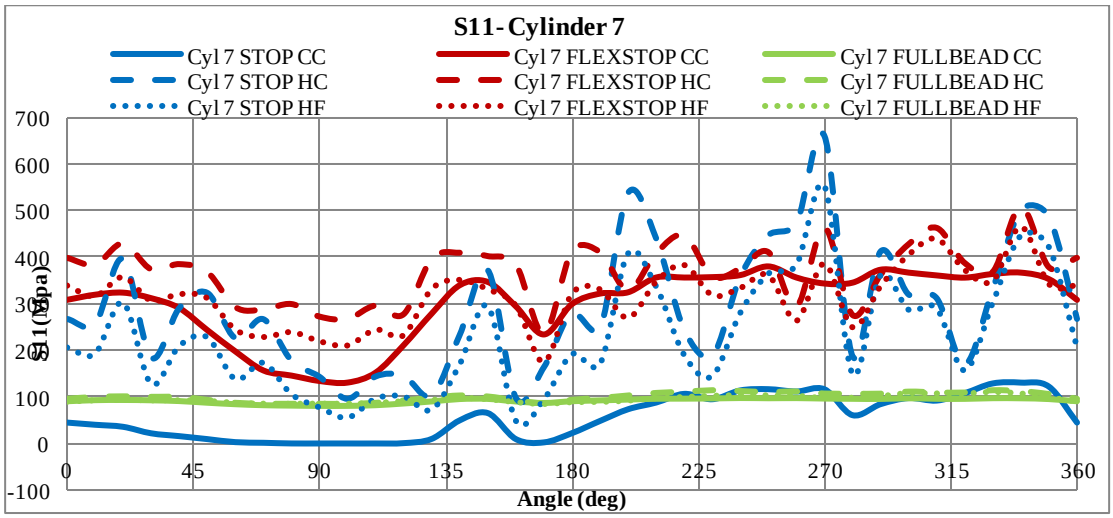

Figure 94: S11 Pressure values at Cylinder 7 for all Conditions

5.3.11 Gasket Membrane Shear stresses

The membrane stress, S23 was determined for the three beads for the cold clamping, hot clamping and hot firing situations. This was done for all cylinder on the right bank of the engine and shown in Figures 95-98 below. The membrane stresses fluctuate, but only peak at approximately 12MPa at cylinder 7. Due to the small values, it unlikely that the shear stresses contribute significantly to the gasket failure.

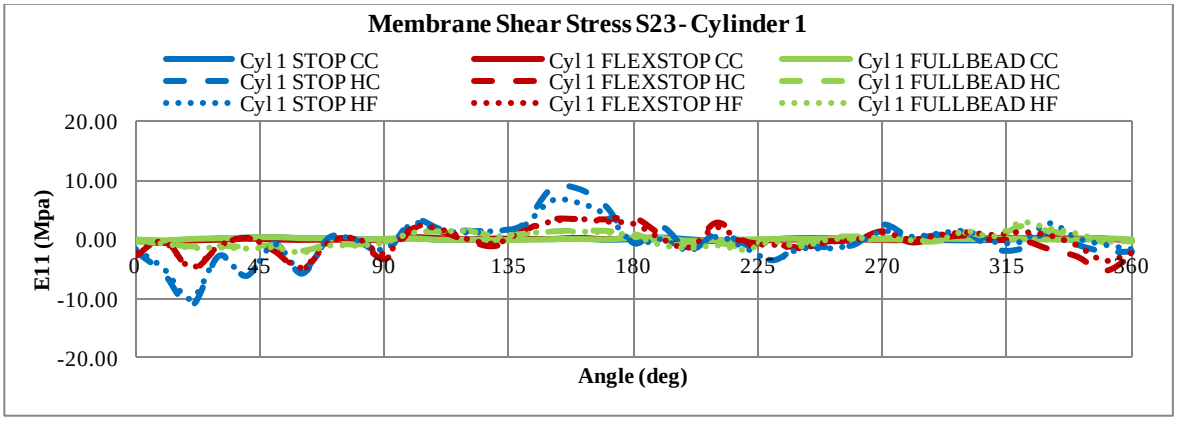

Figure 95: S23 Membrane Shear Stress for Cyl 1, Cold Clamping, Hot Clamping and Hot Firing

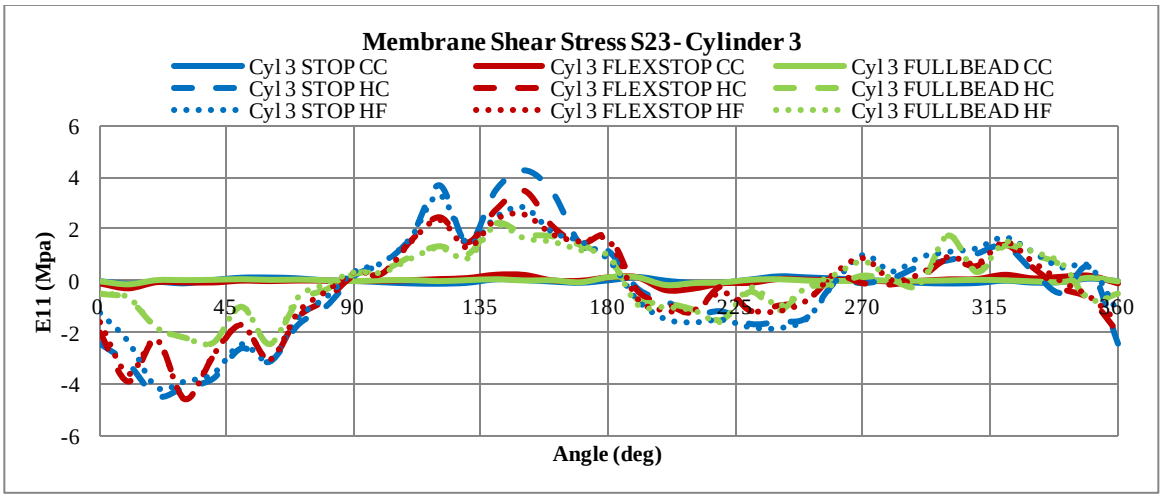

Figure 96: S23 Membrane Shear Stress for Cyl 3, Cold Clamping, Hot Clamping and Hot Firing

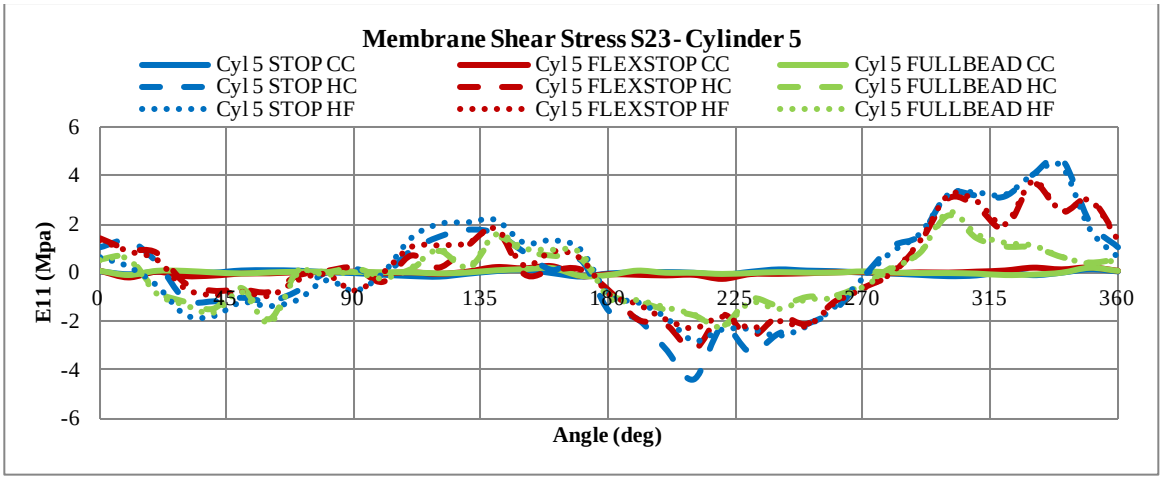

Figure 97: S23 Membrane Shear Stress for Cyl 5, Cold Clamping, Hot Clamping and Hot Firing

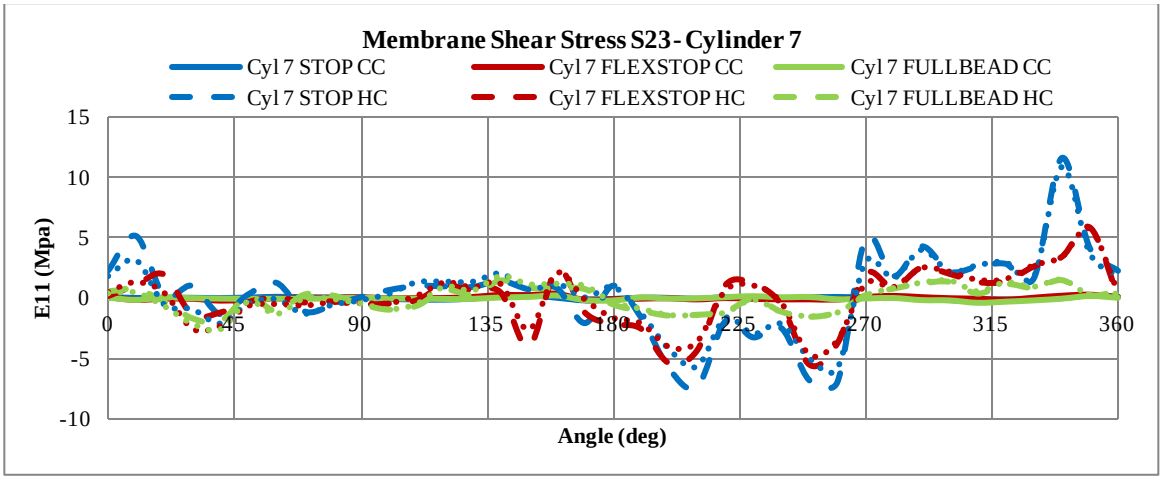

Figure 98: S23 Membrane Shear Stress for Cyl 7, Cold Clamping, Hot Clamping and Hot Firing

5.3.12 Full Bank Discussion

The studies conducted in Series 2 attempted to determine a method to analyze a full bank model, with a compromise between good results and acceptable analysis times. A distinctive method was created and then applied to the Full bank Model of Series 3. Both left and right bank simulations were able to complete in approximately 20 hours while taking 23 iterations to converge. The runs were completed on a server using 16 CPUs. For a half engine analysis with 1.8 million nodes, this is acceptable. If a gasket analysis of the cold clamping case is required by the designer, this method can provide relatively quick and reliable results.

5.4 Root Cause of Gasket Failure

It was shown in the results section that the S11 pressure on the gasket significantly reduces at the location closest to the exhaust ports. For the 100% bolt load hot firing case, the pressures around

the gasket are increased as a result of the head expansion. However, at the 170° location, the pressure dips to below cold clamping values. This tends to occur for all of the engine operating conditions.

As the head is clamped to the block with the gasket in between, a cupping effect occurs in which the outer edges of the head displace more than the inner areas. Due to the decreased stiffness of the head at the exhaust side, the cupping is much more pronounced than at the intake side. The intake side of the head is much stiffer, simply due to the increased bulk of the geometry at these locations. The combination of the different stud clamping forces and head local stiffness's causes the head to deform in such a way that the clamping pressures at the 170-190° locations are reduced. Even during the cold clamping case, there exists dips in pressure at these cylinder locations. This effect is exaggerated when the thermal map is applied to the head and block and the parts experience thermal expansion. Over the entire circumference of the cylinders, the addition of the thermal map causes an increase of thermal pressure on all areas of the gasket. However, at the 180° locations, there exists negative percentages of gasket pressure. During hot firing, the S11 pressures at this location decreases to values below the cold clamping values. So, over the entire span of engine analysis (Cold clamping, Cold firing, Hot clamping, Hot firing), compared to other cylinder circumferential values, the 180° location shows decreased contact pressures and decreased gasket displacement for all cases. When the cylinders are in the hot firing stage at maximum rpm of 9000, the 180° areas are experiencing the largest amplitude in pressure oscillation. Cylinder 5 and 7 have higher peak pressures compared to cylinders 1 and 3, so this effect is slightly increased. This was shown in Figures 87-90 where the area at 180° had the highest percentages decrease in clamping pressures for cylinders 5 and 7. These occur for all of the beads of the gasket elements.

There are two major factors that like cause the gasket failure in the common regions. The first is due to the increased pressure in the two rear cylinders. The higher magnitude of pressure in cylinders 5 and 7 results in higher lift off of the head at these locations. Secondly, the physical geometry of the head and the stud locations appear to be the main contributors to the failure at these locations. There is a constant reduction in contact pressure and closure of the gasket occur at the 180° locations. This causes higher cyclic amplitudes of displacement as the engine is fired. It has been shown that high amplitudes of cyclic stresses are a major contributor to gasket failure. As was discussed in the literature review a major contributor to gasket failure is bead fatigue. This occurs in areas of highest head lift during the dynamic motion of the cylinder head, which results in high cyclic stresses of the gasket area. Cylinder 5 and cylinder 7 are the areas that are subject to

the highest stress fluctuations. Gasket failures are a result of high stress amplitudes, and this is occurring at these locations. The shear stresses found in the gasket do not appear to be large enough to be a major cause of gasket failure.

There was not a single, distinct test that showed that a gasket failure might occur, rather a number of different tests that pointed to the region that failure is likely to occur. The analyst must apply experience and good judgment to recognize the areas of potential failure.

5.5 Fuji Pressure Film Resolution

The high level of detail seen on the Fuji Pressure film can be attributed to the resolution of the microcapsules in material. The capsules are approximately 5-15 microns in diameter. Finite element results are based off of the size of the mesh itself. In order to match the resolution of the Film, the size of the Finite Elements in the mesh would have to be of relatively the same size, at both the head and deck faces. The result would be likely in the billions of elements and would require a gigantic amount of processing power. For this reason, the methods are still based on computational power and must scale down the information available in the gasket.

Fuji Film can be viewed as FE component with a mesh size of 5-15 microns (0.005-0.015mm). In order to achieve this resolution in simulations, deck faces and gasket would need this resolution. This is currently impossible for a full bank analysis due to computational limitations. This should still be an area of study due to computational availability increasing in the future.

5.6 Contact Pressure Verification

It was important to have a method of validating the experimental results with calculated results. Knowing the total force that the studs applied and the surface area of the gasket and block deck, the total pressures were calculated for each surface. These are shown in Table 16 below. The experimental average pressures were determined using the results in ABAQUS and shown in Table 17. These are completed only for the single cylinder using Gasket elements.

Surface Area Block Deck (mm^2)	6582
Surface Area of Gasket (mm^2)	6245
Bolt Force Long Stud 1 (N)	30350
Bolt Force Long Stud 2 (N)	30350
Bolt Force Long Stud 3 (N)	30350
Bolt Force Long Stud 4 (N)	30350
Bolt Force Long Stud 5 (N)	33360
Bolt Force Long Stud 6 (N)	33360
Total Force (N)	188120
Calculated Pressure on Block Deck (N/mm^2)	28.58
Calculated Pressure on Gasket (N/mm^2)	30.12

Table 16: Contact Pressure Calculation

Experimental Sum of Gasket S11 (N/mm^2)	186560
Number of Elements	6848
S11 Pressure Average (N/mm^2)	27.243
Experimental Sum of Deck Pressure (N/mm2)	359056
Number of Elements	15062
Pressure Average	23.8386

Table 17: Contact Pressures at Gasket and Block Deck Face

The experimental S11 average pressure value of 27.2 MPa on the gasket is close to the calculated value of 30.1 MPa. The experimental average pressure of 23.8 MPa on the block deck face is substantially less than the calculated pressure of 28.6 MPa. The differences in magnitude are likely due to different contact areas at the gasket and head, which would result in different contact pressures.

5.7 Future Studies

The studies completed on the gasket element gave good information on static analyses using this type of gasket representation. The thermal map was able to be applied and different engine conditions were studied. Regarding future studies, the other topics could each be focused on as a full investigation, depending on the depth of information needed. The scope for each topic was simply too large to completely cover in one master's thesis. Previous studies have been done by groups of professionals on creating ways to determine the residual stresses in the gasket layers due to the forming process. This was then applied to a program that exported the residual stress values to an input file that can be used in a FE program for further analysis. It is an important step in understanding the interactions between the gasket layers. As was discussed previously, a factor affecting the location of gasket failure is the difference in pressures between the rear and front cylinders. A future study could focus on the reason for the difference in cylinder pressures.

The analyses completed using the shell elements were inefficient and future studies could find more efficient analysis methods. As with any type of finite element based analysis, refinement studies could be completed in order to converge on the exact, real world data. The full gasket models using either shell elements or 3D elements are important for full understanding of the gasket behaviour. These methods should be a major focus for future studies. Gasket layer interactions are a very important aspect of gasket normal stresses and shear stresses. This information is crucial for understanding the relative slip between the block and the head. The interaction of the layers is crucial for durability analysis as well. Also, residual stresses should not be ignored. In past simulations, the analyst was concerned about computational efficiency, so these types of "full gasket" analyses were not considered. However, now the CPU power is available to the FE Analyst and will only continue to increase in the future.

Chapter 6: Conclusions

The axisymmetric analyses were able to complete using different sections of the gasket. The method strengths include: High efficiency, as simulations were able to converge on a PC in under 30 minutes, the information at all layers and fire ring can be studied, the resolution of mesh can be very high due to small scale of test, it is relatively easy procedure to mesh/assembly, and the stiffness of gasket can be determined at each section of gasket. Some of the Axisymmetric method weaknesses include; the method is not truly a an axisymmetric analysis, the head and block geometric stiffness data not present, it's difficult to determine proper bolt loads due to varying locations and magnitudes of bolt force on real engine, the results are difficult to correlate, and the residual stresses from gasket forming process are not present. Residual forming stresses should not be ignored and there are programs that will include the stresses in the gasket such as Proteus®. The lack of correlation methods is a major concern, so future studies should focus on this subject as well.

The single cylinder 3D study showed the strengths and weaknesses of altering parameters at the gasket interfaces and altering the element information. The interaction study gave good insight into the many options available at the deck interfaces and their impact on the simulation results. Stiffness of head and block was present, but not fully accurate due to the cutting of the assembly. When using gasket elements, normal directions of the gasket must be added to input file before submitting the analysis to eliminate gasket spiking. The resolution of results is based on element sizes of the gasket and deck faces; decreasing the size of the element resulted in higher resolution of results at the expense of computational cost. Using specialized gasket elements was most efficient, but the gasket makes many assumptions regarding gasket behaviour. The gasket assembly using Conventional Shell elements was able to converge with realistic results, however these took approximately 24 hours to converge on Chrysler servers. The gasket assembly using 3D Continuum Elements and Continuum Shell elements were unable to converge or gave unusable results and took upwards of 48 hours on Chrysler servers only to fail. Future studies should focus on using shell elements or 3D continuum elements to represent the real world gasket.

The full bank analyses under varying engine operating conditions were completed using the specialized gasket elements. For future studies, ABAQUS should not be used for meshing complicated assemblies. Using Gasket elements is an efficient way to complete Full Bank Analyses as the analyses took approximately 24 hours using Chrysler servers. This type of analysis was appropriate for determining behaviour of head and block as full assembly during

different engine operating conditions since stiffness of head an block is fully present. The conditions of the simulations were cold clamping, cold firing, hot clamping and hot firing. In order to apply the thermal map to the simulation, the thermal map input file must be added to master input file. The single layer using gasket elements does not fully represent real world gasket with multiple layers, as many assumptions are made to reduce computational cost. Many of the results suggested a potential issue at the 180° location (dips in pressure, reduced closure, etc) due to the geometry of the head. The head is less stiff at the exhaust location compared to the intake location, which causes high fluctuations of contact pressure and closure of the gasket under different operating conditions. Also, in-cylinder pressures are higher for cylinders 5 and 7 compared to cylinders 1 and 3. It can be concluded that the gasket failure at this location is being caused by high amplitudes of cyclic stresses of the gasket which cause fatigue failure.

When studying an engine assembly and gasket, there is not a single test that will pinpoint gasket failure, only various tests and results that will give good indication of areas that will be prone to failure. As a trend, FE results always tend to be higher than real world values. The possible cause of this is the residual stresses in gasket tending to return the layer to a flat piece of metal. Different FE tests are appropriate for different results: if information is needed regarding gasket layers, FE methods needs to include gasket layers (dynamic, fatigue tests).. The use of Gasket elements gives most efficient analysis and allows for study of full head and block behaviour. The techniques being used to study gasket in industry are improving due to the increase in available processing power. Future studies should focus on the accuracy of solutions instead of efficiency, as was done in the past. Recommendations for future studies are: methods for determining residual gasket layer stresses due to forming, refinement of 2D axisymmetric method and correlation, refine 3D gasket shell/Layered methods and correlation, investigate benefits of using multiple layers of Gasket Elements, create Virtual dynamic tests to more accurately represent real world engine conditions, create virtual fatigue durability tests of gasket assembly, and the study of actual engine to determine causes for uneven peak pressures.

REFERENCES/BIBLIOGRAPHY

Baig, M., Chang, CC., (2007). Multi-Layer Steel Head Gasket Durability Analysis using Stacked GASKET Element Model.

Bathe, Klaus-Jürgen, and Klaus-Jürgen Bathe. Finite Element Procedures. Englewood Cliffs, NJ: Prentice Hall, 1996. Print.

Belingardi, G. Il Metodo Degli Elementi Finiti Nella Progettazione Meccanica.Levrotto & Bella di Gualini T. & C, 1995. Print

Bosch Automotive Handbook. Hoboken, NJ: Wiley, 2007. Print.

Budynas, Richard G. Advanced Strength and Applied Stress Analysis. The McGraw-Hill Companies, Inc. 1999. Print.

Cengel, Yunus A., and Michael A. Boles. *Thermodynamics: An Engineering Approach*. Boston: McGraw-Hill, 2002. Print.

Chang-Chun Lee, Kuo-Ning Chiang, Wen-King Chen, Rong-Shieh Chen, (2005). Design and analysis of gasket sealing of cylinder head under engine operation conditions. Finite Elements in Analysis and Design 41, pp. 1160–1174

Chang-Chun Lee, Kuo-Ning Chiang, Wen-King Chen, Rong-Shieh Chen, (2005). Design and analysis of gasket sealing of cylinder head under engine operation conditions. Finite Elements in Analysis and Design 41, pp. 1160–1174

Chen T. Y. , Zwick, J., Tripathy B., Novak, G., (2002). 3D Engine Analysis and MLS Cylinder Head Gaskets Design. SAE Paper No. 2002-01-0663.

Cho S.S., Hann B.K., Lee J.H., Chang H. and Kim B.K., (2005). Fatigue Durability Assessment of Full-Bead of MLS Gasket Using Finite Element Analysis. International Journal of Automotive Technology, Vol. 6, No. 5, pp. 513-517.

Cho S.S., Hann B.K., Lee J.H., Chang H. and Kim B.K., (2006). Finite Element Modeling and Parameter Study of Half-Bead of MLS Cylinder Head Gasket. . International Journal of Automotive Technology, Vol. 7, No. 1, pp. 109-114.

Chrysler Group LLC: Powertrain Engineering. Cylinder Head Sealing Analysis. SLTI 7008-03. 2010

Chrysler Group LLC: Powertrain Engineering. Meshing Protocol for Full Block Engine Bottom End Durability Analysis. SLDP7025_00. 2010

Graves, S., Utley, T.L., Isikbay, N., (1993). Nonlinear Finite Element Analysis of Diesel Engine Cylinder Head Gasket Joints. SAE Paper No. 932456

Hebert, C., Webster, W., (1998). Cylinder Head Gasket Simulation in Finite Element Analysis. SAE Paper No. 980843

Hibbit, Karlsson & Sorensen, Inc. *ABAQUS/Standard User's Manual, Vol. I & II* (ver. 6.10), (2010). Pawtucket, Rhode Island.

Hibbit, Karlsson & Sorensen. *Getting Started with ABAQUS/Standard Interactive Addition*. (2001). Print.

Kestly, M., Popielas, F., Grafl, D., Weiss, A., (2000). Accelerated Testing of Multi-Layer Steel Cylinder Head Gaskets. SAE Paper No. 2000-01-1188

Logan, Daryl L., and Daryl L. Logan. A First Course in the Finite Element Method. Pacific Grove, CA: Brooks/Cole, 2002. Print.

Mockenhaupt, M. (2003). The 1D CAE Program for Cylinder Head Gasket Design. SAE Paper No. 2003-01-0479.

Olsson, A. (2001). Stainless Steel Plasticity - Material modelling and Structural Applications. Department of Civil and mining Engineering Division of Steel Structures. ISSN: 1402-1544

"Page 21 of Catalogue Cylinder Head Gaskets of Reinz-Dichtungs-GmbH." *The Permanent Load Resistance of Harder Full Beads... [Page 21]*. N.p., n.d. Web. 11 Apr. 2013.

Popielas F., Chen C., and Obermaier S., (2000). CAE Approach for Multi-Layer-Steel Cylinder Head Gaskets. SAE Paper No. 2000-01-1348.

Popielas F., Chen C., and Obermaier S., (2003). CAE Approach for Multi-Layer-Steel Cylinder Head Gaskets- Part 2. SAE Paper No. 2003-01-0483.

Popielas F., Chen C., Mockenhaupt, M., Pietraski, J. (2003) MLS Influence on Engine Structure and Sealing Function. SAE Paper No. 2003-01-0484

Popielas, F., Ramkumar, R., Minkov, M., Alexandrovitsch, A.I., Kornouchov, A.K., (2003). Proteus® - MLS Cylinder Head Gasket Analysis Tool. SAE Paper No. 2003-01-0481.

Rasmussen, KJR (2001). Full-range Stress-Strain Curves for Stainless Steel Alloys. The University of Sydney Department of Civil Engineering. No. R811.

Reddy, J. N. An Introduction to the Finite Element Method. New York: McGraw-Hill, 1984. Print.

Stone, Richard. Introduction to Internal Combustion Engines. Basingstoke: Macmillan, 1985. Print.

van Basshuysen, R., Schafer,F. (2006) Internal Combustion Engine Handbook; Basics, Components, Systems, And Perspectives. van Basshuysen, R., Schafer,F.

(2013) *FUJI PRESCALE PRESSURE MEASURING FILM*. [online] Available at: http://www.spareonweb.com/lllw_man.pdf (May 2013)

APPENDICES

Appendix A: Technique for Angular Analysis

Once the analyses have completed, it is important to have an efficient method for visualizing the results. The pressures at the areas around the bores at the gasket interface are of great importance, and it is beneficial to know the angles about the bore axis for which the pressures occur. Unfortunately, there does not exist a quick and easy method for determining the values at these areas since the gasket element labels are predetermined by the supplier of the gasket model, in this case, FelPro. Simply picking the element labels and reading their stress values is far too time consuming and must be repeated every time a new simulation is completed. A method was created in order to simplify the process of determining the pressures at predetermined angular spacing and will allow the user to complete various graphs of the data, such as those shown in Figure A.1. The step by step procedure is described below, which can be completed once the block and gasket are assembled in the FEA program.

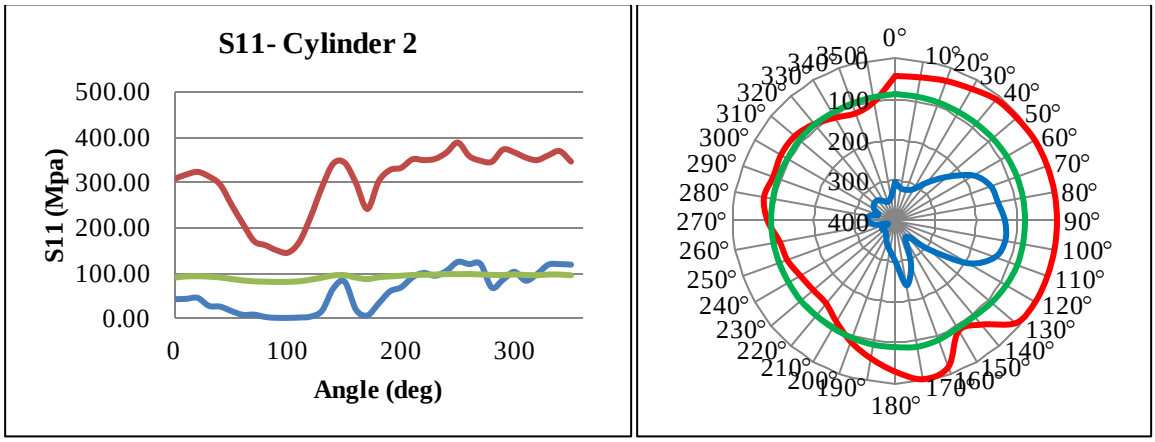

Figure A.1: Example of the types of graphs that can be created using the procedure

Step 1. The first group of steps is aimed at determining the Element IDs at a decided upon angular spacing. Firstly, Save the analysis as different file, as the procedure might cause issues with any previous meshes, interactions, constraints, etc. This new saved file can be used just for the beginning stages of the procedure and will not be used for the actual analysis.

Step 2. Create a dummy part that is a cylinder with an arbitrary radius. On top of this sphere, create a shell formation with equally spaced "beams" that extend beyond the limits of the gasket. The shells should be extruded to be about twice as thick as the gasket. The number and spacing of

the beams depends on the needs of user. For example, the cylinder in Figure A.2 uses 36 equally space beams, which will allow for a visualization of the pressure at every 10° of the bore. More beams would allow for a smaller increment for each angle.

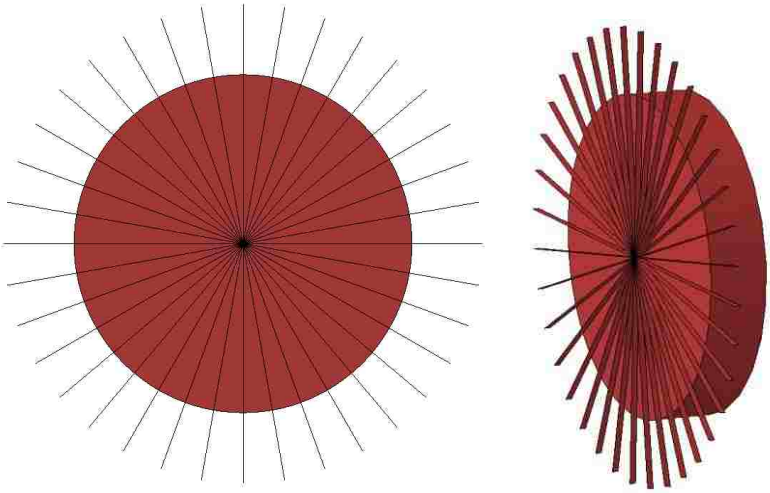

Figure A.2: Geometry of the cylinder and angular beams

Step 3. Assemble the dummy part into a single bore of the block such that the cylinder is face is coincident with the deck. Ensure that that one of the beams is in line with the local coordinate of the gasket and block. This is important as it will correspond to the 0° (also 360°) elements on the gasket. Duplicate the part for each cylinder of the block. The assembly should look similar to Figure A.3 below.

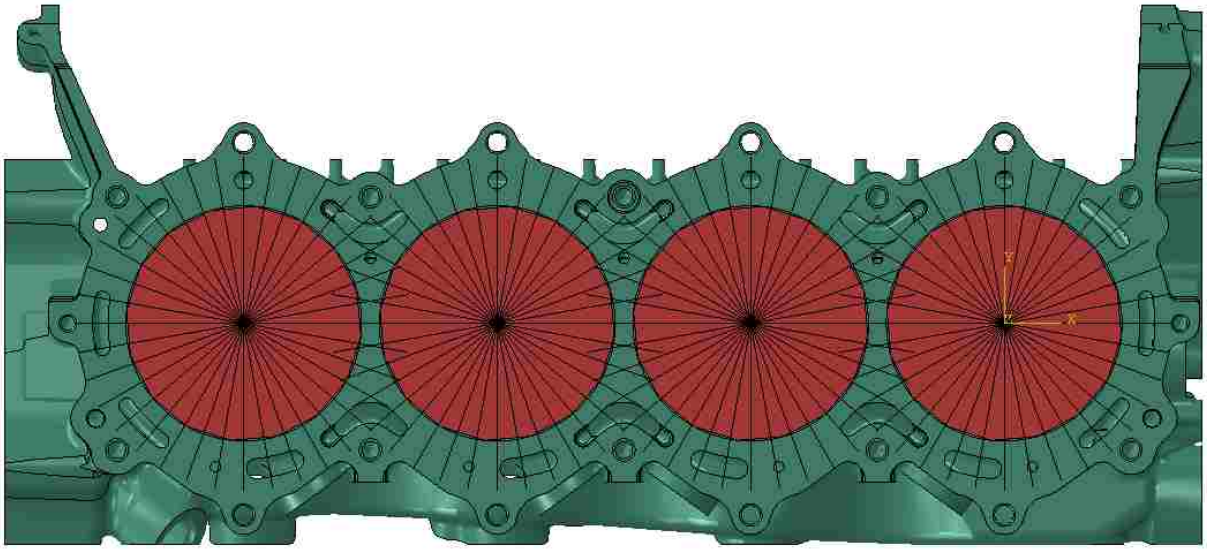

Figure A.3: The assembly with the beams

Step 4. Leaving the dummy parts shown, hide the entire block. Also, show the gasket areas of interest, which should be contained in separate Sets within the program. Figure A.4 below shows the dummy parts with 4 of the gasket sections; Full Bead, Flexstop, Half Bead and Stop. For the example analysis, it was decided to have the 0° beam located vertically upwards, such that 0° is always located at the inner area of the engine assembly.

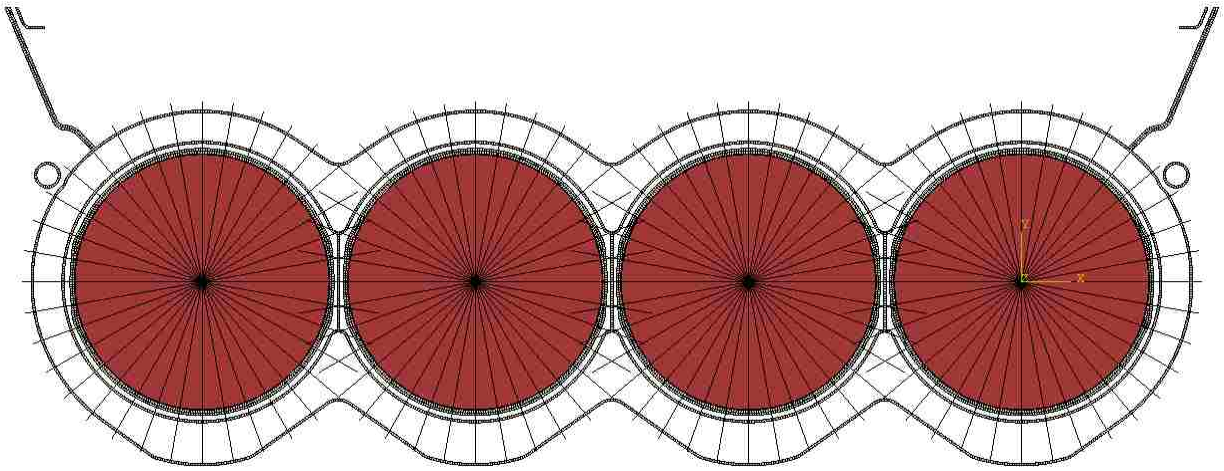

Figure A.4: Gasket beads and Angular beams

Step 5. It is now a simple, but tedious matter of starting at the decided upon 0° beam, and querying the elements that intersect with the beam for every intersection of beam and element in a clockwise or counter clockwise manner. If the beam crosses through two separate elements, choose the one which the larger area of the element is being intersected.. Figure A.5 shows the Element IDs for each Gasket Section being selected at the 10° increment. Abaqus will give the Element ID in the message area of the program which can then be typed or copied and pasted into an Excel spreadsheet, as shown in Table A.1. The Element IDs are only shown for the first 50° of selections, however will be completed for all 360°. Although the process is relatively long and tedious, it only has to be completed once for each gasket, since the Element IDs should remain constant throughout each analysis. If there is a re-meshing of the gasket, this procedure will have to be redone.

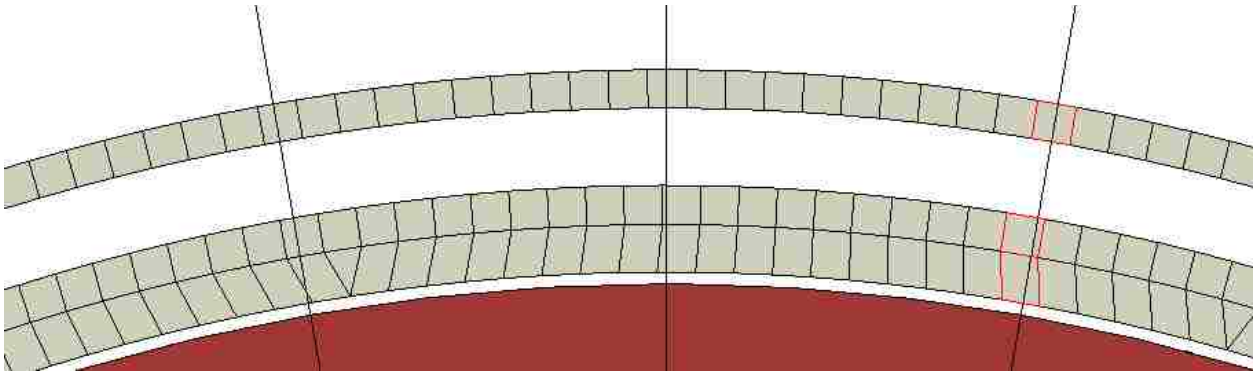

Figure A.5: Query of the Gasket Element IDs at the 350° beam (CCW method).

	Cylinder 2			Cylinder 4			Cylinder 6		
	ELEMENT ID			ELEMENT ID			ELEMENT ID		
Angle	**STOP**	**FLEXSTOP**	**FULL BEAD**	**STOP**	**FLEXSTOP**	**FULL BEAD**	**STOP**	**FLEXSTOP**	**FULL BEAD**
0	271633	269576	268397	272464	269944	268251	272049	270295	269427
10	271653	269566	268387	272482	269935	268241	272066	270286	269416
20	271678	269556	268377	272509	269925	268231	272094	270276	269406
30	271705	269547	268367	272537	269915	268221	272124	270266	269396
40	271725	269537	268357	272551	269905	268211	272143	270256	269385
50	271724	269527	268347	272557	269896	268201	272144	270247	269375

Table A.1: Partial table of all of the element IDs selected

Step 6. The elements must now be copied into a text file in the following format:

Cyl 2 STOP

271633,271653,271678,271705,271725,271724, ...(etc)

Cyl 2 FLEXSTOP

269576,269566,269556,269547,269537,269527, ...(etc)

Cyl 2 FULL BEAD

268397,268387,268377,268367,268357,268347, ...(etc)

Cyl 4 STOP

272464,272482,272509,272537,272551,272557, ...(etc)

Cyl 4 FLEXSTOP

269944,269935,269925,269915,269905,269896, ...(etc)

…..... (etc, for all cylinders and elements)

Step 7. In the Microsoft Excel Program, custom lists must now be created using the preceding element labels. This method corresponds to Microsoft 2007, however will be similar for all versions. Click the Microsoft button in the top left corner of the window to find "Excel Options." In this window, under "Top options for working with excel," click "Edit Custom Lists..." Now, copy and paste the elements from each section in Step 4 into the List entries. This must be done for each bead and each cylinder, so there should be a total of 12 custom lists. The custom lists should be added in a logical order. For example, the first list would correspond to the Stop of Cylinder 2, the second list to the Flexstop of Cylinder 2, and the third list to the FullBead of Cylinder 2. The next three lists would be for Cylinder 4, the next three for Cylinder 6, and the last three for Cylinder 8. Also, these lists will save within the Excel program so they will exist every time Excel is used. There might be issues if there are server or license resets every time Excel is closed. Figure A.6 shows the typical Excel window.

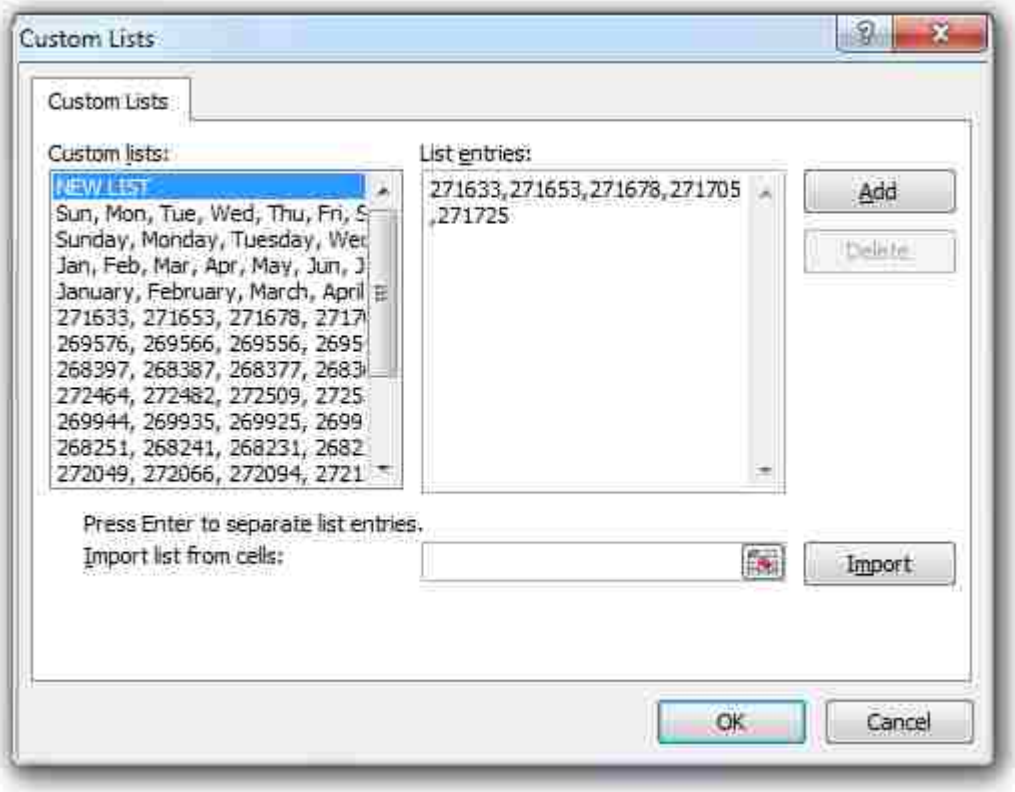

Figure A.6 Showing the Custom Lists created for each bead at every cylinder. There are 12 custom lists in total.

Step 8. In the Abaqus Viewer program, where the results of the analysis can be viewed, create a display group containing only the elements corresponding to the gasket beads of interest. The elements corresponding to the Stop, Flexstop and FullBead should be the only elements on the

screen. Create a report by clicking "Field Output" under "Reports." Under Output Variables, Position," choose "Centroid." Check the box of whatever Field output is desired. For this case, only S11 was chosen. Different options, such as the report name and layout, can be altered under the "Setup" tab. Click OK or Apply to create the report. It is usually saved under the default Abaqus working directory.

Step 9. Open the resulting Report created in Step 8. Abaqus lists the results in order of Element ID, not by the angle. Copy the rows of Element IDs and their corresponding S11 pressures. Other text elements at the top of the report are not required to be copied, only the 2 columns. Paste the results in an Excel Spreadsheet. The results will be pasted into 1 column, and therefore must be split into 2 columns using the "Text to Columns" command under the Data tab. Do this for all of the sections of results from the Report file.

Step 10. Since the results are in increasing order corresponding to the element labels, the columns must be sorted into the proper angular order needed for the charts. Note that there must be column labels such as "Element ID" and "S11 Pressure" above the corresponding columns. These labels are needed for the Excel Sort command. Select the entire two columns of results in the Excel spreadsheet including their element labels. Under the Data tab, select "Sort." Under "Column, Sort by" select the column label corresponding to the element labels, ie "Element ID." Leave the default Sort On option to "Values." Under Order, select "Custom List..." The Custom Lists window that was used earlier will appear. Select the list corresponding to the Column Selected, ie the first list if the columns Cylinder 2 Stop were selected. Click Ok twice. The columns of Element ID and S11 Pressures should now be in the order of the lists, which correspond to the sequence of angles around the circumference of the cylinder. Repeat this step for the remaining columns.

Step 11. It is now a simple matter of using the sorted data to create useful graphs using standard Excel methods. graphs can be overlaid on top of each other to observe differences in pressures along the circumference. If a new Analysis is completed using the same Gasket Model, only Steps 8-10 need to be repeated. Note that an add-on is needed to create the Polar Graphs of Figure A1 above.

Appendix B: Engine Data

File	Parameter	Unit	Mean	Std Dev	Maximum	Minimum
PMEP.Cyl1	Cyl1PMEPRT	psi	-12.51258	0.40972	-11.23787	-13.41237
Peak.Cyl1	Cyl1PeakRT	psi	1262.4963	111.119	1506.6169	943.5584
Peak Loc.Cyl1	Cyl1Peak LocRT	deg	14.196996	2.21909	20.671997	7.171997
NMEP.Cyl1	Cyl1NMEPRT	psi	218.81754	2.54445	225.74635	207.6209
Max Rise.Cyl1	Cyl1Max RiseRT	psi/deg	52.214391	10.6965	79.862305	24.92018
Max Rise Loc.Cyl1	Cyl1Max Rise LocRT	deg	2.429497	1.94292	8.171997	-2.328003
IMEP.Cyl1	Cyl1IMEPRT	psi	231.33013	2.52722	237.34454	220.7436
CA90.Cyl1	Cyl1CA90RT	deg	24.051996	4.01567	35.671993	14.672
CA75.Cyl1	Cyl1CA75RT	deg	16.584496	3.44653	27.171995	9.671997
CA50.Cyl1	Cyl1CA50RT	deg	9.026997	2.79043	17.171995	2.671997
CA25.Cyl1	Cyl1CA25RT	deg	1.876997	2.0647	8.171997	-2.328003
CA10.Cyl1	Cyl1CA10RT	deg	-4.525503	1.78808	0.671997	-8.828003
Burn1090.Cyl1	Cyl1Burn1090RT	deg	28.577499	3.01002	36.5	21.5
PMEP.Cyl2	Cyl2PMEPRT	psi	-14.35817	0.35769	-13.47831	-15.37701
Peak.Cyl2	Cyl2PeakRT	psi	1560.6761	113.579	1786.093	1244.511
Peak Loc.Cyl2	Cyl2Peak LocRT	deg	10.811997	2.83776	17.171995	1.671997
NMEP.Cyl2	Cyl2NMEPRT	psi	228.24632	2.47096	235.52136	221.0968
Max Rise.Cyl2	Cyl2Max RiseRT	psi/deg	71.310952	13.819	126.44613	41.88681
Max Rise Loc.Cyl2	Cyl2Max Rise LocRT	deg	-0.518003	2.25863	5.671997	-6.328003
IMEP.Cyl2	Cyl2IMEPRT	psi	242.6045	2.62657	250.50186	235.0073
CA90.Cyl2	Cyl2CA90RT	deg	19.636996	3.64263	30.171995	10.672
CA75.Cyl2	Cyl2CA75RT	deg	10.734497	3.55526	20.171995	1.671997
CA50.Cyl2	Cyl2CA50RT	deg	3.964497	3.04355	12.171996	-3.328003
CA25.Cyl2	Cyl2CA25RT	deg	-2.233003	2.23908	2.671997	-7.828003
CA10.Cyl2	Cyl2CA10RT	deg	-7.905503	1.93203	-2.828003	-12.828
Burn1090.Cyl2	Cyl2Burn1090RT	deg	27.542499	2.55919	34.999996	21
PMEP.Cyl3	Cyl3PMEPRT	psi	-11.2401	0.39709	-10.07072	-12.0925
Peak.Cyl3	Cyl3PeakRT	psi	1250.171	112.891	1510.9338	908.5082
Peak Loc.Cyl3	Cyl3Peak LocRT	deg	14.749496	2.35802	21.171997	8.671997
NMEP.Cyl3	Cyl3NMEPRT	psi	215.0498	3.36787	222.19437	203.0837
Max Rise.Cyl3	Cyl3Max RiseRT	psi/deg	51.814099	10.6843	84.865959	25.5579
Max Rise Loc.Cyl3	Cyl3Max Rise LocRT	deg	3.089497	2.05838	10.671996	-2.328003
IMEP.Cyl3	Cyl3IMEPRT	psi	226.28991	3.37474	233.48802	213.9561
CA90.Cyl3	Cyl3CA90RT	deg	23.091996	3.79158	34.671993	14.172
CA75.Cyl3	Cyl3CA75RT	deg	15.966996	3.39786	26.671997	8.171997
CA50.Cyl3	Cyl3CA50RT	deg	8.854497	2.77181	17.671995	3.171997
CA25.Cyl3	Cyl3CA25RT	deg	2.134497	2.14239	8.671997	-2.328003

CA10.Cyl3	Cyl3CA10RT	deg	-4.198003	1.97373	1.171997	-8.828003
Burn1090.Cyl3	Cyl3Burn1090RT	deg	27.289998	2.78719	35.499996	19
PMEP.Cyl4	Cyl4PMEPRT	psi	-11.23628	0.46583	-9.583865	-12.34109
Peak.Cyl4	Cyl4PeakRT	psi	1424.0491	130.925	1707.9412	959.3674
Peak Loc.Cyl4	Cyl4Peak LocRT	deg	13.469496	2.37913	19.171995	7.171997
NMEP.Cyl4	Cyl4NMEPRT	psi	231.26603	3.25704	238.11678	220.1773
Max Rise.Cyl4	Cyl4Max RiseRT	psi/deg	61.753895	12.9293	97.179123	22.92053
Max Rise Loc.Cyl4	Cyl4Max Rise LocRT	deg	2.014497	2.39352	8.671997	-3.828003
IMEP.Cyl4	Cyl4IMEPRT	psi	242.50232	3.36998	249.72269	231.7825
CA90.Cyl4	Cyl4CA90RT	deg	22.736996	3.90426	34.671993	11.672
CA75.Cyl4	Cyl4CA75RT	deg	14.976996	3.6207	26.671997	7.171997
CA50.Cyl4	Cyl4CA50RT	deg	7.421997	3.1245	18.671995	1.171997
CA25.Cyl4	Cyl4CA25RT	deg	0.851997	2.5928	10.171997	-4.328003
CA10.Cyl4	Cyl4CA10RT	deg	-5.293003	2.35187	2.671997	-10.328
Burn1090.Cyl4	Cyl4Burn1090RT	deg	28.029999	2.56595	37.999996	20
PMEP.Cyl5	Cyl5PMEPRT	psi	-10.65663	0.44157	-9.519325	-11.72844
Peak.Cyl5	Cyl5PeakRT	psi	1391.3997	116.617	1658.738	955.9318
Peak Loc.Cyl5	Cyl5Peak LocRT	deg	12.286996	2.41128	19.671997	4.671997
NMEP.Cyl5	Cyl5NMEPRT	psi	218.42976	2.42779	223.72322	210.8578
Max Rise.Cyl5	Cyl5Max RiseRT	psi/deg	63.822141	12.1182	96.835556	24.78558
Max Rise Loc.Cyl5	Cyl5Max Rise LocRT	deg	1.006997	2.01873	8.671997	-4.828003
IMEP.Cyl5	Cyl5IMEPRT	psi	229.0864	2.48317	234.8584	221.5784
CA90.Cyl5	Cyl5CA90RT	deg	20.166996	3.87911	37.171997	11.672
CA75.Cyl5	Cyl5CA75RT	deg	12.739496	3.54495	27.171995	3.671997
CA50.Cyl5	Cyl5CA50RT	deg	5.654497	2.937	17.671995	-0.828003
CA25.Cyl5	Cyl5CA25RT	deg	-0.570503	2.34786	9.671997	-5.828003
CA10.Cyl5	Cyl5CA10RT	deg	-6.510503	2.29575	2.171997	-11.828
Burn1090.Cyl5	Cyl5Burn1090RT	deg	26.677499	2.75586	35.999996	19
PMEP.Cyl6	Cyl6PMEPRT	psi	0	0	0	0
Peak.Cyl6	Cyl6PeakRT	psi	14.693111	0	14.693111	14.69311
Peak Loc.Cyl6	Cyl6Peak LocRT	deg	-90.32801	0	-90.32801	-90.32801
NMEP.Cyl6	Cyl6NMEPRT	psi	0	0	0	0
Max Rise.Cyl6	Cyl6Max RiseRT	psi/deg	0	0	0	0
Max Rise Loc.Cyl6	Cyl6Max Rise LocRT	deg	-89.828	0	-89.828	-89.828
IMEP.Cyl6	Cyl6IMEPRT	psi	0	0	0	0
CA90.Cyl6	Cyl6CA90RT	deg	109.172	0	109.172	109.172
CA75.Cyl6	Cyl6CA75RT	deg	94.171989	0	94.171989	94.17199
CA50.Cyl6	Cyl6CA50RT	deg	71.671997	0	71.671997	71.672
CA25.Cyl6	Cyl6CA25RT	deg	48.171997	0	48.171997	48.172
CA10.Cyl6	Cyl6CA10RT	deg	29.671995	0	29.671995	29.672

Burn1090.Cyl6	Cyl6Burn1090RT	deg	79.499992	0	79.499992	79.49999
PMEP.Cyl7	Cyl7PMEPRT	psi	-13.30274	0.34025	-12.41343	-14.00437
Peak.Cyl7	Cyl7PeakRT	psi	1387.9467	129.702	1627.2112	886.8003
Peak Loc.Cyl7	Cyl7Peak LocRT	deg	12.976996	1.97154	19.671997	9.171996
NMEP.Cyl7	Cyl7NMEPRT	psi	221.21767	2.61377	228.32176	208.0277
Max Rise.Cyl7	Cyl7Max RiseRT	psi/deg	62.991559	12.5522	101.39525	27.80034
Max Rise Loc.Cyl7	Cyl7Max Rise LocRT	deg	3.131997	5.01731	11.171996	-3.328003
IMEP.Cyl7	Cyl7IMEPRT	psi	234.52042	2.66338	241.3862	221.6907
CA90.Cyl7	Cyl7CA90RT	deg	21.539496	3.89085	37.171997	10.672
CA75.Cyl7	Cyl7CA75RT	deg	14.034496	3.74598	29.171993	5.671997
CA50.Cyl7	Cyl7CA50RT	deg	7.791997	3.39125	19.671997	-1.328003
CA25.Cyl7	Cyl7CA25RT	deg	0.411997	2.93128	10.671996	-5.828003
CA10.Cyl7	Cyl7CA10RT	deg	-5.645503	2.23617	1.671997	-11.328
Burn1090.Cyl7	Cyl7Burn1090RT	deg	27.184999	2.50964	35.499996	21
PMEP.Cyl8	Cyl8PMEPRT	psi	-13.59111	0.38982	-12.62927	-14.52035
Peak.Cyl8	Cyl8PeakRT	psi	1225.718	117.15	1487.093	953.0016
Peak Loc.Cyl8	Cyl8Peak LocRT	deg	15.094496	2.49404	22.671997	10.172
NMEP.Cyl8	Cyl8NMEPRT	psi	224.33815	3.65839	231.2897	213.6951
Max Rise.Cyl8	Cyl8Max RiseRT	psi/deg	48.456498	10.9745	75.986916	23.30135
Max Rise Loc.Cyl8	Cyl8Max Rise LocRT	deg	3.001997	1.98522	8.171997	-0.828003
IMEP.Cyl8	Cyl8IMEPRT	psi	237.92927	3.57082	244.68877	227.2049
CA90.Cyl8	Cyl8CA90RT	deg	26.364496	4.02109	36.671997	14.672
CA75.Cyl8	Cyl8CA75RT	deg	18.439496	3.56226	27.171995	9.671997
CA50.Cyl8	Cyl8CA50RT	deg	10.474497	2.87615	18.171997	3.671997
CA25.Cyl8	Cyl8CA25RT	deg	3.329497	2.12637	9.671997	-1.828003
CA10.Cyl8	Cyl8CA10RT	deg	-2.925503	1.82668	1.671997	-6.828003
Burn1090.Cyl8	Cyl8Burn1090RT	deg	29.289998	3.01553	35.999996	21.5
RPM.Timer	RPMRT		8999.8444	5.30777	9009.3467	8986.407
PMEP.EA	EAPMEPRT	psi	-10.8622	0.13644	-10.55583	-11.2644
NMEP.EA	EANMEPRT	psi	194.67063	1.07094	197.31769	191.7175
IMEP.EA	EAIMEPRT	psi	205.53284	1.05166	207.94231	202.6958
EncErrors.EA	EncErrorsRT		0	0	0	0
CycleNumber.Timer	CycleNumberRT		100.5	57.7343	200	1
CAIGN.Cyl8.Ign8	Cyl8CAIGNRT	deg	-31.89051	0.24969	-31.32801	-32.32801
CAIGN.Cyl7.Ign7	Cyl7CAIGNRT	deg	-34.29551	0.32046	-33.328	-34.82801
CAIGN.Cyl6.Ign6	Cyl6CAIGNRT	deg	-34.63301	0.29065	-33.828	-35.32801
CAIGN.Cyl5.Ign5	Cyl5CAIGNRT	deg	-34.55301	0.32692	-33.828	-35.32801
CAIGN.Cyl4.Ign4	Cyl4CAIGNRT	deg	-32.6855	0.26635	-32.32801	-33.328
CAIGN.Cyl3.Ign3	Cyl3CAIGNRT	deg	-32.783	0.51524	-31.82801	-33.828
CAIGN.Cyl2.Ign2	Cyl2CAIGNRT	deg	-33.6255	0.28327	-32.828	-34.32801
CAIGN.Cyl1.Ign1	Cyl1CAIGNRT	deg	-31.94551	0.31216	-31.32801	-32.828

CA50.EA	EACA50RT	deg	15.60762	1.07378	18.984493	12.9845
Burn1090.EA	EABurn1090RT	deg	34.261555	0.89868	36.687492	31.56249

Appendix C: Cold Clamping S11 Pressures for All Cylinders

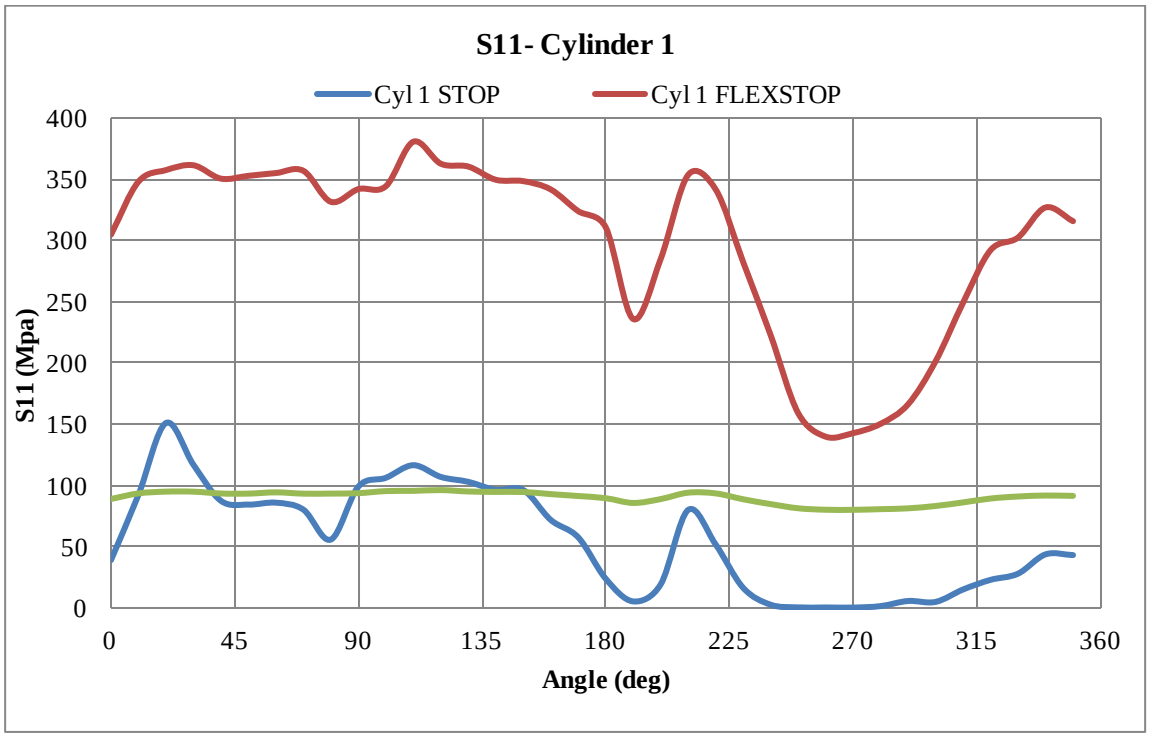

Figure C1: Circumferential S11 Pressures on all Bead Areas for Cylinder 1

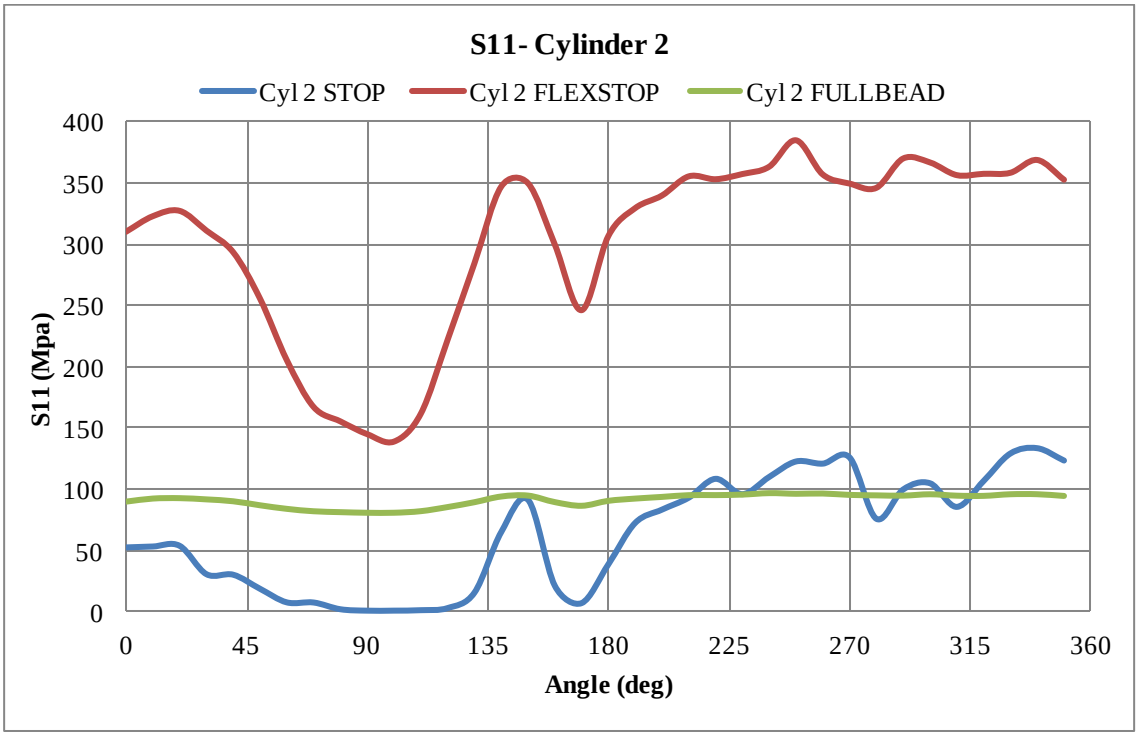

Figure C2: Circumferential S11 Pressures on all Bead Areas for Cylinder 2

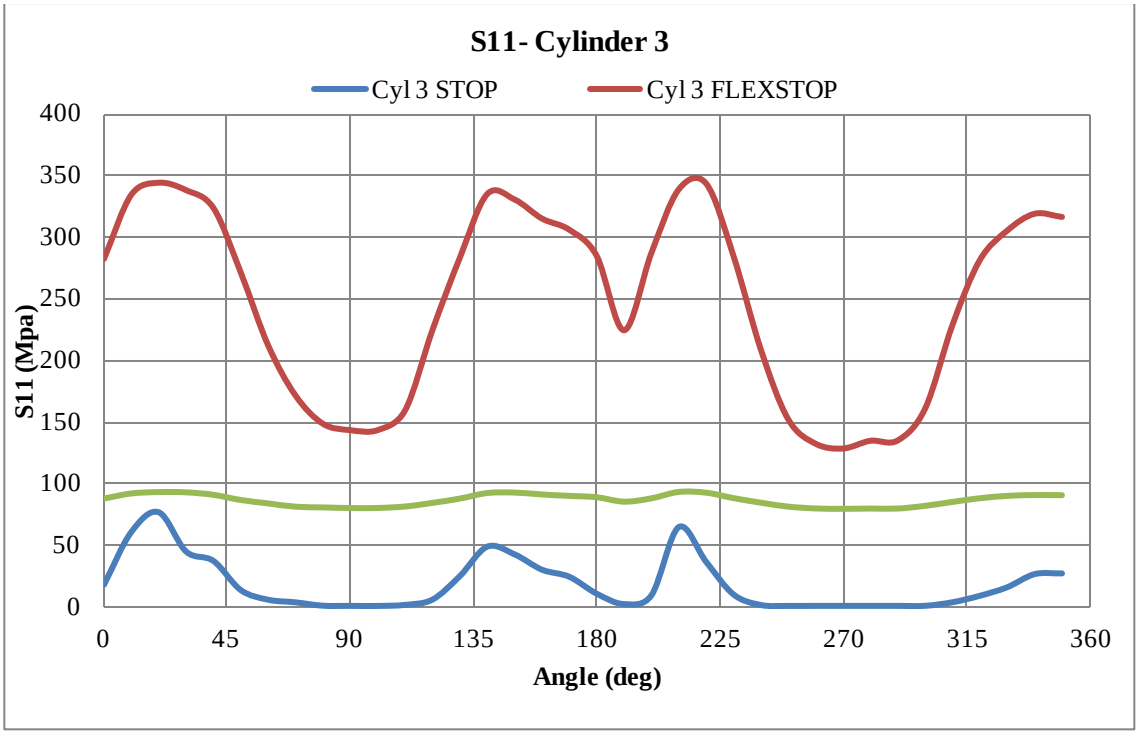

Figure C3: Circumferential S11 Pressures on all Bead Areas for Cylinder 3

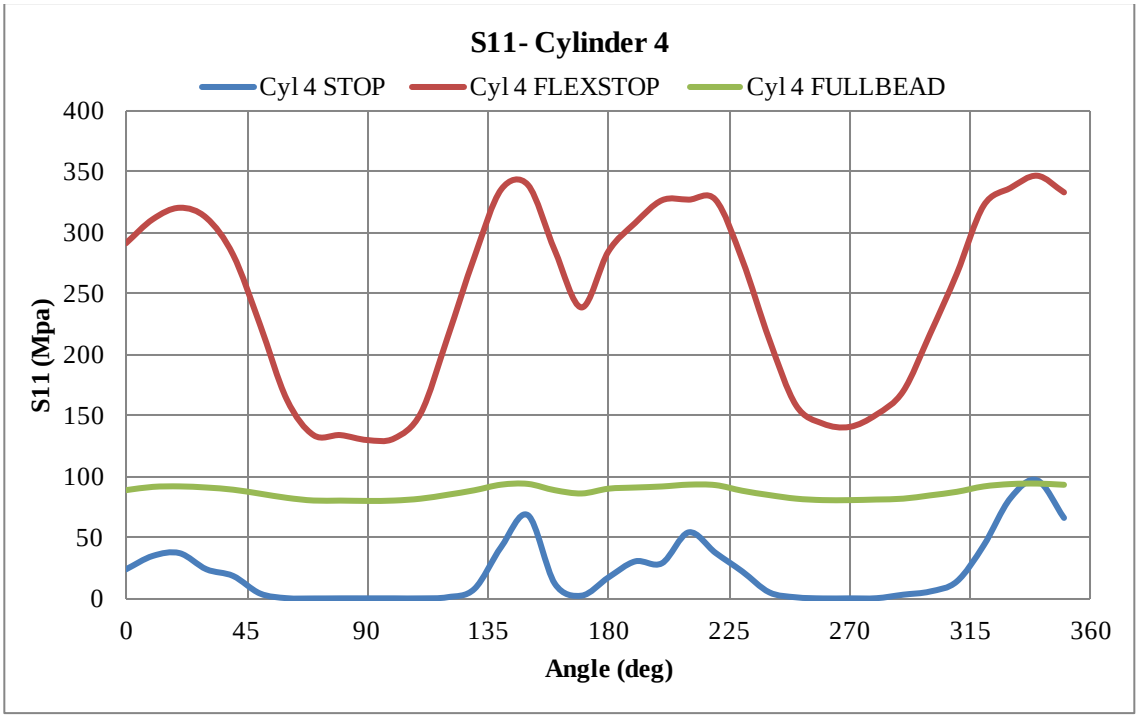

Figure C4: Circumferential S11 Pressures on all Bead Areas for Cylinder 4

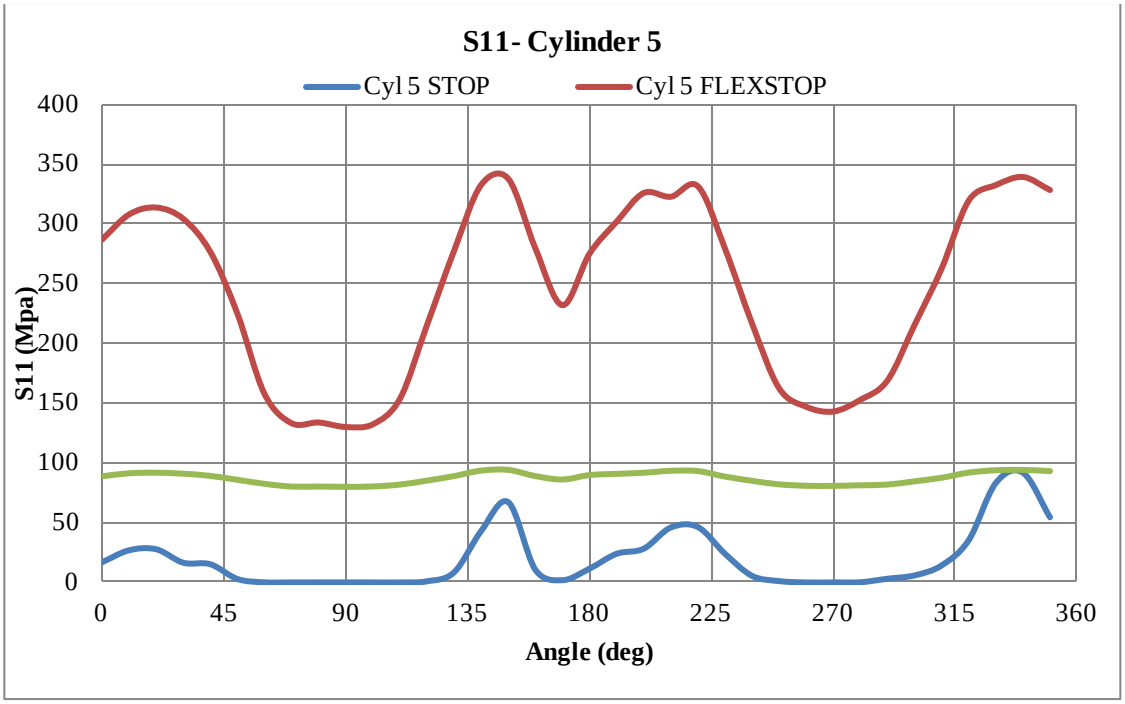

Figure C5: Circumferential S11 Pressures on all Bead Areas for Cylinder 5

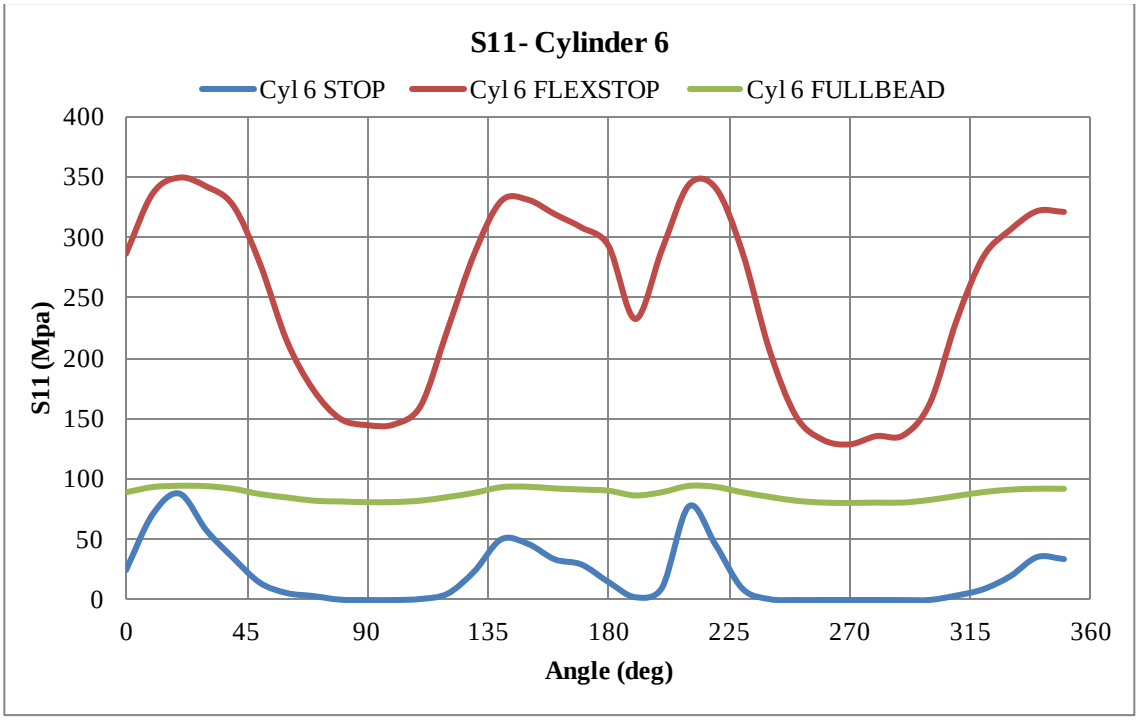

Figure C6: Circumferential S11 Pressures on all Bead Areas for Cylinder 6

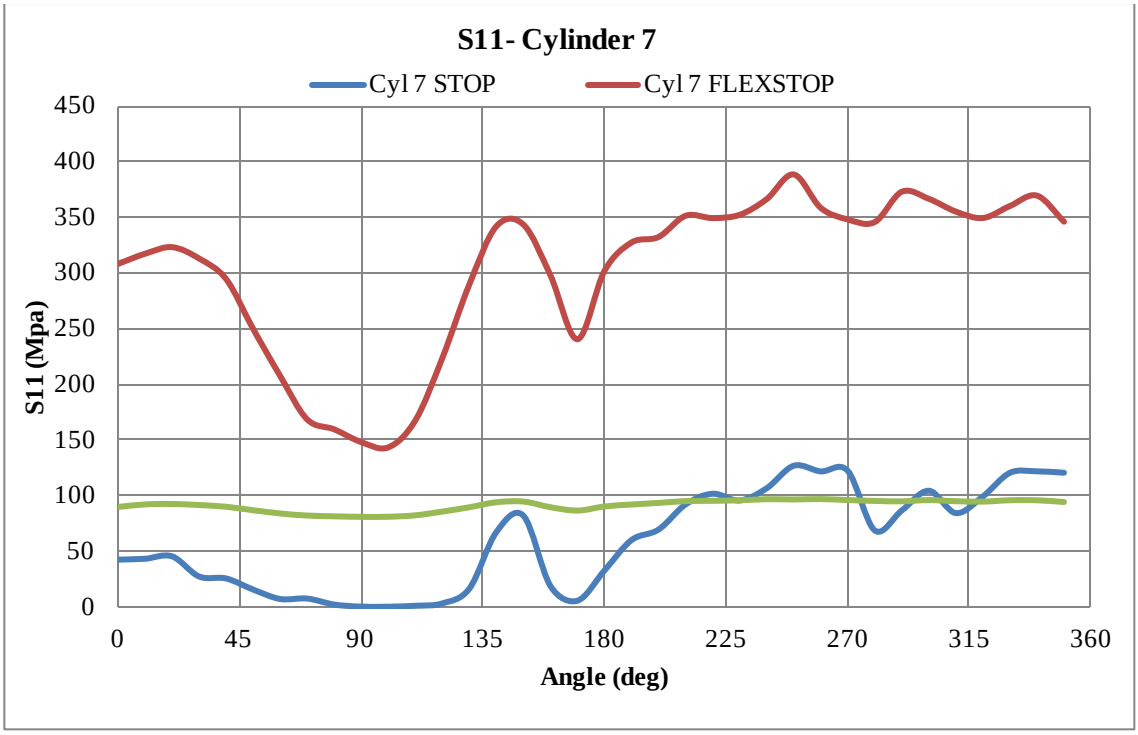

Figure C7: Circumferential S11 Pressures on all Bead Areas for Cylinder 7

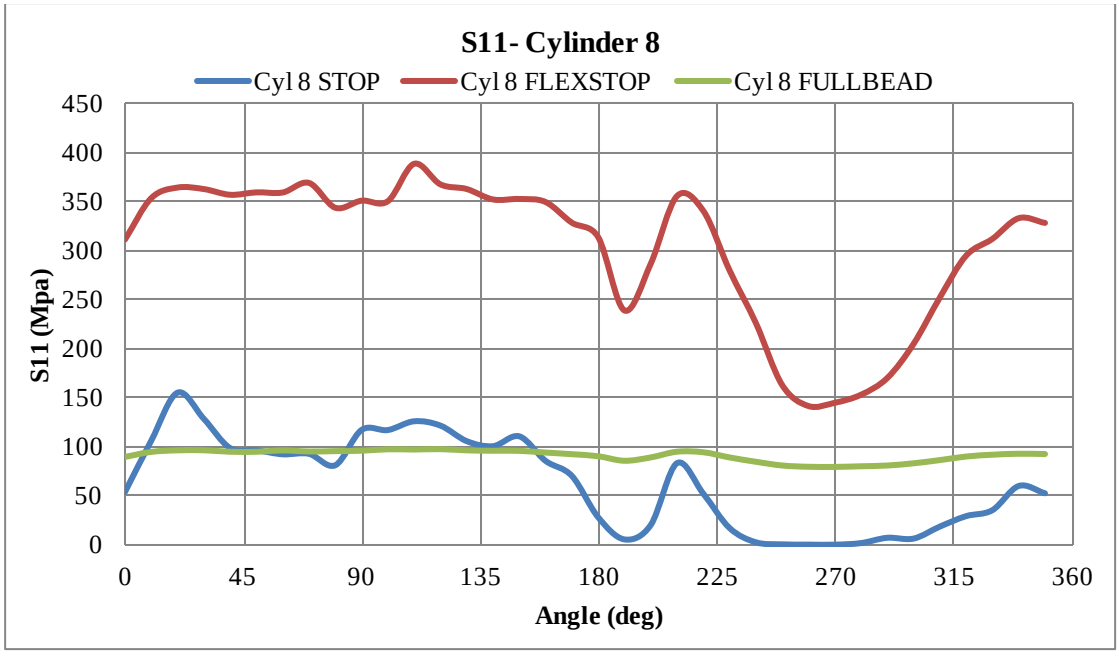

Figure C8: Circumferential S11 Pressures on all Bead Areas for Cylinder 8

VITA AUCTORIS

NAME:	Jeffrey Scott Eagleson
PLACE OF BIRTH:	Sarnia, ON
YEAR OF BIRTH:	1983
EDUCATION:	Lord Elgin High School, Burlington, ON, 2002
	University of Windsor, B.Sc., Windsor, ON, 2010
	Politecnico di Torino, M.Sc., Torino, IT, 2013
	University of Windsor, M.Sc., Windsor, ON, 2013